QUANTITATIVE ESTIMATES OF COARSE ROOT BIOMASS USING 3-D GPR

QUANTITATIVE, NON-DESTRUCTIVE ESTIMATES OF FOREST COARSE ROOT BIOMASS USING 3-D GROUND-PENETRATING RADAR (GPR)

BY

MICHELLE MOLON, B.Sc (Hons)

A Thesis Submitted to the School of Graduate Studies in Partial Fulfillment of the Requirements for the Degree Master of Science

MASTER OF SCIENCE (2012)	MCMASTER UNIVERSITY
Geography and Earth Sciences	Hamilton, Ontario
TITLE:	**Quantitative, non-destructive estimates of forest coarse root biomass using 3-D ground-penetrating radar (GPR)**
AUTHOR:	Michelle Molon, B.Sc (Hons) (McMaster University, Hamilton, 2010)
SUPERVISOR	Professor Altaf M. Arain
CO-SUPERVISOR	Professor Joe I. Boyce
NUMBER OF PAGES	xi, 104

ABSTRACT

In this study we evaluated 3-D imaging of coarse root structure and biomass using ground-penetrating radar (GPR). GPR surveys were conducted in a white pine forest in southern Ontario, Canada. GPR profiles were obtained across two test plots (6 and 17 m^2 area), using 1 GHz GPR and a MEMS (micro-electro-mechanical systems) accelerometer. Test plot surveys evaluated the effects of micro-topography, soil moisture content, and root diameter and spacing. In addition, with the aid of the outcome of the control test plots two other plots (25 and 400 m^2 area) were surveyed with varying line sample spacing to investigate the restraints on resolution brought about by line sampling density.

Accounting for antenna tilt is necessary to determine an accurate and more precise position of root mass. The antenna tilt was >45^o pitch, >28^o roll and up to 10^o yaw due to surface micro-topography of the forest floor. Vector 3-D imaging enhanced the diffraction amplitude (15.5% increase) and centralizes the position of the root compared to that of the non-vector images. Radial surveys provided root continuity and produced better root imaging.

GPR largely underestimates coarse root biomass when a line spacing of 25 cm is used. However similar results are found with smaller line spacing (12.5 cm). A maximum line spacing of 10 cm provided continuous root structure and the differentiation of roots spaced 10 cm apart and greater. A sampling line spacing of 5 cm and an inline sampling interval of 0.5 cm in low soil moisture conditions provided the detection of roots that were a minimum of 1.4 cm in diameter; compared to 1.9 cm root diameter in high soil

moisture. This study showed that 3-D imaging of root structure is possible with the correct field procedure and technique, leading to the estimation of coarse root biomass.

ACKNOWLEDGEMENTS

First and foremost I would like to thank my supervisors, Dr. Altaf Arain and Dr. Joe Boyce. I would not have gotten to where I am without the opportunity given to me by them. This was a new collaboration for them and I am grateful that I was able to be a part of it. Both of you have taught me to learn independently and have helped me expand my knowledge for the future. Thank you both for believing in me and continuing to help me along the way.

I would also like to thank everyone in the hydrometeorology and climatology lab, especially Rob Thorne. Rob, thank you for helping me dig numerous holes, carry out GPR surveys as well as providing me with your knowledge and advice. Jason Brodeur and Samantha Mackay, thank you both for being there for me and answering any question I had. Last but not least, I would not have been able to do this without Beth Hooper, who gave her time to help me on numerous occasions.

Thank you to my sponsors, NSERC, MOE, and OMNR, for their funding and support. This was an exciting and challenging experience that I would do all over again.

Thank you mom and dad for supporting me with my decision of pursuing a Masters and being there for me from beginning till end. I only hope to amount to what you both have; you are the perfect role models. Jeremy, Nicole and Danielle, thank you for being interested in my work, and your support. Especially Danielle, thank you for coming to the field with me when no one else could/would. We make a great team. To Daryl Sivakumaran, thank you for pushing me when I needed it and not letting me give up. It means a lot to know that I have you to count on.

TABLE OF CONTENTS

LIST OF FIGURES

CHAPTER 1

CHAPTER 2

CHAPTER 3

LIST OF TABLES

CHAPTER 1

CHAPTER 3

CHAPTER 1: INTRODUCTION

1.1 Background and Rationale

The Intergovernmental Panel on Climate Change (IPCC) foresees extreme changes in climate events if current trends of carbon dioxide emissions are continued in the future (IPCC, 2007). Carbon allocation in forests has garnered increased interest because of their potential to sequester atmospheric carbon dioxide (CO_2) to offset anthropogenic emissions and help in mitigating climate change. It is necessary to determine forest carbon stocks and to estimate any changes that may occur. In particular, the estimation of belowground biomass, which is composed of live roots, is important for greenhouse gas inventory in forests. Roots are responsible for providing nutrients, water and stability in ecosystem functioning. They act as a carbon sink that account for 20-40 % of global forest biomass (Hirano et al., 2009). Roots consist of 10-65 % of a tree's total biomass varying with factors such as age, species, water and nutrient availability, and competition (Barton et al., 2004). Coarse roots (>5mm diameter) are important for carbon storage in forest trees while fine roots (<2mm diameter) are important in tree to soil carbon fluxes and carbon storage in the soil (Hirano et al., 2008). Therefore it is important to accurately sample and measure root biomass for carbon allocation. Common practices for calculating belowground biomass include destructive techniques (e.g. excavation, air spading and coring) and non-destructive geophysical methods (e.g. ground-penetrating radar) (XiHong et al., 2010).

1.2 Destructive Techniques

Soil coring is typically done for the estimation of fine root biomass using a metal cylinder or auger. With a known volume, the roots can be sampled and converted into root biomass per unit area (Lassoie and Hinckley, 1991). Coarse root biomass is mainly obtained by automatic excavation machinery, manually using hand tools and/or high-pressure methods such as air spading. Entire root zones are excavated using one or more of these methods. For instance, soil cores have been used to determine fine root biomass of Norway spruce in a forest located in the Fichtelgebirge mountains in southeast Germany (Gaul et al., 2008). Together with excavation data, total belowground biomass can be estimated. Peichl and Arain (2006) used soil coring for fine root biomass and excavation for coarse root biomass at Turkey Point Flux Station (TPFS). Fine root biomass was performed in a similar manner as mentioned and 5 white pine trees were excavated manually and with machinery. Belowground biomass was separated into root stump, medium root (0.5-2 cm), small roots (<5 mm) and large roots (≥2 cm) (Peichl and Arain, 2007). This was done at 4 sites that varied with stand age resulting in a total belowground biomass estimate and a biomass estimate for each belowground component for each tree, given in Table 1.1. These values were used to calculate the total belowground biomass for each site with allometric equations and the use of stem density.

Root to shoot ratios are used extensively to estimate belowground biomass. However the large degree in variation of the ratios shows a need to estimate belowground biomass using species or forest specific equations (Vadeboncoeur et al., 2007). This can

Table 1.1: Partitioning of belowground biomass in the 2-, 15-, 30-, and 65-year old white pine sites (Peichl and Arain, 2007).

Tree Component	Biomass (kg/tree)			
	2-year old	15-year old	30-year old	65-year old
Root stump	0.02 ± 0.01	5.9 ± 6.1	6.8 ± 5.3	38.9 ± 14.0
Large roots (≥2cm)	0	5.7 ± 4.4	7.9 ± 7.7	51.1 ± 23.5
Medium roots (0.5-2cm)	0.03 ± 0.03	1.1 ± 0.7	2.0 ± 1.4	7.6 ± 0.9
Small roots (2-5mm)	0.04 ± 0.03	0.3 ± 0.1	0.5 ± 0.5	0.9 ± 0.2
Total belowground	0.09 ± 0.07	13 ± 11	17 ± 14	99 ± 40

be done by means of allometric equations and regression analysis. Allometric equations are based on results and relationships from data collected by destructive techniques. Root dry weights are used to develop regression equations that estimate coarse root biomass from measurements of tree diameter at breast height (DBH, 1.3 m) (Lassoie and Hinckley, 1991). Several studies have found significant regressions describing dry root biomass as a function of DBH for various forests and tree types (Bolte et al., 2004; Cairns et al., 1997; Ouimet et al., 2008). The model that has come to form is:

$$y = b_1 \times DBH^{b_2} \tag{1}$$

where y is the root biomass (kg) and b_1 and b_2 are equation constants (Ouimet et al., 2008). This model has proven useful for estimating the amount of belowground biomass for site-specific trees types. Difference in climatic region, the amount of DBH samples taken, and the range in size of DBH samples can explain the differences in the models. Therefore the relationships are site-specific and should be completed for each individual site.

Similar studies have been conducted in various locations with different species and stand age. Peichl and Arain (2007) obtained an allometric equation for stands of varying age at TPFS composed of white pine forests in southern Ontario. In each site, 5 trees were randomly selected for excavation, covering the range of DBH in each stand within the dominant canopy layer (Peichl and Arain, 2007). They found belowground biomass to be highly correlated with DBH across the entire age sequence. There was also a decrease in the relationship between tree component biomass and stem volume for belowground biomass and total tree biomass with increasing stand age (Peichl and Arain, 2007). This shows that total tree biomass changes with age and should be considered in allometric equations, making site-specific allometry important. Their allometric equation for each site was multiplied by stem density in order to obtain total belowground biomass for each individual site.

Destructive techniques have the ability to quantify fine and coarse roots; soil coring for quantifying fine roots and excavation for coarse roots. Excavation gives a direct estimate of root biomass and the introduction of air spading can provide a picture of the entire root zone and root structure can be analyzed. Allometry is an easy way to quantify a large spatial extent once excavation is complete. If allometric equations are available for an entire region the belowground biomass can be estimated. However these methods are unrepeatable, time consuming, labour intensive, and limited with respect to the area that can be evaluated (Butnor et al., 2003). This makes it difficult to acquire adequate samples (XiHong et al., 2010). For instance, coring requires a significant amount of replicate samples to detect significant differences between samples, but processing time limits the amount of samples that can be taken over a year (Lassoie and Hinckley, 19991). The allometric equations should also be species and site-specific since the root zone differs with soil type and species. Site-specific factors include varying tree density, soil moisture, nutrients, light exposure, topography, and disturbance (Peichl and Arain, 2006). Destructive techniques prevent the study of the entire tree root system or root branching patterns and give little to no resolution on root structure or distribution (Butnor et al., 2003; Hruska et al., 1999). This makes it difficult to determine spatial variability over a large area.

1.3 Geophysical Measurement of Root Biomass

Several studies have demonstrated the successful application of geophysical methods such as: electrical resistivity tomography, seismic refraction tomography, X-ray computed tomography, nuclear magnetic resonance and ground-penetrating radar (GPR) to detect and estimate root biomass (Amato et al., 2008; Heeraman et al., 1997; Leucci, 2010; Zenone et al., 2008). However GPR has been used most widely as it can detect coarse root location in large areas, estimate root biomass and has the potential to create three-dimensional (3-D) images of root structure. The costs of these other techniques are higher than GPR and are difficult to apply in the field (XiHong et al., 2010). GPR has been used to detect roots in lab and field environments. Controlled lab experiments entail burying roots in a sand pit to compare the estimated root biomass that GPR obtains versus the actual root biomass as well as discovering the minimum root diameter that can be detected by GPR. Barton and Montagu (2004) used 500 MHz, 800 MHz and 1 GHz antennas to detect roots and determine their root size in a sandpit. Native hardwood roots of various diameters (1-10 cm) were buried at 50 cm and roots with the same diameters were buried at various depths (15-155 cm) without overlap and in optimal orientation. The authors found that the 800 MHz antenna resulted in the clearest radar profiles in terms of the identification of hyperbolas since it gave the best compromise between penetration and resolution. However, the centre of the root detected with the 500 MHz antenna, after processing, correlated well with root diameter compared to the other antennas. Using half of the 500 MHz data a multiple regression model was created, which was able to predict root diameters as small as 1 cm with a root mean squared error of 0.6

cm. Similar results were found in an experiment conducted by Hirano and colleagues (2009) who buried *Cryptomeria japonica* roots varying in diameter from 10 mm to 78 mm. A 900 MHz antenna was able to detect roots greater than 19 mm, varying with the volumetric water content of the roots. Roots with high volumetric water content were easily detected while roots with volumetric water content of 20 % or less were not found (Hirano et al., 2009). Closely spaced roots were also not detected by GPR individually. Slight differences between experiments could be due to soil and root water content, interval between roots and sand composition, which could lead to an underestimation of root biomass (Hirano et al., 2009). A recent study performed by XiHong et al (2010) used a much higher antenna frequency of 2 GHz to calculate *Ulmus pumila* root biomass in sand. After surveyed at 10 cm intervals and processed, results showed that coarse root biomass for root diameters greater than 0.5 cm could be estimated using bulk volume and density of coarse roots since the density of coarse roots greater than 0.5 cm in diameter were found to be uniform (XiHong et al., 2010). Root diameter was estimated with the time between when the wave reaches the root bottom and when it reaches the root top (XiHong et al., 2010). This was then used in the estimation of coarse root biomass, assuming the root is cylindrical (XiHong et al., 2010). They found that their GPR based model was capable of estimating coarse root biomass.

Field experiments apply these findings to various sites to determine the belowground biomass. Excavation and/or soil cores are required for direct observation and can be related to GPR reflection. Destructive techniques are also used for verification of GPR results. Butnor et al (2001) used 1.5 GHz and 400 MHz antennas to determine the best soil conditions for the detection of loblolly pine roots using GPR and to calculate root biomass. Several sites were surveyed with varying soil conditions and the Georgia and Carolina Sandhills in southeastern United States gave the best results since they are composed of sandy, excessively drained soils. The 1.5 GHz antenna was used for root sizing and biomass estimates since it had a higher capacity to resolve roots compared to the 400 MHz antenna. Grids were surveyed with 25 cm spacing and then harvested for actual root biomass up to a 40 cm depth. Roots as small as 0.5 cm were detected with the 1.5 GHz antenna to a depth of 50 cm, but dead roots and taproots were poorly detected (Butnor et al., 2001). Total root biomass was correlated with manual reflection tally (the number of reflections within a certain threshold range) and high amplitude area. Both variables were found to be directly proportional to changes in root biomass. Reflector tally indicated a statistically significant difference ($P = 0.0152$) compared to that of high amplitude area, which was therefore not significant. This showed that GPR could be a valuable tool for root biomass estimation (Butnor et al., 2001). Butnor et al (2003) performed a similar study with a 1.5 GHz antenna to estimate belowground biomass of loblolly pine and sweetgum located in Decatur County, Georgia. The site is composed of Troup and Lucy soils, which allowed for a maximum penetration depth of about 70 cm. Several plots were surveyed in 60 cm intervals in both directions creating a square grid. GPR estimates were calculated and compared to soil coils that were taken along the same transect. GPR root biomass estimates were based on the correlation of root biomass per core with the number of pixels within a certain threshold range. The correlation coefficient was also highly significant, agreeing with the Burtnor et al (2001) data.

Another study by Zenone and colleagues (2008) used 900 MHz and 1.5 GHz antennas in a circular and square grid transect in a poplar plantation and pine wood forest. For poplar trees, high frequency antennas (1.5-2 GHz) are best for the detection of small roots (Zenone et al., 2008). This proved to be the case in this study especially for trees with a dominant radial expansion of the root system (Zenone et al., 2008). The study used air spading to see morphological information on the root zone and then scanned the excavated trees with portable on ground scanning LiDAR. This resulted in a 3-D image of the root structure showing the potential for 3-D mapping with GPR data, as long as the appropriate software is available. GPR-SLICE, processing software, has the potential to create 3-D images of root structure from GPR data, however this has not been explored in literature.

To summarize this discussion, I can state that the limitations and pitfalls of destructive techniques give rise to the evaluation of GPR for biomass detection. There is an issue with discrete sampling and therefore having to upscale to a larger area through stem density. Allometric equations can only be as accurate as the given sample size; the greater the number of trees excavated the more accurate the regression equation. In addition, destructive techniques destroy the root zone through excavation and coring eliminating the possibility of 3-D imaging of root structure.

1.4 Study Objectives

In this study I created 3-D images of root structure and distribution using ground-penetrating radar and developed a standard field procedure. It also introduced a new method for obtaining coarse root biomass estimates. The main objectives for this study were to:

1) evaluate vector guided GPR and the effects of surface micro-topography on the acquisition of radar data.

2) quantify the spatial distribution and volume of coarse roots using the high-resolution 3-D GPR resulting in a coarse root biomass estimate.

3) provide a survey method technique by investigating the relationship between line spacing, volumetric moisture content, root diameter, root spacing and root continuity with the gridding of GPR data.

4) perform a comparative analysis of the allometric equation method and GPR, to improve on existing belowground biomass estimates.

1.5 Study Area

This study was conducted in a 73-year-old (planted in 1939) white pine forest, located 12 km South of the town of Simcoe and 3 km North of Lake Erie in Southern Ontario Canada (Figure 1.1). The forest is part of an age-chronosequence of three white pine plantations that make up the Turkey Point Flux Station (TPFS). Carbon dioxide and water vapour fluxes have been continuously measured at TPFS since 2003. The forest is dominated by eastern white pine (*Pinus strobus L.*) (>82 %), some other tree species within the area are balsam fir, and native Carolinian species. The ground cover vegetation consists of mosses (eg. *Phlox subulata*), poison ivy (*Rhus radicans* (L.) Kuntze ssp. radicans), bracken fern (Pteridium aquilnum (L.) Kuhn), Canada mayflower

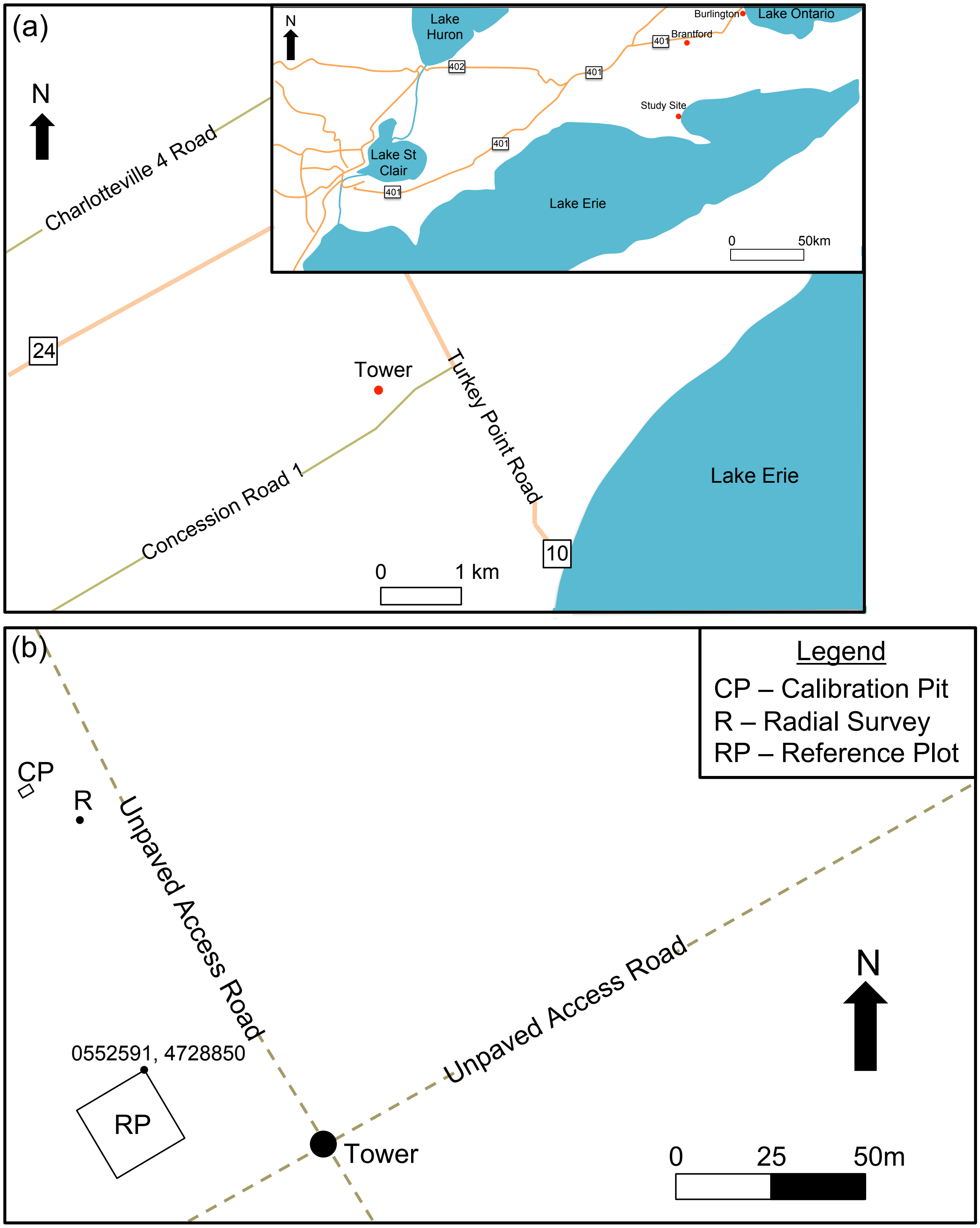

Figure 1.1: (a) Location of study area and Turkey Point Flux Station (TPFS) 1939 in southern Ontario with an inset of a regional map of the area. (b) Site map, with the UTM coordinates of the north-east corner of the reference plot.

(*Maianthemum canadense* (Desf.)), and allegheny raspberry (*Rubus allegheniensis* (Porter)) (Arain and Restrepo-Coupe, 2005; Peichl and Arain, 2006). The average diameter at breast height (DBH) is 34 cm, the average tree height is 21.8 ± 1.7 m, the stand density is 421 ± 166 stems ha^{-1} (Peichl et al., 2010b) and the leaf area index (LAI) is 8 m^2 m^{-2} (Chen et al., 2006).

The 30-year annual mean temperature is 7.8 ^oC and the mean annual precipitation is 1010 mm. Between May and September there is 438 mm of rainfall and 133 mm falls as snow in the winter (Meteorological Services of Canada climate records at Delhi, ON, located ~20 km West of TPFS). The water table is at 7 m below ground surface. The forest grows on well-drained sandy soil with a low moisture holding capacity (Arain and Restrepo -Coupe, 2005). The soil is a very fine brunisolic grey-brown luvisol, with a sandy texture, composed of ~98 % sand, 1 % silt and <1 % clay. The site is located on lacustrine sandy plains that were only modified by wind action (Peichl and Arain, 2006). The bulk density of the upper 10 cm is 1.35 gcm^{-3} (Peichl et al., 2009).

1.6 Methods

1.6.1 Background of Ground-Penetrating Radar

GPR is a non-invasive, near surface (<50 m) geophysical technique that is used to detect buried objects. It can predict the depth, position and size of matter that is buried using the time and character of reflected waves (Hirano et al., 2009). GPR consists of short pulses of radio frequency electromagnetic energy (10-2000 MHz) being radiated to detect and image electrical discontinuities in the subsurface from a transmitting antenna

(Figure 1.2). A spectrum of frequencies is generated that extends above and below the centre frequency of the transmitting antenna (Butnor et al., 2001). Heterogeneities in the subsurface cause a portion of the energy to be reflected back to a receiving antenna, while the remainder of the energy is transmitted further into the subsurface. Heterogeneities in the subsurface are created by layers with different electromagnetic properties due to water content, dissolved minerals, and expansive clay and heavy minerals (Butnor et al., 2001). Relative permittivity (ε_r), relative magnetic permeability (μ_r) and electrical conductivity (σ) determine how electromagnetic energy will behave in a given medium (Neal, 2004). Relative (dielectric) permittivity is the capacity of a material to store a charge when an electric field is present compared to that in a vacuum, measured in farads per meter. Relative magnetic permeability is the ability of a substance to sustain a magnetic field relative to free space, in henrys per meter. Conductivity measures the ability to transport charge in the presence of a static electric field (Neal, 2004). The receiving unit measures the intensity, velocity and propagation time of the signal (Stover et al., 2007). If the velocity of the electromagnetic pulse is known then the depth to the reflector can be calculated using the formula:

$$d = vt/2 \tag{2}$$

where d is the depth to the reflector, v is the propagation velocity, and t is the two way travel time. The propagation velocity is also related to the relative dielectric permittivity by:

$$v = \frac{c}{\sqrt{\varepsilon_r}} \tag{3}$$

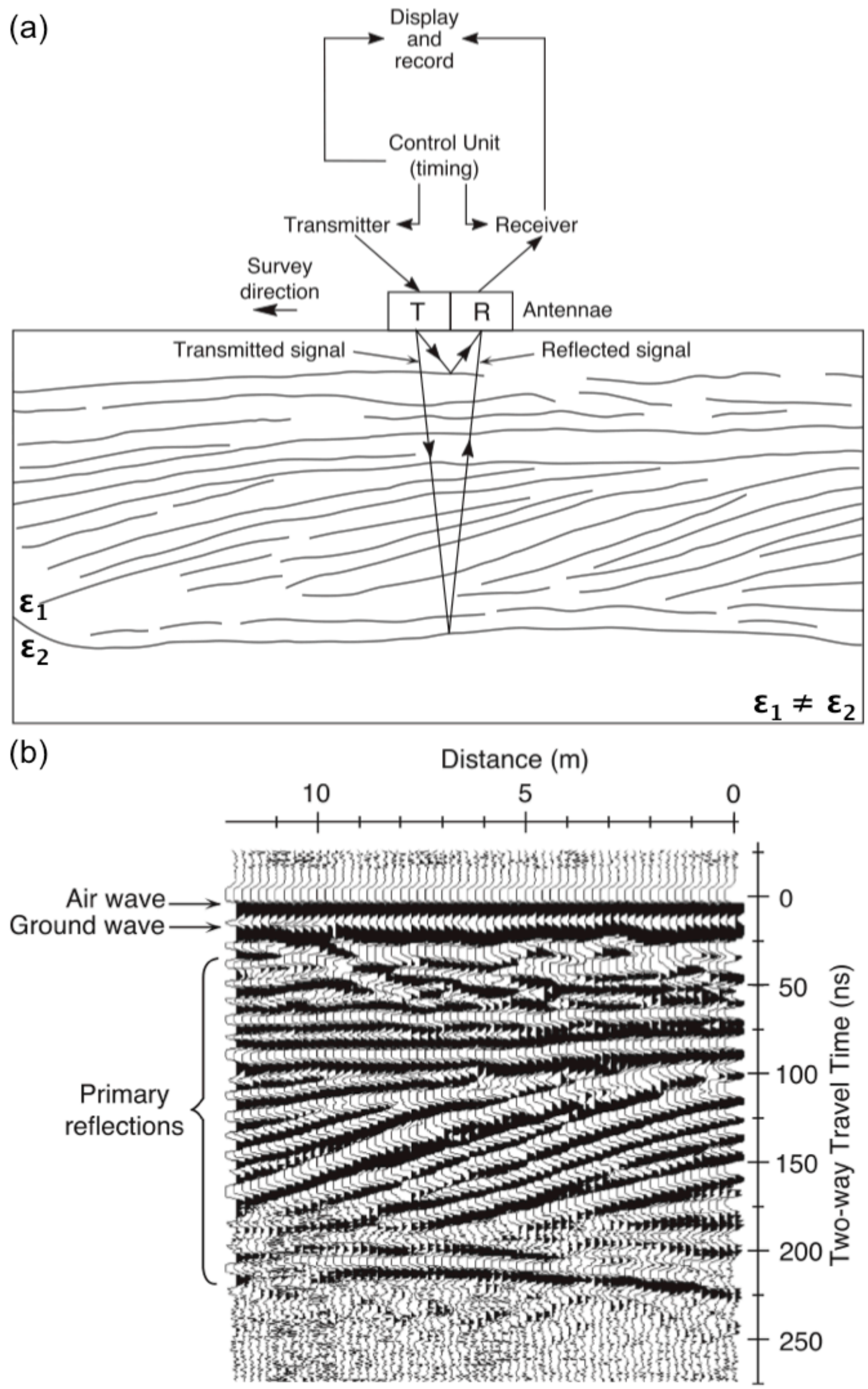

Figure 1.2: Principle of ground-penetrating radar (GPR) (Neal, 2004). (a) Transmitter sends a high frequency radar impulse into the subsurface that is reflected due to boundaries with differences in relative permittivity. The receiver antenna records the arrival of the reflected impulse and the two way travel time. (b) The direct waves are visible in this radargram (air and ground wave) and the primary reflections.

where c is the electromagnetic wave velocity in a vacuum, 3 x 10^8 ms^{-1}, and ε_r is the relative dielectric permittivity. This is a simplified equation in the presence of a low-loss material where the conductivity is negligible and the relative magnetic permeability is 1, as for most geologic materials. The wave velocity is therefore governed by the relative permittivity. The contrast in relative permittivity between the medium and buried matter cause reflections visible in the receiving unit that is attached to a video screen (Barton and Montagu, 2004). The contrast of relative permittivity determines the strength of the reflection and is measured by the reflection coefficient, R

$$R = \frac{\sqrt{\varepsilon_{r2}} - \sqrt{\varepsilon_{r1}}}{\sqrt{\varepsilon_{r2}} + \sqrt{\varepsilon_{r1}}} \qquad (4)$$

where σ and μ_r are negligible and ε_{r1} and ε_{r2} are the relative dielectric permittivity of the two mediums that are adjacent to one another (Neal, 2004). The electromagnetic wave velocity is equal to the product of the wavelength (λ) and the frequency (f) (Beres and Haeni, 1991). The reflected energy is sampled and amplified and converted into a waveform in a lower frequency wave (Butnor et al., 2001). Roots have a higher water content than the surrounding soil matrix therefore they provide a permittivity contrast that can be detected with GPR (Cui et al., 2010). The relative permittivity of unsaturated sand is 2.55 - 7.5 whereas the relative permittivity of fresh water is 80 (Neal, 2004). Recent studies using frequencies as high as 1.5 GHz have been able to detect roots as small as 0.5 cm (Butnor et al, 2001).

The displayed image, known as the radargram, shows the two-way travel time of the pulse passing through the surface, hitting an object and then returning to the surface.

This two-way travel time, in nanoseconds, is displayed on the vertical axis of the radargram, with the distance of the survey along the horizontal axis. Roots produce hyperbolic patterns and higher amplitudes of reflected waves in comparison to the surrounding matter that can be observed on the radargram. The hyperbolic pattern is created as the root is sensed, before and after the antenna is moved directly over the root (Zenone et al., 2008). The apex of a hyperbola represents the antenna passing over a root (Butnor et al., 2001). Post-processing can be done to reduce clutter in the data and minimize the effects of multiple hyperbolic functions (Butnor et al., 2003). When deciding upon a frequency to use it is important to note that there will be a tradeoff between penetration depth and resolution. A high frequency radar signal has high resolution but low penetration depth and vice versa. Under ideal conditions the resolution is equal to a quarter of the wavelength, but velocity uncertainties and waveform variations result in a resolution that is one-third to half of the wavelength (Benson, 1995; Beres and Haeni, 1991). Signal processing must be done to make the radargram into an image that can be better interpreted.

1.6.1.1 Advantages of Ground Penetrating Radar

The uncertainty in GPR can be eliminated by the presence of optimal conditions. Optimal soil conditions would be well-drained sand. Processing techniques also eliminate many of the limitations. For example, processing can eliminate clutter and the interference of objects in the ground other than roots (Butnor et al., 2003). Corrections for topography and tilt of the antenna over uneven terrain can also be corrected through processing of GPR data with digitized contour maps as outlined in Goodman et al. (2006) using GPR-SLICE software. The addition of horizontal and vertical bandpass filtering and migration in the processing routine may help discriminate closely spaced roots and improve imaging of the root structure in the field (Butnor et al., 2001). Uncertainty can be measured and eliminated by using other methods in conjunction with GPR, such as soil cores for fine root biomass. GPR is a good supplement and possible alternative to destructive methods, since it is fast, non-destructive and therefore repeatable and can be done over a large area (Butnor et al., 2003). The non-destructive nature of GPR can lead to exploring the spatial and temporal variability of belowground biomass. High frequencies together with smaller measurement intervals can provide resolution of a survey of less than 1 cm (Hruska et al., 1999). Although GPR primarily detects coarse roots, this is the bulk of belowground biomass. Fine roots are normally ignored because they are not easily distinguished from soil organic matter. In addition, even though high frequency antennas have limited penetration under optimal conditions, this is where the majority of roots reside. A 1.5 GHz antenna with penetration of up to 70 cm in optimal conditions would provide high-resolution surveys for the root zone. While the root zone is site-specific, dependent on water and nutrition availability, soil type, and species, an appropriate frequency can be chosen for the area under investigation. Unlike non-geophysical techniques, such as soil cores, GPR is capable of creating a 3-D structure of the roots belowground, in addition to quantifying belowground biomass.

1.6.1.2 Limitations and Uncertainties of Ground Penetrating Radar

GPR is a relatively new technique that is being used to a greater extent in root detection, however it has its limitations and restrictions. Soil properties impact GPR penetration greatly. This is due to spherical spreading and the conversion of electromagnetic energy to thermal energy causing attenuation losses. GPR works best in sandy soils with low water content because of the high conductivity of water and its effect on the attenuation of the electromagnetic wave. Clay also has a high conductivity resulting in a decrease in signal penetration. As the electromagnetic wave travels through the medium its amplitude (A) exponentially declines from its initial value (A_0) with depth (z), which varies with frequency. This is calculated by:

$$A = A_0^{-\alpha z} \tag{5}$$

where α is the attenuation constant (Neal, 2004). The attenuation constant for low-loss materials is frequency independent and can be calculated by:

$$\alpha = \frac{\sigma}{2}\sqrt{\mu/\varepsilon} \tag{6}$$

where σ is the conductivity and μ is the magnetic permeability (Neal, 2004). This equation clearly shows that conductivity has the greatest influence on the attenuation constant.

When choosing a frequency, a trade-off must be made between penetration depth and resolution. A high frequency will result in high resolution, but low penetration depth with the reverse trend for a low frequency. Therefore a frequency of 100 MHz, for example, can provide information down to depth of 30 m under optimal conditions, whereas a 2 GHz system would provide information up to 0.2 m in depth (Barton and Montagu, 2004). The highest resolution obtained using a 1.5 GHz frequency is greater than 5 mm roots, but only reaches a depth of 0.5 m (Hirano et al., 2009). Fine roots, less than 2 mm, cannot be detected using GPR (Stover et al., 2007). GPR is only capable of mapping roots in the horizontal plane, making it impossible to detect roots that are vertically oriented, such as taproots. If a root is not perfectly perpendicular to the profile then the classic hyperbolic anomaly shape may be lost and its true position will not be identified (Zenone et al., 2008). This can also cause clusters of roots to remain undistinguished, appearing as elongated and obscured (Butnor et al., 2001). Uneven terrain and litter can further complicate this issue. Removing understory and clearing the area before use can help eliminate this problem. In addition, it is hard to distinguish live roots from dead or decaying roots since dead roots can take on the properties of the soil overtime (Hirano et al., 2009). Dead roots also have less of a contrast in relative permittivity from the surrounding soil since its water content will decrease significantly, leading to an underestimation of carbon stock. Unexpected features within the soil can reduce the quality of the data by creating clutter leading to a misinterpretation of the data. However, post-collection processing can eliminate this (Butnor et al., 2003). Lastly, processing techniques may differ depending upon the site characteristic, radar system, software system used and objective. A GPR model should be carefully calibrated and validated according to species and local environmental conditions (XiHong et al., 2010).

1.6.2 Equipment and Software

A high frequency antenna of 1 GHz was used. A Noggin Plus 1 GHz smart handle profiling system was rented from Sensors and Software (Mississauga). Ideally a 1 GHz frequency would provide a resolution of 2.5 cm to a depth of about 1.5 m in dry sand. All surveys were completed with an OS5000 series accelerometer attached to the GPR unit. A program called GPR-Slice (version 7) was used for processing the radargrams. GPR-Slice v7 allowed for 3-D images to be created as well as a processing flow and model. OASIS was used alongside GPR-Slice in order to process and image the antenna tilt obtained from the accelerometer. A soil moisture probe was used to collect the soil moisture at a depth of 20 cm.

1.6.3 Calibration Pit

A 2 x 3 m trench was excavated in order to act as a calibration pit for the reference plot and determine the minimum root diameter that could be detected. The trench was excavated to a depth of 0.6 m and white pine roots were reburied at around 0.4 m. Roots were collected while digging, and fourteen roots were reburied. Each root was weighed, numbered and measured for diameter and length in the field. The roots were reburied at various orientations and with varying diameter (Figure 1.3a). The roots varied in diameter from 0.5 cm to 12 cm. Five roots with similar diameter were placed 4 cm, 5 cm, 10 cm and 20 cm apart. This would determine the minimum spacing detected by GPR before the roots were no longer individually detected. A root was also placed vertically to show the

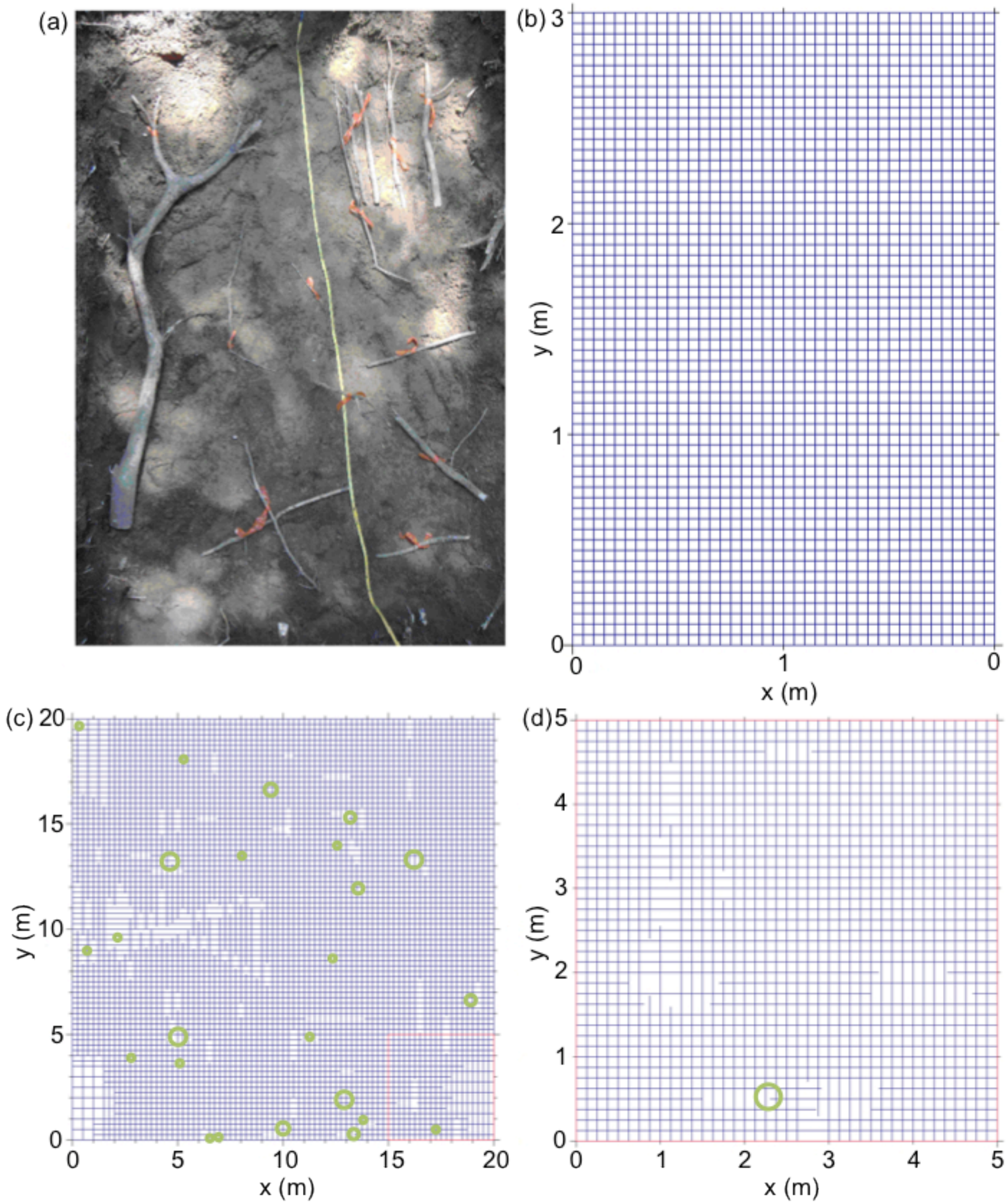

Figure 1.3: (a) Photo showing layout of roots. (b) GPR survey grid for 2 x 3 m calibration pit. (c) Survey grid for 20 x 20 m reference plot, with the inset outlined in red and tree represented as green open circles. (d) Survey grid for 5 x 5 m inset of reference plot, with trees represented as green open circles.

inability of GPR to detect roots that are perpendicular to the survey layout, since white pine trees have several main roots that extend horizontally and vertically.

A survey was performed before and after a 13.69 mm rainfall in order to determine the effect of soil moisture content. A 0.05 x 0.05 m grid was created on a plastic tarp to ensure that the survey was repeated in the same manner before and after rainfall (Figure 1.3b). The plastic tarp also provided a smooth surface that the GPR could be dragged along without any interference from the ground surface. The GPR system was pulled over the grid smoothly and slowly. The surveys were conducted with an inline sampling rate of 0.005 m. The soil moisture pre-rainfall was about 6 % at a depth of 20 cm compared to 11 % post-rainfall. The test pit was also used to help create a standard field procedure by determining the environment and survey size that is best.

1.6.4 Reference Plot

A 20 x 20 m reference plot was used to apply the GPR technique and compare biomass measurements with the allometric equation. A 0.25 x 0.25 m grid was created with string within the 20 x 20 m reference plot (Figure 1.3c). A smaller grid of 0.125 x 0.125 m was created in a 5 x 5 m area within the reference plot (Figure 1.3d). An inline sampling rate of 0.005 m was used for both surveys. Both surveys consisted of dragging the GPR system along the strings for consistency over top of the understory vegetation. When an obstacle was encountered, such as a log or tree, the line was stopped and continued past the obstacle. The GPR system was dragged slowly and carefully in order to minimize any tipping or bouncing of the system.

The DBH and coordinates of the trees within the reference plot were recorded as well as 5 m around the perimeter of the plot. There were 24 large (DBH > 9 cm) trees within the reference area. Small trees were ignored, as the allometric equation does not take them into account. There were 16 small trees in the 20 x 20 m reference plot. This data was used to calculate an allometrically derived biomass value that could be compared to the GPR value. A map of tree location with their corresponding biomass (kgC) value was created.

1.6.5 Radial Survey

Radial surveys were performed around a tree with a DBH of 11.8 cm. The survey began 50 cm away from the tree in a circular fashion, at an interval of 10 cm and inline sampling of 0.005 m. A rope marked every 10 cm was attached to the GPR unit and tied around the tree. This allowed the GPR unit to be moved around the tree and ensured that the survey grid was consistent. The rope was attached and reattached every 10 cm and the survey ceased once a large tree interfered.

1.6.6 Accelerometer

The accelerometer recorded the pitch, roll and yaw of the unit. This was done to correct for antenna tilt created from any offset of the GPR unit due to micro-topography. The roll, pitch and yaw are used to describe the rotation of the GPR unit around the x, y, and z axis respectively. This is discussed further in Chapter 2 of the thesis.

1.7 Subsurface Modeling and Data Processing

1.7.1 Gain Recovery and Background Removal

Gain recovery and the removal of DC drift were performed on all of the radargrams before further processing was done. This step was imperative in order to account for radar wave attenuation through spherical divergence. This step restores the signal amplitudes with increasing two-way travel times (Reynolds, 1997). Time zero adjustment was also performed to set the ground surface to zero on the vertical scale. Background removal was used to eliminate surface reflections, airwaves and ground waves. Objects on the surface of the ground being detected from reflected waves generate surface reflections. Air and ground waves are direct waves from the antenna to the receiver.

1.7.2 Bandpass Filtering

A high pass filter retains hyperbolic reflections and suppresses flat lying events, while low pass filtering has the opposite effect (Sensors and Software Inc, 1999). Therefore high pass filtering was applied to the radargrams, as dipping events identify roots. A bandpass filter of 761 – 2605 MHz was used. This would preserve the hyperbolic reflections generated from roots and eliminate stratigraphic events.

1.7.3 Stolt Migration

Migration collapses diffraction hyperbolas to their correct geometrical position (Reynolds, 1997). A point source, such as a root, generates a hyperbola that can be compressed back to a point using the correct velocity and aperture width. The aperture width is the number of traces that are chosen adjacent to the hyperbola (Reynolds, 1997). When the radar wave velocity is slow then the hyperbola is steep and a small number of traces are required. For a fast velocity and therefore wide and flattened hyperbolic curvature a large number of traces are chosen. A point is created at the apex of the hyperbola. A velocity of 0.11 m/ns was determined and a width of 501 was used.

1.7.4 Hilbert Transform

The last step of the processing flow was Hilbert transform, which calculates the envelope of the radargram pulse. Hilbert transform connects the positive amplitudes of the signal thereby creating more intact looking roots. This step is useful since we are interested in the areas with strong reflections and therefore high amplitudes.

1.7.5 Grid Parameters

The 2 x 3 m area was processed with three different gridding parameters. This was done to calibrate the reference survey along with its subset survey. The first grid was 0.05 x 0.05 m, the second 0.1 x 0.1 m and the last 0.25 x 0.25 m. With the known volume calculated from the roots before being buried, it was possible to determine the volume threshold for each interval spacing scenario. This volume threshold was then applied to the corresponding reference area. This ensured that we were not over-estimating or under-estimating root mass/volume. All of the surveys were processed with the same processing flow and each corresponding survey used the same grid parameters.

The volume of roots within the isometric volume was generated using GPR-Slice. GPR-Slice determines the volume of the root mass within the isometric volume. The isometric surface is created using the marching cubes algorithm. The surfaces displayed within the plot area are of equal amplitude in the 3-D volume (Goodman and Klein, 2012).

The antenna tilt was processed with GPR-Slice and OASIS. GPR-Slice calculated the vector of the antenna position using the roll, pitch and yaw angles recorded by the accelerometer. The radargrams with their vector position were displayed in GPR-Slice and exported to be gridded in OASIS. This was done for both the 2 x 3 m calibration pit and radial survey. In attempt to smooth the radial vector data, a time correction was applied to the accelerometer and global positioning system (GPS) data. The time correction involved the addition of milliseconds to the time stamp of the data sets. A 15-point box step filter was also applied to the accelerometer data. The box step filter smoothed the accelerometer data, reducing error brought about by the system.

1.8 Layout of Thesis

This thesis is presented as a “sandwich thesis” where Chapter 2 and Chapter 3 are formatted for submission to an academic journal. Chapter 2 focuses on methodology and vector guided radar imaging of roots using GPR. The effects of micro-topography are investigated with the use of radargrams and an accelerometer. 3-D images are created to compare the differences of root location with and without vector imaging applied. The study shows that vector guided radar imaging is necessary to obtain precise and accurate positions of roots. Chapter 3 is a test case that evaluates the effects of line spacing, soil moisture, root diameter, and root spacing on the detection of roots using GPR. We also attempt to estimate root biomass using total root volume estimated from isometric surfaces calculated on the Hilbert-transformed radargrams. We then compare the GPR estimates to the estimates from the site-specific allometric equation. With the generation of 3-D images, the study identifies that these variables all influence the outcome of the GPR survey, which in turn have an effect on the accuracy of the biomass estimate obtained.

CHAPTER 2: 3-D GROUND PENETRATING RADAR (GPR) IMAGING OF ROOT STRUCTURE IN A TEMPERATE PINE FOREST, TURKEY POINT, ONTARIO

Abstract

Tree root biomass is an important component of carbon storage in forest ecosystems. Ground-penetrating radar (GPR) has been employed successfully to map root systems and to estimate root diameter but previous studies have focused largely on interpretation of root structures in 2-D profiles. In this study, we evaluated 3-D imaging of root structure in a temperate pine forest in southern Ontario, Canada using high-resolution (1 GHz) GPR. High-resolution imaging was achieved using high sampling density (inline = 0.5 cm, inter-line spacing 5-10 cm) and post-survey correction of antenna tilt induced by surface micro-topography. Antenna motions were recorded with a MEMS (micro-electro-mechanical systems) accelerometer and used to calculate the antenna attitude (pitch, roll, yaw) and the transmit beam vector. Surveys were performed on a grid-wise basis across a 2 x 3 m test pit (5 cm spacing) and using a radial survey method (10 cm lines) to determine the most effective acquisition strategy. Radargrams were corrected for beam angle, migrated using Stolt (F-k) migration and interpolated to a quasi-3-D volume using an inverse distance algorithm. Root volumes were estimated from isosurfaces calculated on the Hilbert-transformed amplitudes using a marching cubes algorithm.

The results show that the forest floor micro-topography induced significant antenna tilt (pitch > 45°, roll > 28°) and yaw (up to 10°), leading to errors in the

positioning of root diffraction events in 2-D radargrams and 3-D radar volumes. The vector migrated GPR amplitudes showed a 15.5% increase and improved imaging of root structures due to focusing of diffraction energy. The radial scanning produced better root imaging and continuity due to the larger number of root crossings when compared to the rectilinear survey grid. Isosurfaces calculated on Hilbert-transformed amplitudes provide a rapid means of quantifying the root diameter and total biomass volume.

Keywords: Ground-penetrating radar, 3-D imaging, root structure, antenna tilt, accelerometer, vector corrections

2.1 Introduction

Tree roots account for a large proportion of the total biomass in forests (30-65%) and are an important terrestrial carbon sink comprising about 40% of belowground carbon (Dixon et al., 1994; Peichl and Arain, 2006; Goodale et al., 2012). Knowledge of carbon storage in root systems is critical to understanding carbon cycling in forest ecosystems and for predicting of CO_2 drawdown resulting from reforestation and afforestation programs (Arora and Montenegro, 2011). Root biomass is one of the least understood components of the terrestrial carbon cycle due to the difficulty in observing and measuring buried roots. Inventory of root biomass is conducted conventionally using destructive methods, including soil coring, test pitting, air spading (soil removal using air jets) and increasingly, using non-invasive geophysical methods (Hruska et al., 1999; Butnor et al., 2001, 2003). Geophysical methods have the advantage of being non-destructive and can be repeated, allowing assessment of spatial and temporal changes in root biomass.

A number of geophysical methods have been applied successfully in tree root detection and biomass estimation but electrical resistivity and ground-penetrating radar (GPR) have been used most widely (Zenone et al., 2008; Satriani et al., 2010; Leucci, 2011). Tree roots are commonly observed in GPR radargrams but in many studies they have been viewed as a source of noise rather than targets of interest. The first studies to evaluate GPR imaging of root structures were conducted by Hruska et al. (1999) and Butnor et al. (2001). Hruska et al. (1999) employed 450 MHz GPR (5-cm line spacing) to map oak roots (Quercus petracea) in a sandy loam and were able to image coarse roots >

3 cm diameter. Root networks were mapped in plan view by manual 2-D tracing of root diffractions identified in radargrams. Butnor et al. (2001) evaluated GPR mapping of roots across a broad range of soil conditions in southeastern USA. Using 1.5 GHz radar and 25 cm line spacing they were able to resolve roots as fine as 0.5 cm and estimate root diameter (0.5 to 6.5 cm) through analysis of radargram diffraction amplitudes. Butnor et al. (2001) concluded that GPR had great potential for biomass estimation in sandy resistive soils and advocated high-resolution imaging using small line spacings (< 5 cm). In several subsequent studies, statistically significant correlations between radar amplitudes, root diameter and root biomass were determined by experimental studies on natural and simulated root networks (Stokes et al., 2002; Butnor et al., 2003, 2005; Barton and Montagu, 2004; Stover et al., 2007; Dannoura et al., 2008; Hirano et al., 2009). Most studies employed the root diffraction amplitude or derived amplitude parameters (e.g. Butnor et al., 2003; Barton and Montagu, 2004) to develop empirical equations relating root diameter to GPR amplitude parameters.

While these studies demonstrate the great potential for GPR estimation of root biomass, several important limitations of GPR were identified: 1) GPR image quality and resolution is site specific and strongly controlled by soil conditions (moisture, clay content and soil texture); imaging is optimal in resistive, well-drained sandy soils and degraded in water-saturated and highly-conductive clay rich soils, 2) small roots (< 0.5 cm) and closely-spaced roots are difficult to image unless lines are collected at very high density (e.g. 2-5 cm) and with sufficient inline sampling so that diffraction hyperbolas are clearly recorded in radargrams, 3) soil heterogeneities (e.g. presence of clasts, soil layering, plant debris) can produce significant background noise and clutter in radargrams, making it difficult to distinguish root diffractions, 4) root diffraction characteristics vary with root moisture content and density, and are also a function of the antecedent conditions (e.g. rainfall or period of drought), 5) root volumes estimated from 2-D profiles may underestimate root biomass; accurate characterization of root structure and volume requires 3-dimensional (3-D) mapping of the entire root networks.

The limitations of 2-D GPR methods for imaging 3-D subsurface structures were recognized more than a decade ago for applications in geology, archaeology and civil engineering. These disciplines now routinely employ either fully 3-D or quasi-3-D rendering of GPR volumes (Grasmueck, 1996). Full 3-D imaging requires recording of reflections over a range of transmitter-receiver offsets (e.g. common mid-point data). Such data are typically acquired using multi-channel GPR systems and processed in a manner similar to 3-D seismic methods (Grasmueck, 1996). 3-D GPR volumes can be produced by interpolation of common-offset GPR 2-D profile data when they are acquired as a grid work of closely spaced profiles (Neale, 2004). GPR data volumes generated in this fashion are termed 'quasi-3-D' because they do not contain a wide range of reflection azimuths and offsets necessary for full 3-D imaging. To date, few studies have attempted quasi-3-D imaging of root networks. Wielopolski et al. (2002) generated quasi-3-D volumes of artificial roots in a 2-m^2 sandbox by interpolation of closely spaced 1.5 GHz radar profiles. Roots as small as 0.25 cm were rendered in 3-D as an isosurface (surface of constant amplitude) using a marching cubes algorithm (Lorenson and Cline, 1987). Zenone et al. (2008) used 3-D fence diagrams in combination with laser scanning of excavated roots to create a 3-D model of a root network. Roots imaged by the laser scanner corresponded closely with high amplitude diffractions in the radar profiles. Zenone et al. (2008) also evaluated the use of circular (radial) scanning around trees but were unable to produce 3-D volume models due to unavailability of software capable of displaying and analyzing circular scans. More recently, Yokota et al. (2011) produced a 3-D volume model of root structures using a rotary laser to improve the accuracy of radargram positioning.

A further requirement for high-resolution 3-D GPR imaging is correction for surface topographic effects. As shown in Figure 2.1, as a radar antenna is towed across uneven ground the antenna will be subject to tilting (pitch, roll) and rotational motions (yaw). These motions in turn cause the transmit beam to be deflected from the assumed vertical vector and can lead to potential errors in positioning of reflection and diffraction targets in radargrams (Figure 2.2). The magnitude of the sensor and beam axis motions will be a function of the surface roughness and also the bottom surface area of the GPR antenna. Tilt and yaw motions will be exaggerated for high-frequency (> 1 GHz) antennas, which have a relatively small surface area. Errors due to surface topographic effects have been well documented for GPR surveys acquired across rugged topography (Goodman et al., 2006a, 2006b; and Conyers and Leckebusch, 2010) but micro-topographic effects have not been considered, nor corrected for in root biometric surveys. The conventional approach for correction of surface topographic effects is to perform a trace-by-trace bulk shift (static correction) of the radargram traces (in either depth or two-way travel time) to account for the changes in sensor elevation along the profile. Other schemes apply

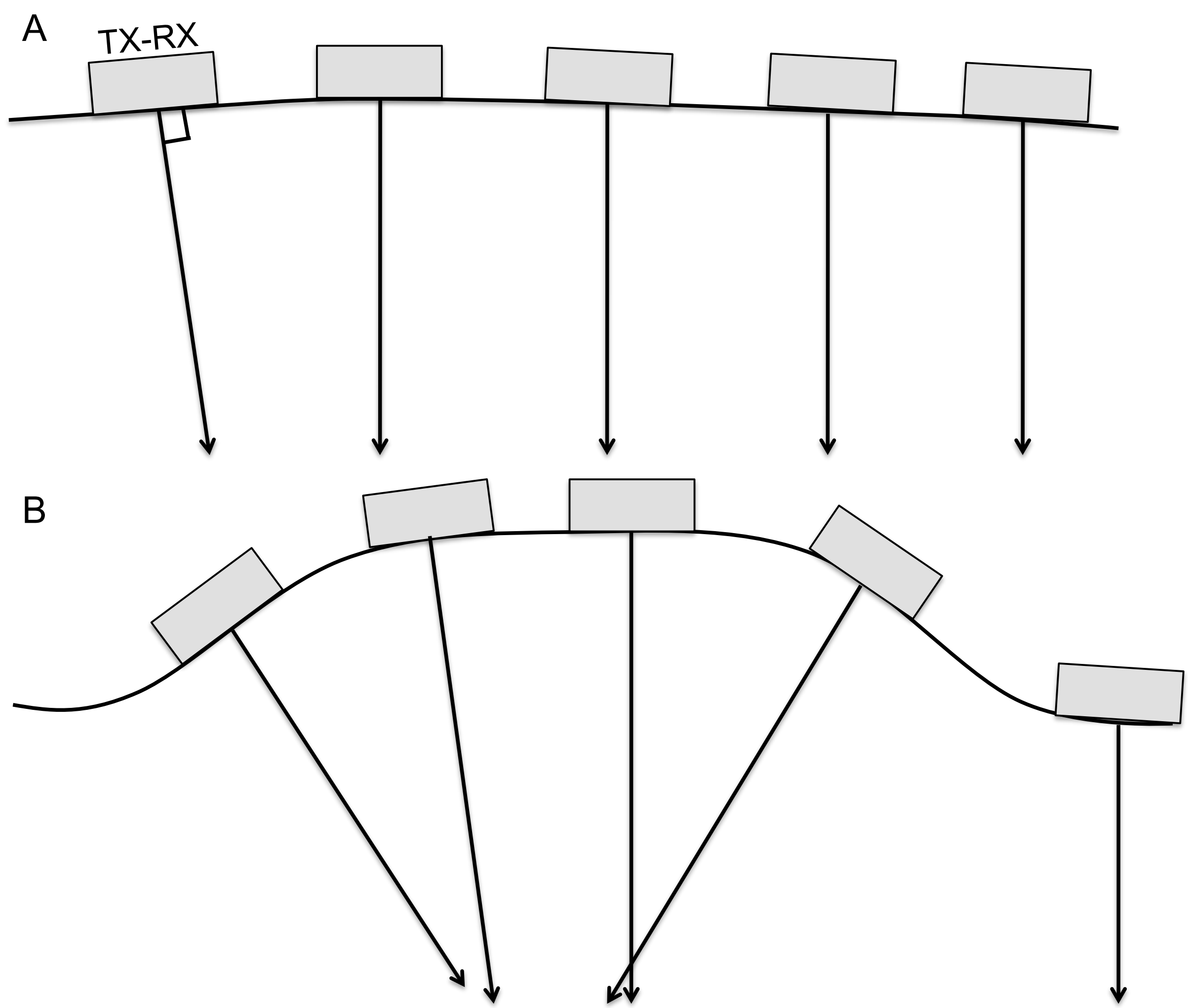

Figure 2.1: Topographic effects on GPR transmit beam. The beam angle (α) is vertical only for the case of a horizontal ground surface. A. Smooth topography. B. Uneven topography (modified from Goodman et al., 2006b).

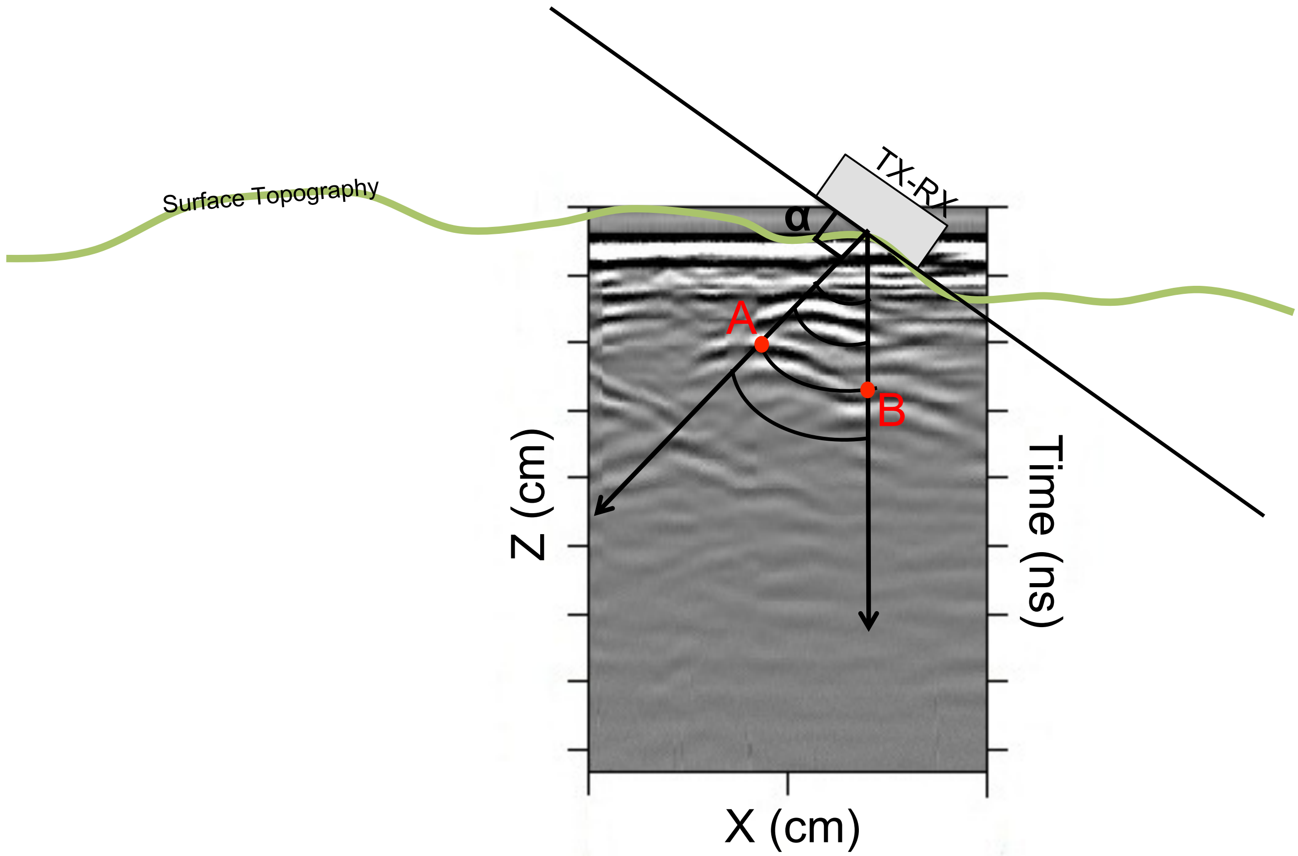

Figure 2.2: Micro-topographic effects on GPR beam angle. Antenna towed across uneven ground surface will be subject to tilt (pitch, roll) and rotational (yaw) motions. Motions are exaggerated when antenna length and width are small relative to wavelength of the ground surface undulations. Root detected at location A will be migrated in down-dip direction to B, resulting in mis-location of diffraction event in radargram.

corrections that estimate the tilt of the transmit beam axis using the vector normal to the surface topography and perform a simple migration of the GPR amplitudes to their correct locations (Goodman et al., 2006a). These schemes work well for correction of large topographic effects using digital elevation models but are not practical for correction of micro-topographic effects, unless high-density surface elevation measurements are available (e.g. from laser scanning). An alternate method for correcting topographic effects is to directly measure the antenna orientation using an accelerometer (Prokhorenko et al., 2012) but this method has not yet been evaluated as a 3-D GPR acquisition strategy.

In this paper, we report on the results of 3-D GPR imaging of root structures in a white pine (*Pinus strobus L.*) plantation in southern Ontario, Canada. The overall objective of the study was to assess the potential for non-invasive belowground biomass estimation using 3-D GPR. This work is part of an ongoing program of long-term carbon flux monitoring at the Turkey Point Flux Station (TPFS) (Arain and Restrepo, 2005; Piechl and Arain, 2006). High-resolution GPR data were acquired at the TPFS on two small test plots (6 and 17 m^2) with high survey line density (5-10 cm) to evaluate the resolving capabilities of a 1 GHz radar system. GPR data were acquired with a tilt meter fixed to the antenna to assess the effects of ground surface micro-topography on sensor motions and 3-D image quality. The results demonstrate that sensor tilt due to relatively minor ground micro-topography can degrade GPR image quality. A new approach is outlined for correction of the antenna tilt and rectification of radagrams using accelerometer data. The quasi-3-D volumes generated from the tilt-corrected radargrams allow enhanced mapping of root networks and estimation of root volumes from isometric surfaces. The approach demonstrated in this study can also be applied more broadly to enhanced 3-D imaging of subsurface structures in archaeology, civil engineering and earth sciences.

2.2 Study Site

The study site is a 73-year old white pine (*Pinus strobus L.*) plantation located near Turkey Point, Ontario, Canada. This site is part of the Turkey Point Flux Station (42^{o}71'N, 80^{o}35'W) that includes a chronosequence of four white pine plantations. The area experiences a temperate climate with a mean annual temperature of 7.8 ^{o}C and annual precipitation of 1010 mm (Peichl and Arain, 2007; Peichl et al., 2010). Approximately 438 mm of this precipitation falls in May to September.

The site is located on a lacustrine plain dominated by thick (up to 20 m) sandy surficial sediments with brunisolic grey brown luvisol soil type (Peichl and Arain, 2007). The soil texture ranges from very fine sandy sediments to fine sandy loam (Peichl and Arain, 2007; Peichl and Arain, 2006). The soil has a low to moderate water holding capacity and is well to perfectly drained (Peichl and Arain, 2006).

2.3 Field Methods

3-D GPR surveys were acquired using a Sensors and Software Noggin 1 GHz GPR system with DVL data monitor/controller. Due to the thick forest canopy at the site D-GPS positioning was impractical and survey positioning was obtained using the

Noggin odometer wheel and by visual reference to grid lines drawn on a polyethylene tarp. All profiles were collected with an inline sample spacing of 0.5 cm and 5 or 10 cm line spacings (Figure 2.3C and 2.3D). All radargram record lengths were set to 30 ns with a 0.1 ns sample interval (300 samples per trace).

The GPR antenna motions were recorded with a Server S-5000-US digital compass/tilt meter mounted on the top surface of the 1 GHz antenna. With this instrument yaw, pitch and roll were recorded at a 20 Hz update rate (0.05 s) and monitored on a tablet computer during the survey. The sensor employs a 3-axis anisotropic magneto-resistance sensor (AMS) and a 3-axis micro-electro-mechanical systems (MEMS) accelerometer to measure pitch and roll with accuracy of 1^{o} and yaw (azimuth) with accuracy of 0.5^{o} (RMS) (OceanServer Technology Inc., 2010). The orientation reference framework and conventions used for measurement of the instrument pitch, roll and yaw angles are shown in Figure 2.4.

2.3.1 Test Plot

A 2 x 3 m test plot was excavated to a depth of 60 cm and all tree roots removed. Fourteen roots were collected and their mass (g), length, and diameter were recorded in the field. The roots varied in diameter from 0.5 cm to 12 cm. The pit was backfilled with 20 cm of native sand and 14 roots were placed in the pit bottom at 40 cm depth (Figure 2.5). Plastic flagging marker tags were placed next to each root and the pit and roots were photographed from a height of 2 m. The pit was then backfilled with the native sand and the surface smoothed and leveled. The 3-D survey was acquired with 5 cm line spacing

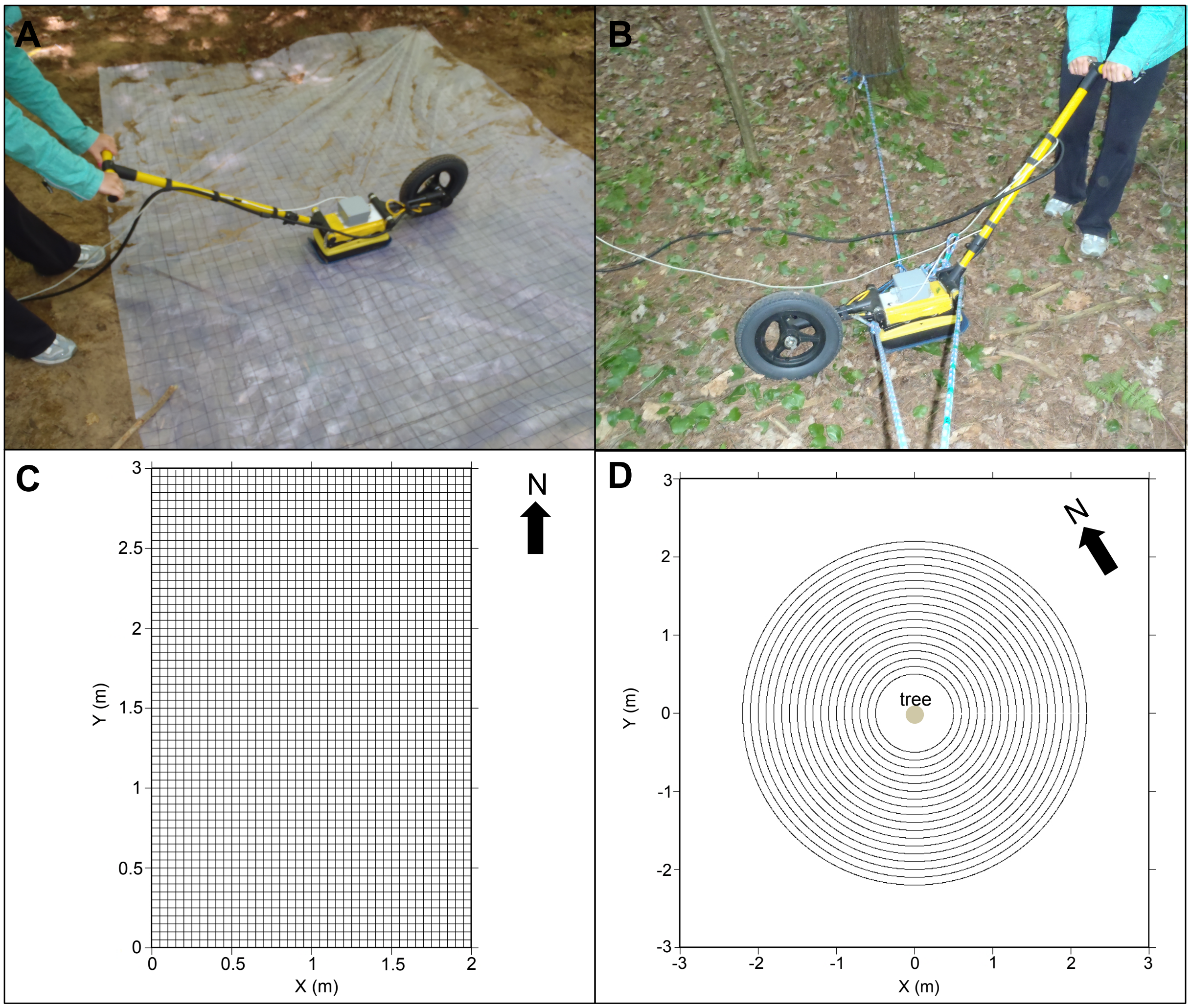

Figure 2.3: A. Collection rectilinear survey over 2 x 3 m test pit using 1 GHz Noggin shielded antenna with MEMS accelerometer mounted on top surface. Grid lines on plastic tarp at 5 cm intervals. B. Acquisition of radial survey around tree. Rope is used to keep antenna at constant radius from tree trunk. C. Survey grid for 2 x 3 m survey with location of buried roots shown. D. Radial survey grid location of tree with a base diameter of about 27 cm. Radial scan collected at 10-cm intervals.

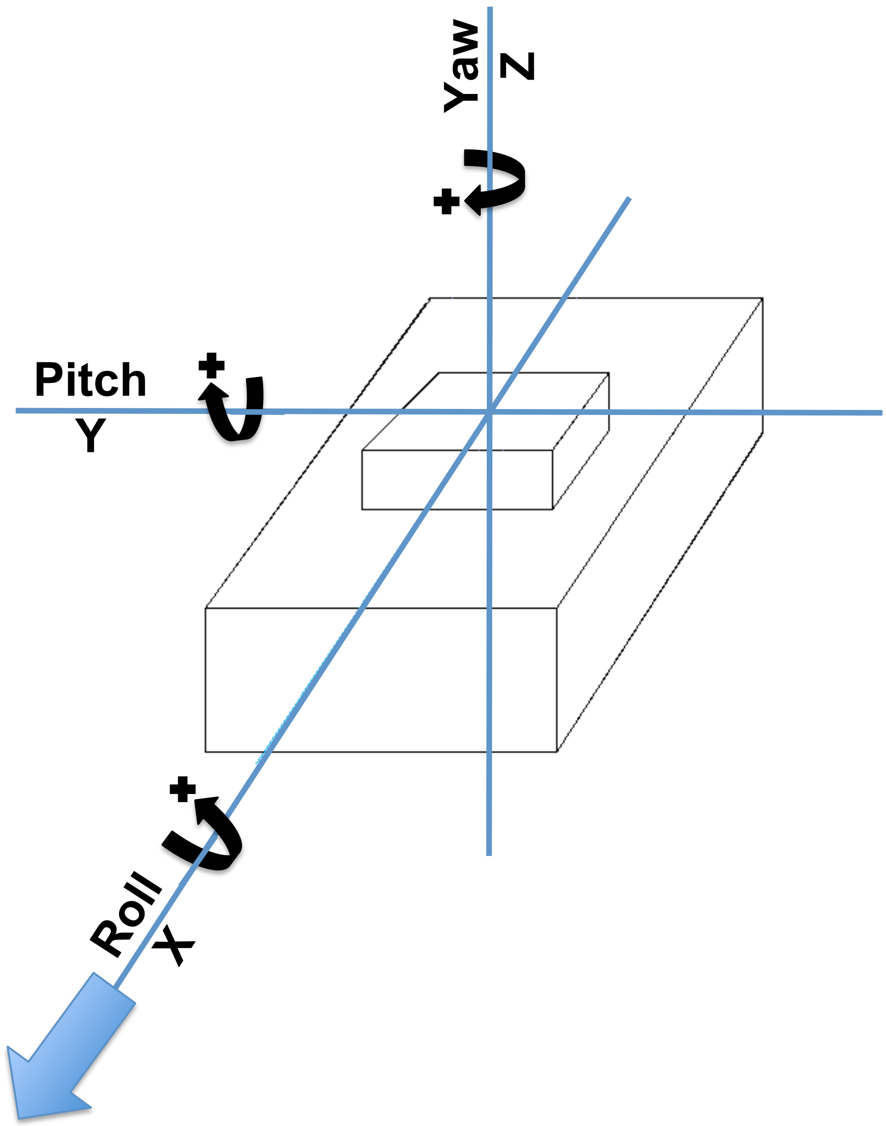

Figure 2.4: Reference framework for measurement of antenna orientation. Pitch is measured in inline (X) direction and roll in cross-line (Y) direction. The antenna rotation or yaw is measured relative to a vertical axis (Z).

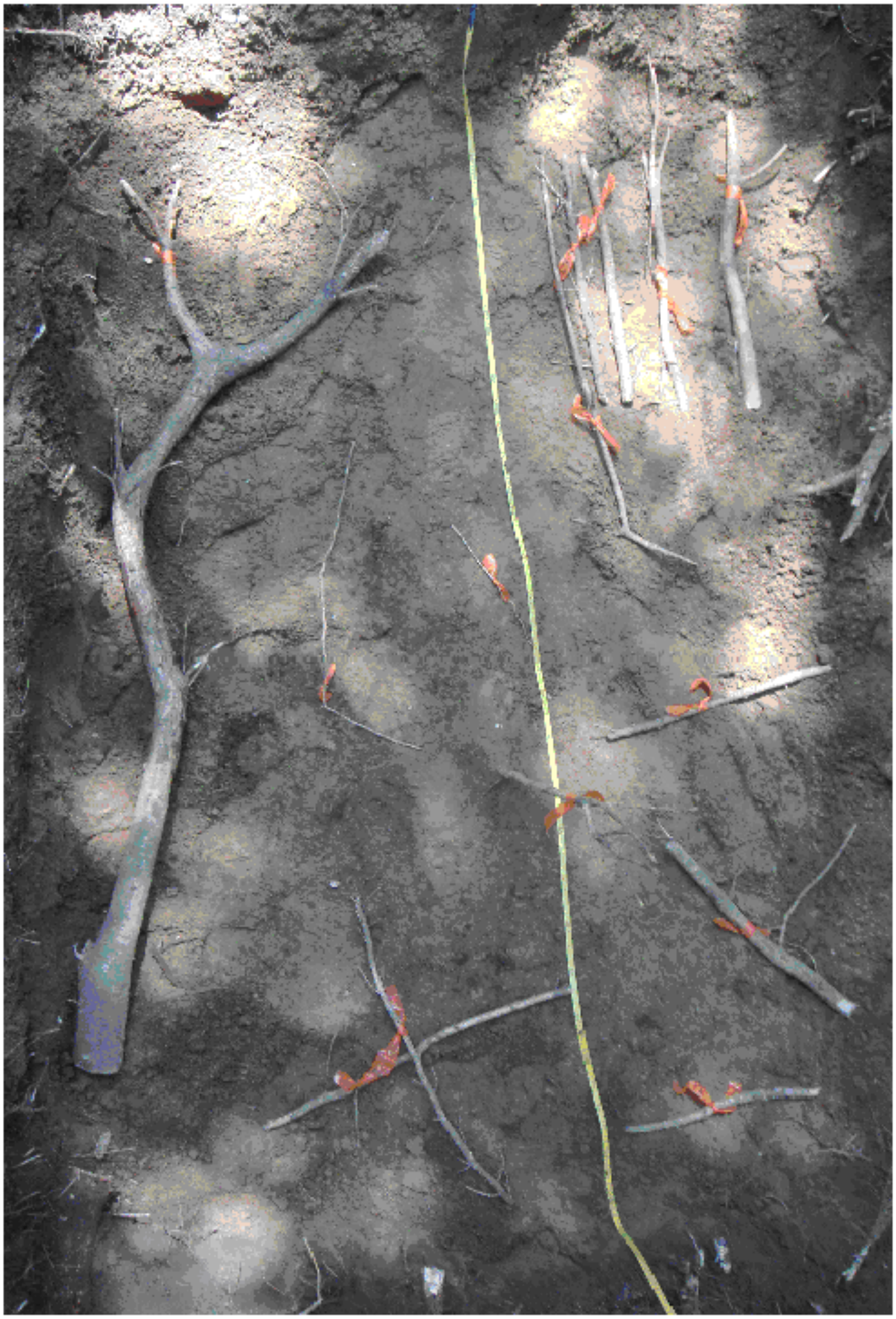

Figure 2.5: Photograph taken from above of root layout.

by towing the 1 GHz GPR antenna slowly across a rectilinear survey grid drawn on a plastic tarp (Figure 2.3A). A total of 102 profiles were collected with an inline sample spacing of 0.5 cm (401 or 601 scans per record).

2.3.2 Radial Surveys

A radial survey, employing circular scanning pattern (Figures 2.3B, 2.3D), was carried out over a 17 m^2 area around a single white pine with a DBH of 11.8 cm and basal diameter of 27 cm. Surveys began at a radius of 50 cm from the tree base and were incremented at 10 cm intervals to a maximum radius of 220 cm (Figure 2.3D). A rope, marked every 10 cm, was tied to the tree base and tethered to the GPR system to keep the antenna at a constant radius from the tree. A second rope was used to maintain an outward tension on the GPR antenna while the operator towed the instrument around the survey line. GPR soundings were collected at 0.5 cm intervals and the positioning determined using the survey wheel odometer (Figure 2.3D). Using this method and with careful towing the positional error was estimated to be $<\pm 2$ cm in the cross-line and <1 cm in the inline directions.

2.4 Data Processing

2.4.1 Accelerometer Data

The accelerometer data were smoothed using 15-point boxcar filter and time-synched to the nearest 0.05 s (20 Hz) with corresponding traces in GPR radargrams. The smoothed roll, pitch and yaw angles were converted to vector coordinates using the following relations:

$$
\begin{aligned}
V_1 &= \left[\sin(p) * \cos(r)\right] * \cos(y) - \left[\cos(p) * \cos(r)\right] * \sin(y) \\
V_2 &= \left[\sin(p) * \cos(r)\right] * \sin(y) - \left[\cos(p) * \cos(r)\right] * \cos(y) \\
V_3 &= \sin(r)
\end{aligned}
\tag{1}
$$

where V_1, V_2, V_3 are the vector components and *p*, *r*, and *y* are the pitch, roll and yaw angles in radians. The vector coordinates were then imported to GPR-SLICE™ software and used to re-project the beam axis. Figure 2.6 shows two examples of the vector-corrected radargrams displayed in 3-D space.

2.4.2 GPR Data

GPR profiles were processed to quasi-3-D volumes in GPR-SLICE™ v.7.1 software (Goodman, 2012). GPR-SLICE ™ was designed specifically for 3-D imaging of GPR data and includes options for vector navigation and correction of beam angles using tilt meter data. The radar processing flow is summarized in Figure 2.7. The initial processing steps included application of linear gain function, background removal, and band-pass filtering (761-2605 MHz) to suppress low frequency reverberations and horizontal reflection events produced by soil stratigraphy. A velocity versus depth function was then determined by curve fitting of root diffraction hyperbolas. An average radar wave velocity of 0.11 m/ns was used to migrate the data using Stolt (frequency-wavenumber) migration. Migration is a critical step for root imaging as it collapses the diffraction hyperbolas to high amplitude foci that are centered over roots. As a final

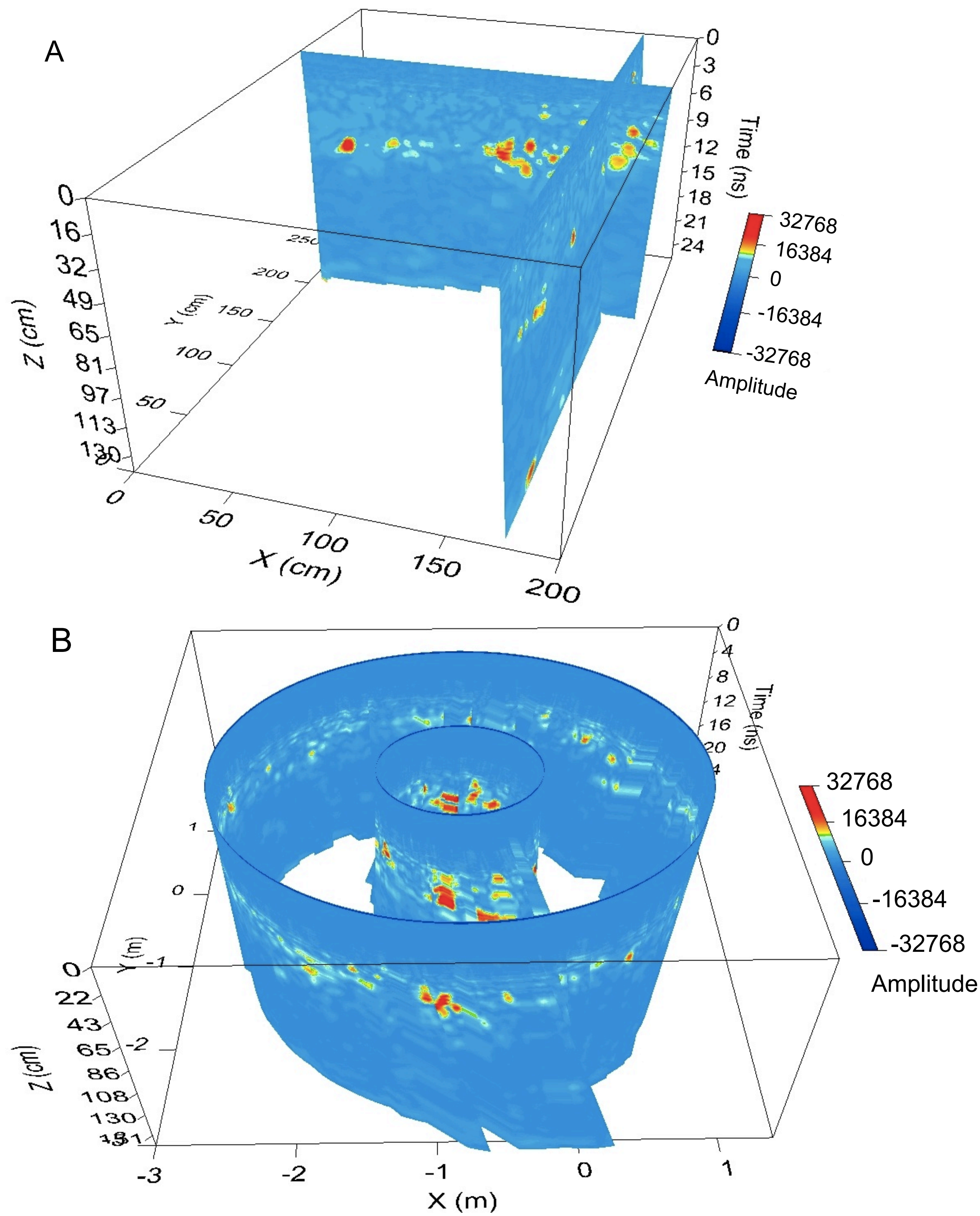

Figure 2.6: Depth-converted radargrams with correction for beam vector corrections applied (2 x 3 m lines 43, 96) B. Tilt corrected radial scans (lines 4, 16). Radargrams show Hilbert-transformed amplitudes. Roots indicated by zones of high amplitude.

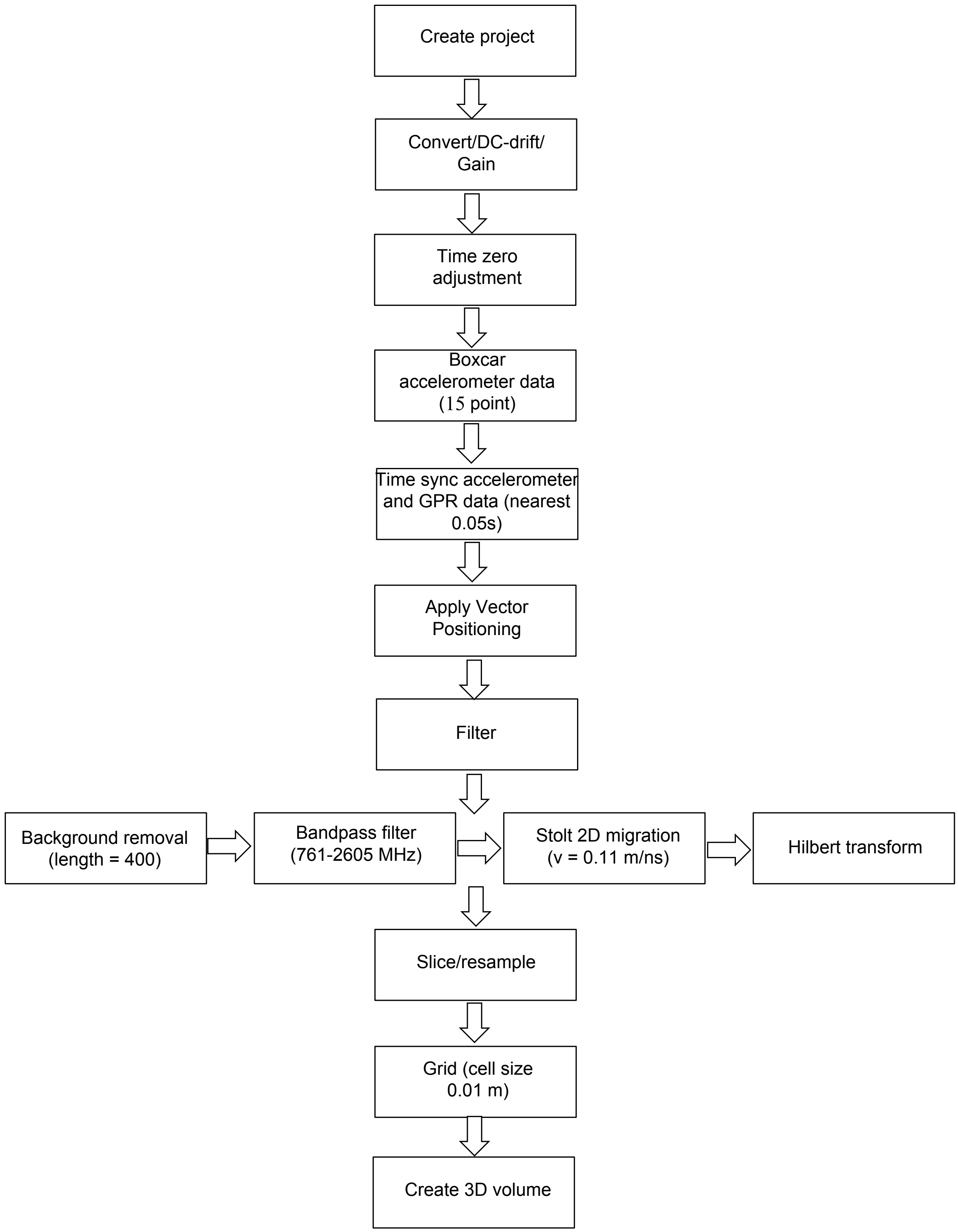

Figure 2.7: Schematic diagram showing processing flow.

filtering step, a Hilbert transform was applied to radargrams to produce a rectified signal envelope. This step results in a significant enhancement of diffracted energy in the radargrams and simplifies interpretation of root structures, particularly when root diffractions are closely spaced and overlapping (Doolittle and Butnor, 2009).

The processed radargrams were corrected for topographic effects and instrument tilt using the calculated transmit beam vectors in GPR-SLICE™ (Figure 2.6). Both the tilt-corrected and uncorrected amplitude data were exported as an ascii flat file (x,y,z, amplitude) to Geosoft Oasis™ and gridded using a 3-D inverse distance algorithm (1 cm grid cells, 5 cm search radius). The resulting quasi-3-D GPR volumes were then depth-sliced at various horizons for visualization of root structures and for comparison of the tilt-corrected GPR with the uncorrected data. Several difference grids were calculated for the 2 x 3 m and radial depth slices to determine the amplitude change resulting from the tilt correction.

2.5 Results

2.5.1 Instrument Motions

The tilt meter data show that the GPR antenna was subject to considerable tilting motion as it was towed across the survey areas (Figures 2.8, 2.9, 2.10). As shown in Figure 2.8, the pitch and roll varied rapidly along the lines with amplitudes of about 2-10°. The variability in the yaw angles (azimuth) was small by comparison (Figure 2.8) and resulted from small changes in the tow direction. The yaw data for the radial survey show a constantly changing heading due to the circular line paths (Figure 2.8B). In

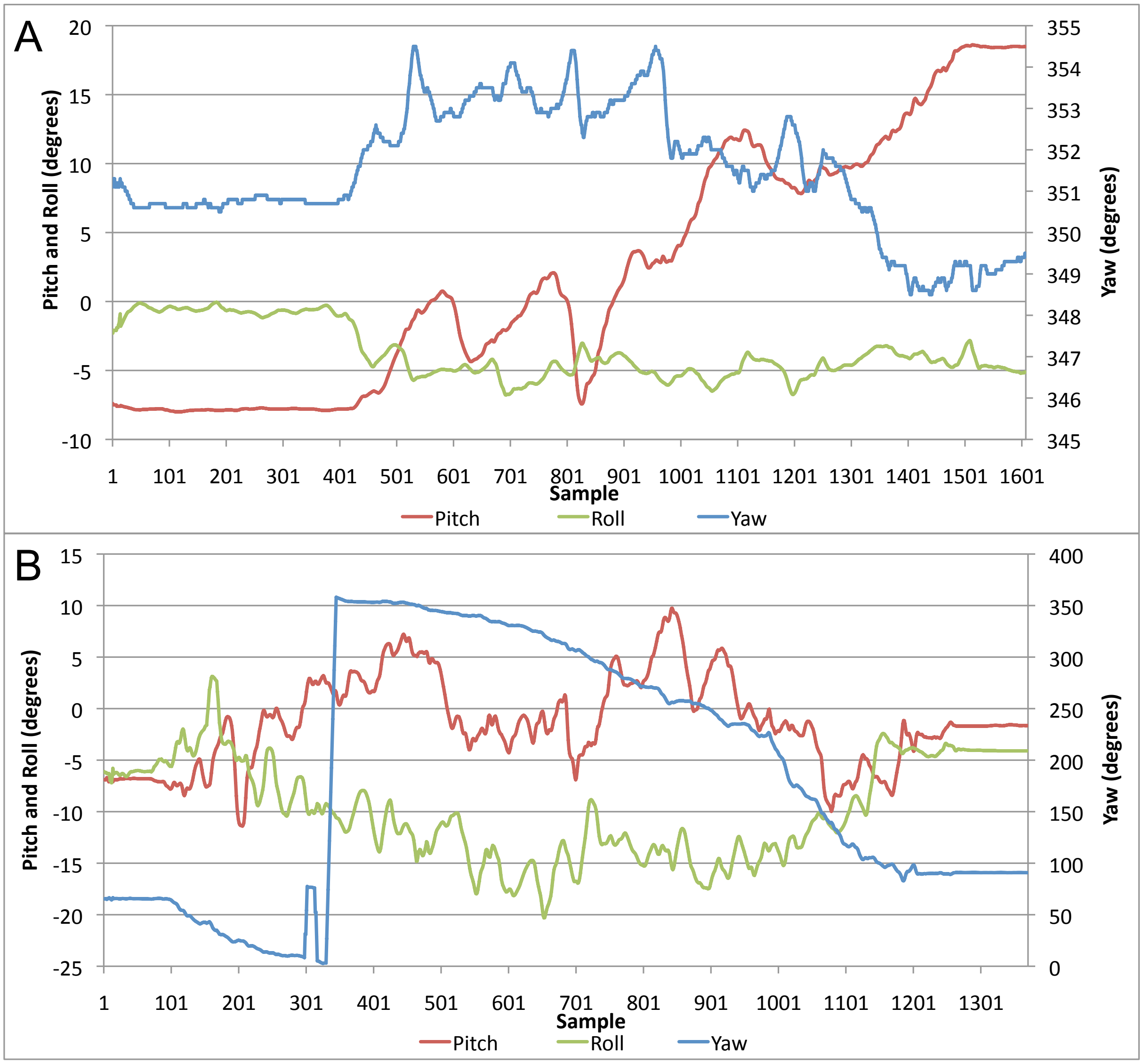

Figure 2.8: Plots showing pitch, roll and yaw data recorded using MEMS tilt sensor. Data were smoothed using a 15-point boxcar filter. A. 2 x 3 m survey line 4. B. Radial survey line 10.

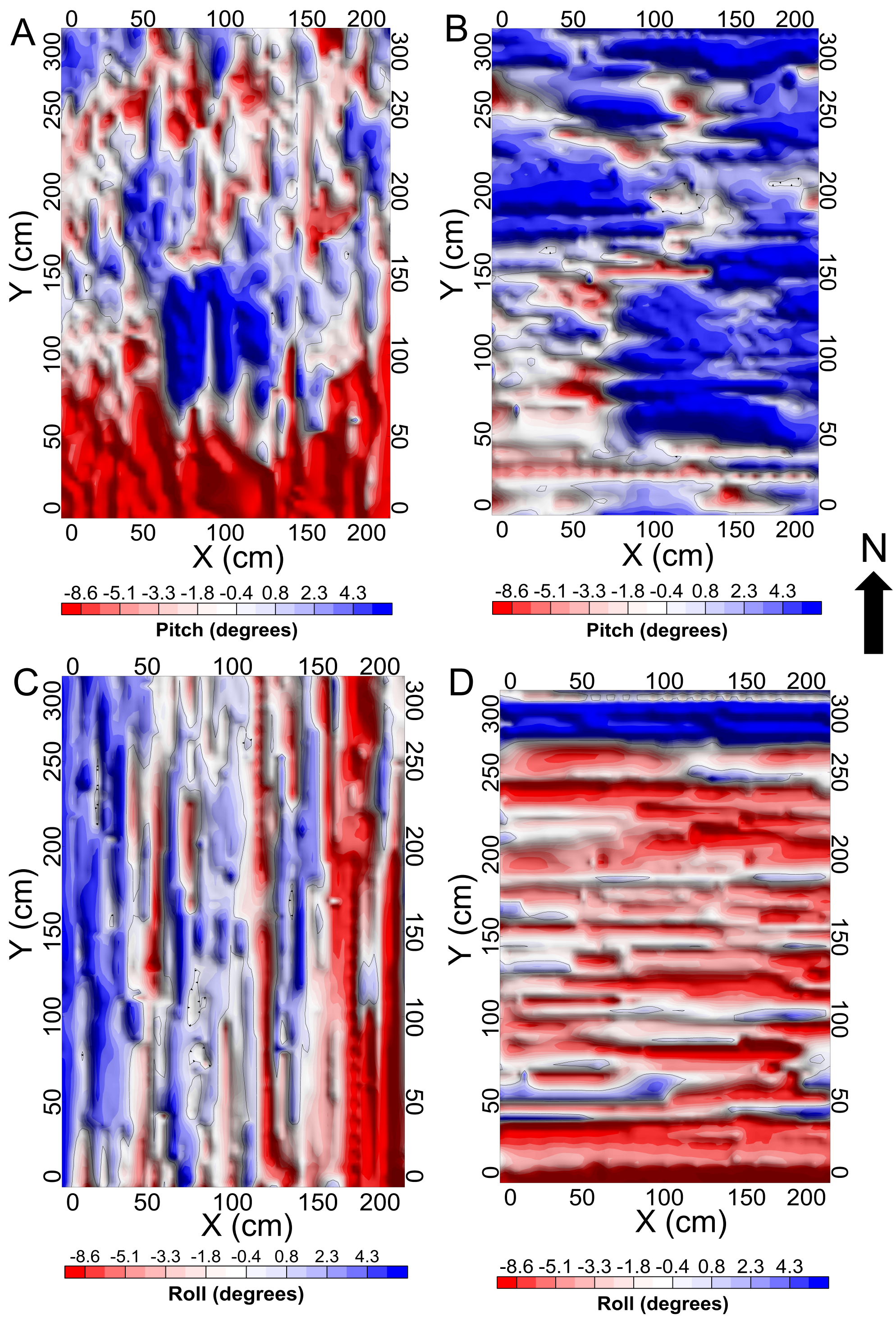

Figure 2.9: Maps showing interpolated pitch and roll values for 2 x 3 m survey. A. Pitch N-S lines. B. Pitch from W-E lines. C. Roll from N-S lines. D. Roll W-E lines. Contour line indicates 0 degrees pitch/roll.

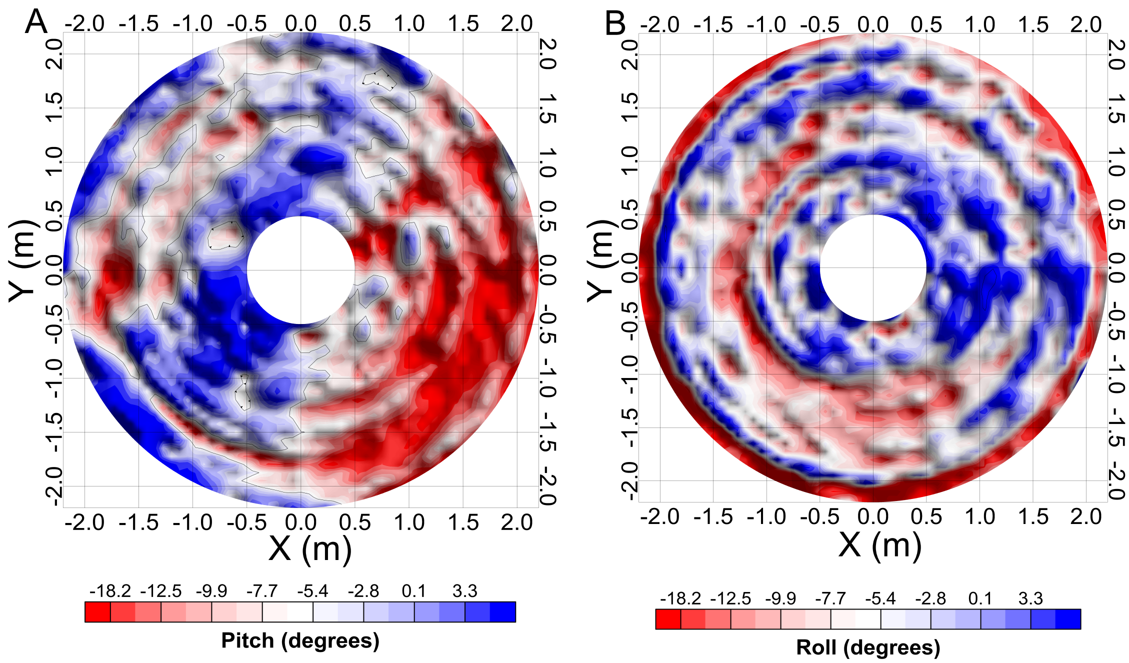

Figure 2.10: Maps showing interpolated pitch (A) and roll (B) values for radial survey. Contour line indicates 0 degrees pitch/roll.

addition, the yaw data for the radial survey is not a sign wave, as the radial distance changed slightly at times due to the difficulty in maneuvering the GPR unit around the tree. The changes in instrument tilt are best visualized in Figures 2.9 and 2.10, which show the interpolated pitch and roll data for the two survey areas. The maximum pitch in the N-S direction was 37 ° (Figure 2.9A) whereas the maximum W-E pitch angle was 19° (Figure 2.9B). The maximum roll angles were 18° in the N-S (Figure 2.9C) and 24° in the W-E direction (Figure 2.9D). The radial survey had larger maximum pitch angles (up to 45°) (Figure 2.10A) and a maximum roll angle of 28° (Figure 2.10B).

The relatively large magnitude of the instrument tilt (Figures 2.9, 2.10) was unexpected, as the survey areas were relatively smooth with a maximum of 10-15 cm in surface relief. The tilt meter data show clearly that the microtopography produced by small ground surface undulations, exposed roots and other minor asperities (e.g. boulders) can produce considerable instrument motions.

The changes in amplitude due to tilt corrections are shown in the depth slices in Figures 2.11 and 2.12. The test plot volume was sliced at a depth of 43 cm, as this is where the roots were best displayed. Figure 2.11A shows the depth slice without tilt corrections and Figure 2.11B the tilt-corrected image. The amplitude difference (Figure 2.11C) clearly shows an increase in the Hilbert amplitude in the root regions (maximum difference of 1526) due to enhanced focusing of the diffraction energy. The maximum increase in amplitude, as shown in Figure 2.11D, was 3.6%. The same procedure was applied to the radial survey data (Figure 2.12) for a depth slice at 26 cm. The difference

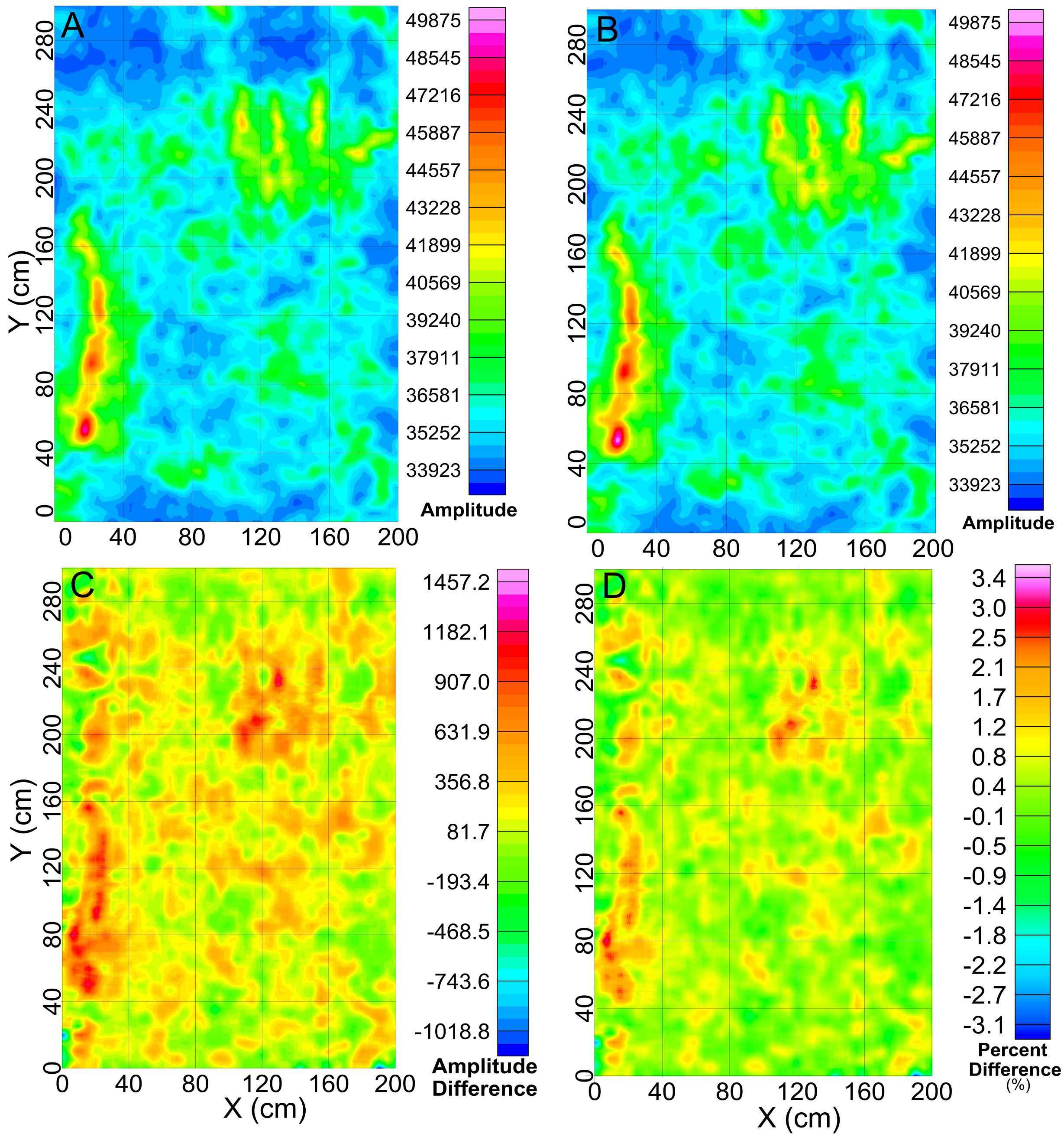

Figure 2.11: Interpolated depth slices (Hilbert-transformed amplitudes) for 2 x 3 m test plot at 43 cm. A. No vector beam corrections applied. B. With vector corrections applied. C. Amplitude difference (C = grid A - grid B). D. Percent amplitude difference (D = grid C/grid B).

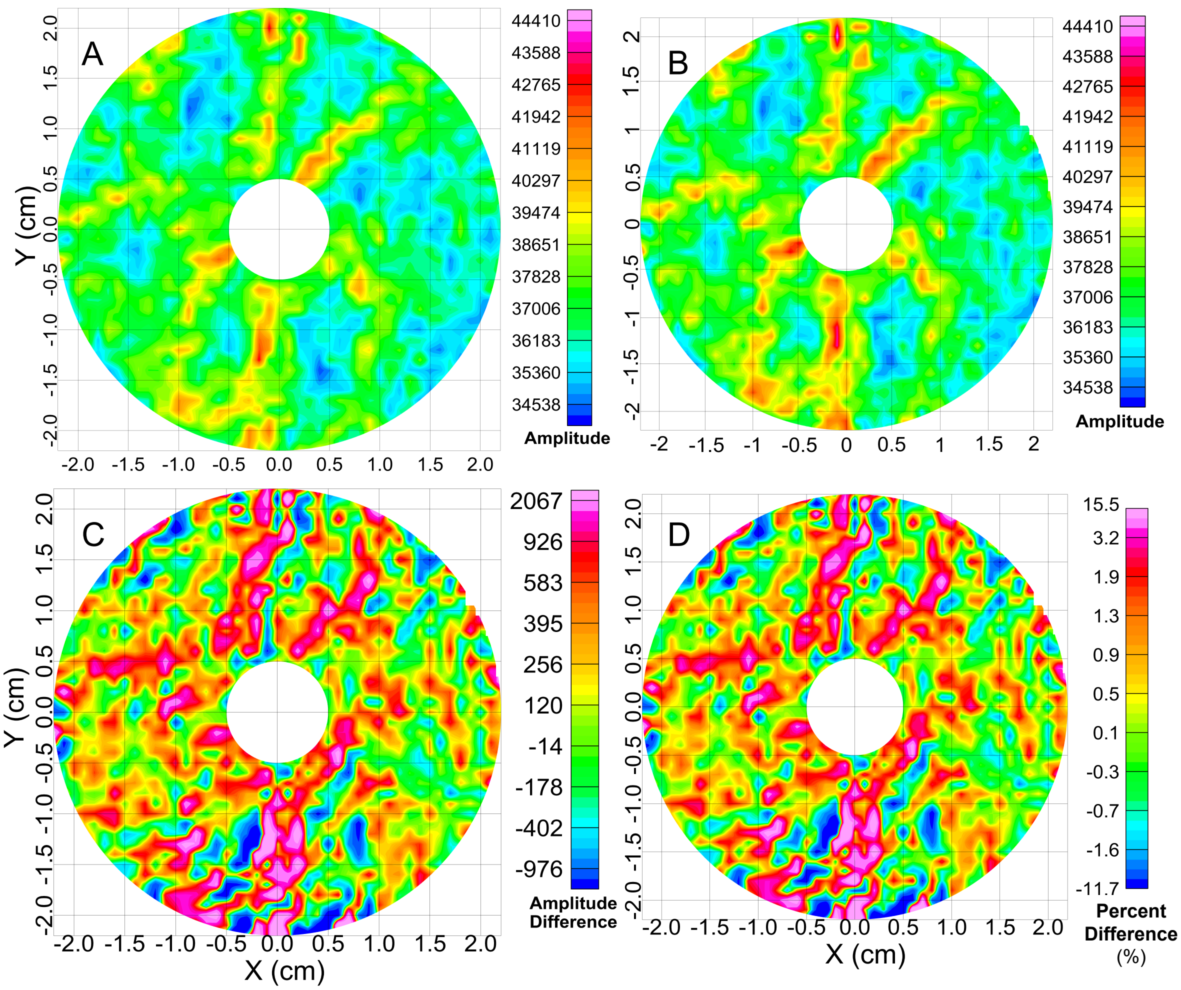

Figure 2.12: Interpolated depth slices (Hilbert-transformed amplitudes) for radial survey at 26 cm depth. Coarse root structures indicated by radiating patterns of high amplitudes. A. No vector beam corrections applied. B. With vector corrections applied. C. Amplitude difference (C = grid A - grid B). D. Percent amplitude difference (D = grid C/grid B).

grids (Figure 2.12C, D) show an increase in amplitude of up to 15.5 % due to tilt correction of the beam angle. In both cases, the tilt-corrections enhanced and localized the high amplitude areas. This was the expected result and can be attributed to the migration of the diffraction energy to its correct location in the subsurface. Because of the limited topographic variation at the test site (< 15 cm relief) the corrections produced a small but measureable increase in the image coherency. In areas with more rugged surface relief (e.g. forest floor with roots and deadfall) it is anticipated that the tilt corrections would contribute to much enhanced GPR 3-D imaging.

2.5.2 Quasi-3-D GPR

2.5.2.1 Test Plot

The fully corrected quasi-3-D GPR volume for the 2 x 3 m test plot is shown in Figure 2.13. The high amplitude areas, denoted by hot colours, indicate diffractions from coarse roots. Within the test plot, 8 of the 14 roots were identified at a depth of 43-49 cm. The high amplitude area at the top right of the volume (Figure 2.13A) is representative of 5 roots that were buried with varied spacing of 4 cm, 5 cm, 10 cm, and 20 cm and with diameter varying from 1.1 cm to 3.9 cm (Figure 2.5). The roots spaced 10 cm and 20 cm apart are identifiable. The three identifiable roots are better distinguished in Figure 2.11A and 2.11B. The smallest root that could be detected was 1.4 cm.

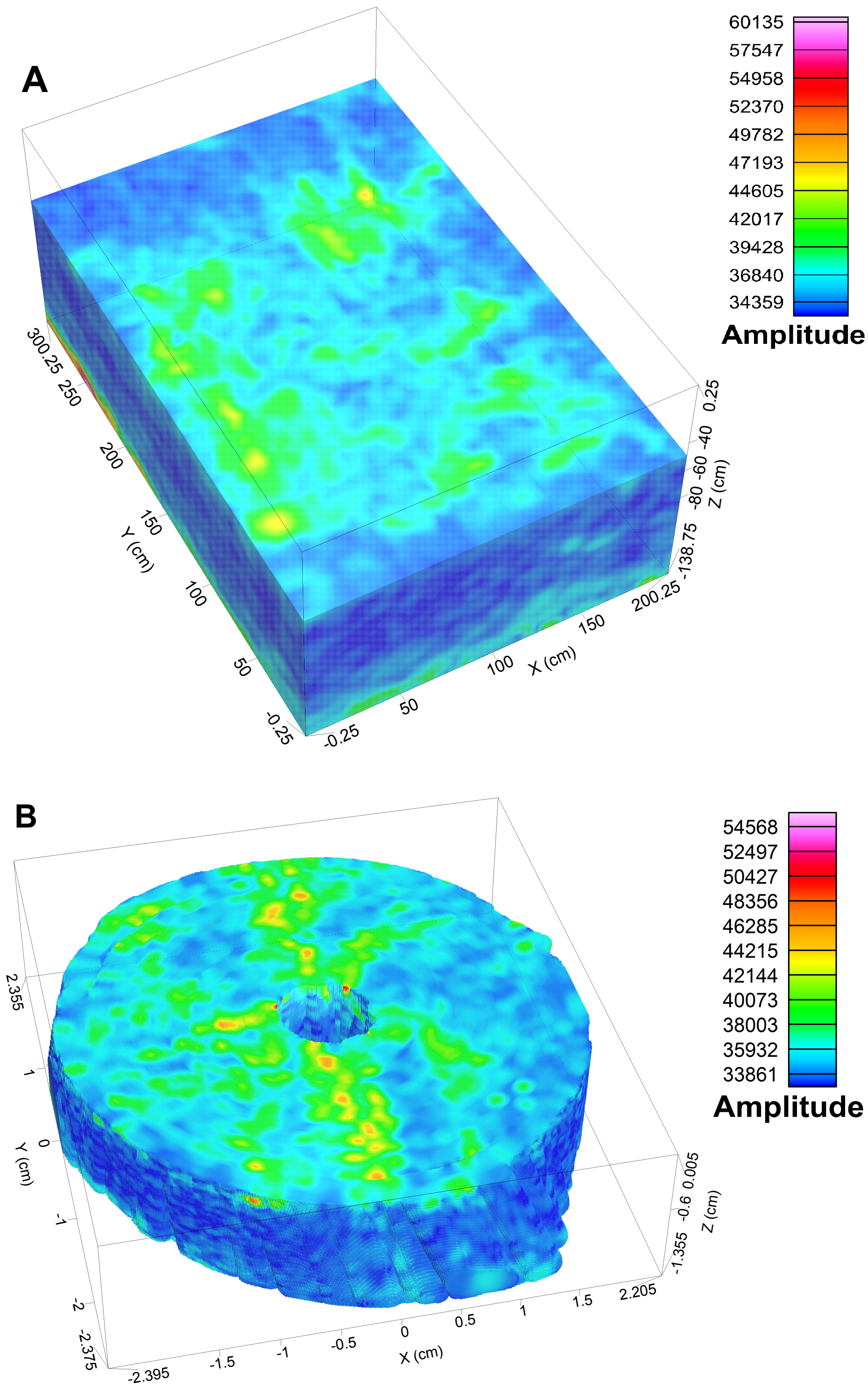

Figure 2.13: Quasi-3-D GPR volumes with tilt corrections applied. A. 2 x 3 m cut at depth of 49 cm. B. Radial survey cut at depth of 35 cm.

2.5.2.2 Radial Survey

Several roots are identified that radiate outward from the tree in the radial survey in Figure 2.13B at a depth of 35 cm as well as in the depth slice shown in Figure 2.12B. The effect of the tilt corrections can be seen in Figure 2.13B, as the volume is not perfectly circular. The radargrams are wavy thereby providing a more precise and accurate root location. The root distribution and density can be seen in Figure 2.13 of both the 2 x 3 m and radial plots.

2.6 Discussion

Mapping pitch and roll over the survey areas (Figure 2.9 and 2.10) shows that even with a relatively smooth topography, there are still micro-topographic effects that arise due to the small size of the high frequency GPR antenna. The tilt-corrected GPR volume allowed enhanced imaging and more precise positioning of roots. Figures 2.11 to 2.12 visualized the effects of micro-topography showing that there was an offset from the tilt of the antenna. The vector data enhanced and localized the high amplitude signal. Figures 2.11D, and 2.12D show that the vector data centralized the root position from the higher amplitude areas.

Zenone et al. (2008) state two issues when performing radial surveys: difficulty in sliding the GPR antenna around the tree due to ground roughness, and software capable of creating 3-D models from the dense circular scans. Our work has managed to overcome these obstacles with the use of an accelerometer. Our method proved to be successful and 3-D models were created using GPR-SLICE™ and Geosoft Oasis™. The

3-D images allowed mapping of the layout of the coarse root network. White pine trees are known to have several main roots that radiate out from the tree. In agreement, several roots were detected from the high amplitude areas radiating horizontally from the base of the tree. The radial survey detected the roots clearly since the GPR antenna runs perpendicular to the root, which is the best survey scenario.

Future work includes the creation of a mound/hill to exaggerate topographic effects with known objects placed underground to which surveys will be completed where micro-topographic and topographic corrections will be applied. Laser scanning could be completed for improved accuracy of the radargram position, with up to millimeter precision. Further improvements could be applied to the algorithm of the calculation for antenna tilt as well as to the correction of the time stamp for the GPS and accelerometer data. There will also be further investigation into the use of other geophysical methods to be used alongside GPR, including multi-channel and multi-frequency GPR. Electrical resistivity tomography (Zenone et al., 2008 and Rossi et al., 2010), borehole GPR and X-ray computed tomography (Heeraman et al., 1997) will also be further experimented. These methods have the potential to improve 3-D imaging of root structure.

Our work has the ability to enhance 3-D root imaging and introduces a necessary step in the GPR survey method for detecting roots. With the detection of root structure being more precise, better models for estimating root diameter can be created. Accurate estimates of root biomass can also be made from the precise locations of roots. Determining root structure and biomass estimates can also add to the expanding work being done to allocate carbon stock within forests. The 3-D root imaging can be applied to an urban setting to detect roots that are interfering with buried infrastructure and associate roots with the tree responsible.

2.7 Summary

The study has demonstrated that with the use of an accelerometer, antenna tilt can be calculated and micro-topographic corrections can be made. Experiments related to mapping tree roots should include an accelerometer for micro-topographic corrections especially when GPS is not available, such as in a forested area due to signal blocking from the canopy. Mapping tree roots also requires the use of high frequency antennas, which are small in size and need to be moved freely throughout the area. Therefore micro-topography becomes an issue that can be eliminated when accounting for antenna tilt. This results in more accurate and precise 3-D vector images of root structure/distribution and location.

2.8 Acknowledgements

This work was supported through Natural Sciences and Engineering Research Council of Canada grants to Boyce and Arain. Project funding was also provided by grants to Ontario Ministry of Environment (MOE), Canadian Foundation of Innovation (CFI), Ontario Innovation Trust (OIT) and the Ontario Ministry of Natural Resources (OMNR) to Arain. We thank Emily Nicholas, Suo Huang, Bin Chen, Robin Thorne and Steve Williams (OMNR) for field assistance. We are very grateful to Dean Goodman (Geophysical Archaeometry Laboratory) for his expert technical advice and for software modifications to GPR-SLICE™ for handling of vector radargrams.

CHAPTER 3: QUANTITATIVE, NON-DESTRUCTIVE ESTIMATES OF COARSE ROOT BIOMASS IN A TEMPERATE PINE FOREST USING 3-D GROUND-PENETRATING RADAR (GPR)

Abstract

Coarse root (> 5 mm) biomass is an important component of carbon storage in forest ecosystems. In this study, we evaluated non-invasive estimation of root biomass using high-resolution 1 GHz ground-penetrating radar (GPR) and compared the results with allometric biomass measurements from a temperate white pine forest in southern Ontario, Canada. 3-D GPR surveys were acquired across three test plots (6, 25 and 400 m^2) with varying line spacing (5-25 cm line spacing) to map coarse root distribution and to determine the resolution constraints imposed by line density. Empirical relations between GPR amplitude, root diameter and soil moisture content were investigated in a controlled test plot (6 m^2). The total root volume was estimated using isometric surfaces calculated on the interpolated 3-D radar volume using a marching cubes algorithm.

Root biomass values estimated by GPR, 22.6 kgC, were comparable to allometric estimates, 12.3 kgC, when smaller (12.5 cm) sampling line spacing was used. However GPR root biomass estimates were less than the allometric estimation, 369 kgC and 2170 kgC respectively, when sparse sampling was used since the large line spacing did not image continuous root structures. A line spacing of 10 cm or less was able to provide continuous root structures, regardless of plot size. Sparse line spacing decreased the resolution of the images created and therefore limited the size of root that can be detected. In addition to sampling line spacing, soil water content heavily influenced images created

using the GPR survey data. High soil moisture decreases the detection of roots due to the lack of permittivity contrast between the soil and roots. A sampling line spacing of 5 cm with soil moisture content of 6% and inline sampling interval of 0.5 cm allowed for the detection of small diameter (up to 1.4 cm) roots. We recommend using high frequency antennas to provide 3-D imaging capabilities in sandy environments with low soil moisture to achieve better contrast between soil and roots.

Our results show that high-resolution 1 GHz GPR provides a viable method for belowground biomass estimation when conducted with small line spacing (< 10 cm) and high inline sampling density. GPR measurements can be employed to refine allometric biomass estimates and have broader applications to mapping of root networks in urban areas to avoid damage to buried drainage infrastructure. Accurate estimates of belowground biomass can also assist in reducing uncertainty in carbon flux estimates in climate models.

Key Words: Ground penetrating radar, root biomass, carbon, temperate forest, *Pinus strobus*

3.1 Introduction

Roots provide water, nutrients and structural stability in trees. Depending upon species, age, water and nutrient availability, approximately 10-65% of a tree's total biomass may be contained within the root system (Barton and Montagu, 2004). In a forest ecosystem about 20-40% of biomass is located in roots (Hirano et al., 2009). Coarse roots (>5 mm) account for a large proportion of this, and hence must be quantified in forest carbon budget studies (Hirano et al., 2009).

Coarse root biomass (CRB) is commonly estimated using destructive techniques such as high-pressure air spading and soil excavation or coring (Butnor et al., 2003). These methods are time consuming, labour intensive, and limited with respect to the area that can be evaluated. Measurements of the exposed root systems are often used to derive allometric equations for estimating CRB. Several studies have developed allometric equations, which relate root biomass to tree diameter at breast height (DBH, 1.3 m above ground level) for various forests and tree types (Lassoie and Hinckley, 1991; Ouimet et al., 2008; Peichl and Arain, 2007; Peichl et al., 2010a Bolte et al., 2004).

Most often, a small sample size is used to determine the allometric equation and only large trees with a DBH greater or equal to 9 cm are used. This introduces error when these allometric equations are used to estimate root biomass for the whole ecosystem. Therefore, there is a need to develop and test alternate methods that may improve the accuracy of CRB estimates and may be used to validate estimates derived using conventional destructive methods.

Geophysical remote sensing techniques (such as ground-penetrating radar, resistivity surveys) may be used to measure root density and biomass (Zenone et al., 2008). Ground-penetrating radar (GPR) is a good alternative to destructive methods as it can be applied over large areas and is non-invasive and repeatable (Butnor et al., 2001, 2003; Nadezhda and Cermak, 2003). In the past, several studies have been conducted to determine root diameter, distribution and biomass. In these studies high frequency antennas ranging from 800 MHz to 2 GHz were used to detect roots. For example, Butnor et al. (2001, 2003, 2005) used a 1.5 GHz frequency GPR system to estimate root biomass with the use of image analysis software that related the amplitude of the radar reflection to the actual root biomass.

Butnor et al. (2001) expanded upon the work of Hruska et al., (1999) who used a 450 MHz frequency GPR to obtain the three dimensional (3-D) distribution of large oak trees to a resolution of 3 cm. Unlike Butnor et al. (2001) who used the reflected wave to estimate root diameter, Barton and Montagu (2004) used a waveform parameter of the reflective wave. The waveform parameter was found to have a better relationship with root diameter than the amplitude of the reflected wave (Barton and Montagu, 2004; XiHong et al., 2010). This waveform parameter was even effective at various depths. Butnor et al. (2001, 2003) derived GPR root biomass estimates based on the correlation of root biomass per core with the number of pixels within a certain threshold range. Their soil cores comprised mainly of coarse roots (>5 mm), which made up 87% of the total root biomass on a dry weight basis (Butnor et al., 2003).

Although GPR is a relatively new method to estimate root biomass several issues have arisen. XiHong et al. (2010) identified the two problems with GPR root biomass studies. Firstly, the effect of radar wave attenuation on root diameter and biomass estimation models and secondly, the inadequate post-processing of GPR data. They set out to solve these problems, as well as estimate root biomass using a root diameter estimation model with 2 GHz radar data. Their model estimated the coarse root density using a waveform parameter, which employed the time difference (ΔT) between the arrival from the root top and bottom. ΔT was in turn used to create a root diameter estimation model (XiHong et al., 2010). In comparison to field experiments, this model was able to estimate CRB, assuming that roots are cylindrical. Hirano et al. (2009) explored the accuracy of detecting roots through varied root volumetric water content, root diameter and interval between roots. These factors were found to be important since roots with less than 20% water content were not detected, roots less than 19 mm diameter were not detected and closely spaced roots were detected as a large root (Hirano et al., 2009). These issues could lead to uncertainty in root biomass estimates.

In the past 3-D radar imaging has not been explored greatly for obtaining root structure and there have been no attempts to estimate root biomass using this advanced imaging. Zenone et al. (2008) state that there is potential for 3-D imaging of root structure, however further refinements are still required. In particular, obtaining software capable of processing raw data into root system architecture. Modeling size, shape and root volume is more difficult than determining root location (Butnor et al., 2005).

In this study an experiment was conducted in a temperate pine forest to estimate root biomass using high resolution (1 GHz) 3-D GPR. The main objectives of the study were to: (1) quantify the spatial distribution, size and volume of coarse roots in varying test plots using 3-D images (2) determine the impact of root diameter, root spacing sampling resolution and soil moisture status on root detection and (3) perform a comparative analysis of the allometric equation method and the GPR derived method to improve existing below ground biomass estimates.

3.2 Materials and Methods

3.2.1 Study Site

The study was conducted at the mature stand of the Turkey Point Flux Station (TPFS) located in southern Ontario, Canada (42^{o}42'N, 80^{o}21'W) (Arain and Restrepo-Coupe, 2005), which is known as TP39 (1939 plantation) or CA-TP4 in global Fluxnet. This white pine (*Pinus strobus* L.) forest grows on sandy, well-drained soil with low to moderate water holding capacity and little organic matter. The soil type is a brunisolic grey brown luvisol, as the site is located on lacustrine sandy plains modified by wind action (Peichl and Arain, 2006). The surficial deposits in the area include > 15 m thick sand overlying glacial lake clays with a water table depth ranging between 4 and 6 m (Peichl et al., 2009). A soil profile in this area typically consists of a 4-5 cm think litter layer, an Ap horizon of 20 cm, a Bm1 horizon up to 60 cm and a Bm2 horizon that reaches up to a depth of 70 cm (Presant and Acton, 1984). Organic matter makes up the majority of the Ap horizon. Soil texture ranges from sand to loamy sand (80-90% sand, 8-18% silt, <5% clay) (Peichl et al., 2009). Bulk density of the upper 10 cm is 1.35 g cm^{-3}

(Peichl et al., 2009). The site has a 30-year mean annual temperature of 7.8 ^{o}C and an annual precipitation of 1010 mm, where 438 mm falls between May and September. Previous root excavation done at TPFS shows that the root zone extends the upper 0 – 30 cm, where more than 90% of the root mass is located (Piechl et al., 2010a). Rooting depth was found to be >2 m (Piechl et al., 2010a).

3.2.2 GPR Data Collection and Field Procedures

GPR data were acquired using a Sensors and Software Noggin 1 GHz shielded antenna. The 1 GHz frequency was chosen as it provided the best compromise between vertical and horizontal resolution and penetration (about 1 m) in sandy soils. GPR surveys were conducted at three spatial scales (2 × 3 m, 5 × 5 m and 20 × 20 m plots) to evaluate the changes in radar resolution as a function of survey line density.

3.2.2.1 Test Plot

A 2 × 3 m trench (0.6 m deep) was excavated for validation of the radargrams generated by GPR and for calibration of the 20 × 20 m grid with a 5 × 5 m inset. This trench was also used to determine the smallest root diameter that can be detected by a 1 GHz antenna. Roots were collected during the excavation of this trench and their wet weight, length, and diameters were recorded. No rocks were found while digging. Several different diameter roots were chosen based on their characteristics. Each root was numbered and reburied with the native sand at about 0.40 m depth at various orientations. Due to the slight topography of some of the roots themselves, the depth ranged from 0.30

– 0.50 m, where the vertical root was placed at 0.40 m to the top of the surface. The orientation, depth and root numbers were also recorded and a photograph of their layout was taken. In total fourteen roots were buried with diameters ranging from 0.5 cm to 12 cm. Five roots with similar diameter were buried 4, 5, 10, and 20 cm apart to determine the minimum spacing that GPR can detect for individual roots. The photograph of the root layout was then used to compare with the radargrams that were collected over the 0.05 × 0.05 m grid within the 2 × 3 m plot at an inline sample spacing of 0.005 m once the trench was refilled. A 0.05 × 0.05 m grid was created on a plastic tarp to make the surface smooth and ensure that the survey lines were consistent while surveying. A survey was performed before and after a 14 mm rain event on 22-23 June. The volumetric soil moisture sampled across the trench plot using a manual probe (CS620, HydroSense Water Content Reflectometer, Campbell Scientific, Inc. (CSI)) before rainfall was 0.06 m^3 m^{-3} (about 6%) at 20 cm depth, while the soil moisture after rainfall was 0.11 m^3 m^{-3} (about 11%). We attribute the low soil moisture values to the pit being refilled, thereby creating larger pores and smaller porosity allowing better drainage.

3.2.2.2 20 x 20 m Survey Area

A 20 × 20 m plot was surveyed with a 25 cm line spacing and inline sampling interval of 0.5 cm. A 5 × 5 m subset of the 20 × 20 m plot was also surveyed with the same inline sampling rate but at 12.5 cm line spacings. All surveying techniques consisted of dragging the GPR along the ground, overtop the litter and small surface vegetation, but stopping and starting a new line at trees and fallen logs if they were located on the grid line. Care was taken while pulling the GPR over obstacles as to minimize any tipping or bouncing (Butnor et al., 2003). The DBH and coordinates of large trees within the 20 × 20 m plot were recorded. These tree DBHs were used to estimate root biomass for the whole plot using the following site-specific allometric equation developed by Peichl et al. (2010a) and Peichl and Arain (2007):

$$B_r = c(DBH)^a \times S \qquad (1)$$

where B_r is the dry root biomass (kgC/m^2), c (0.0027) is an equation constant, a (3.001) is a fitted equation parameter, DBH is tree diameter at breast height (cm), and S is the stem density (stems/m^2). The 16 small trees (< 9 cm DBH) in the plot were not included in Br estimations since the allometric equation does not take small trees into consideration.

3.2.3 Data Processing

GPR data were processed using GPR-SLICE^{TM} software (Goodman and Klein, 2012). Several post-processing steps were performed on radargrams including background removal, bandpass filtering, Stolt 2-D migration and Hilbert transform (Figure 3.1). Due to radar wave attenuation gain recovery was applied to all radargrams. Background removal was used to remove the effects of the airwave and ground wave, which are direct waves from the antenna to the receiver. In addition, background removal eliminates the effect of surface reflections, which also input a large amount of energy that saturates the GPR receiver signal (Fisher et al., 1992). A bandpass filter (761 – 2605 MHz) was applied to enhance the resolution of root diffractions and to discriminate against long wavelength radar signals. Stolt migration was applied to collapse diffractions

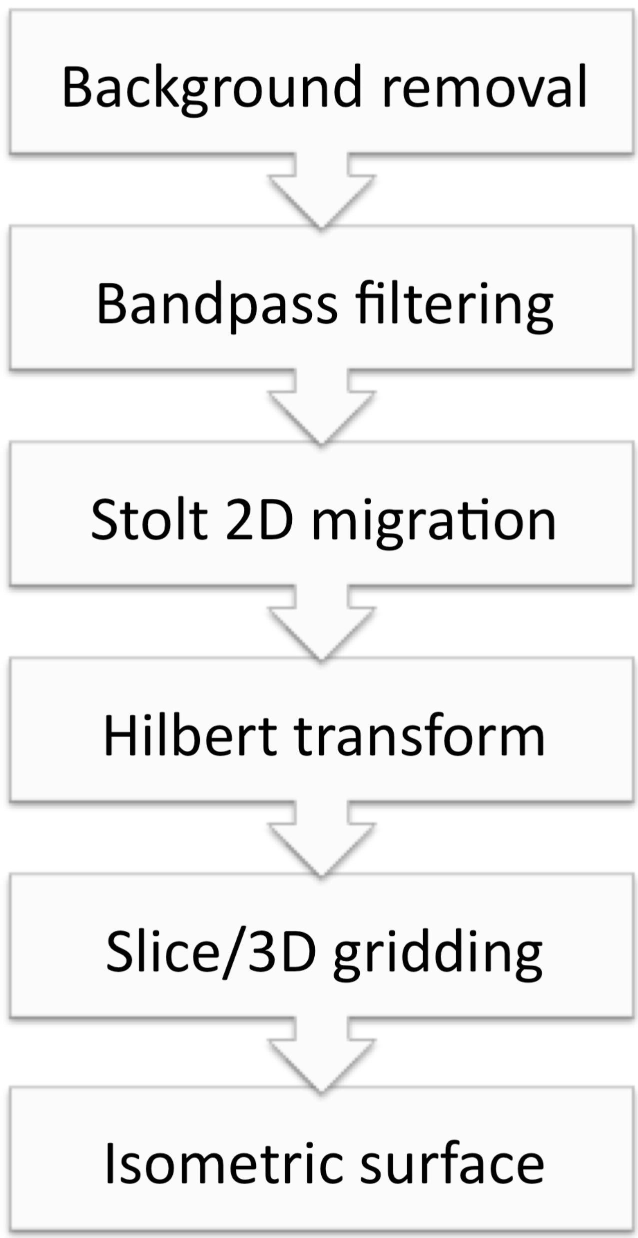

Figure 3.1: Schematic diagram showing radar processing flow.

to single source points using a radar wave velocity of 0.11 m/ns determined by curve fitting to diffraction hyperbolas. Lastly, the data were Hilbert transform (magnitude) to create an envelope of the radargram pulse by removing the rapid oscillations of the signal by connecting the magnitudes of the diffraction amplitudes. This was done to help mask the echoes that were present and create more intact looking roots. GPR-SLICE was used to apply these processing steps and this processing flow was applied to all of the profiles collected.

Root volume was estimated using the actual root mass divided by the average density of eastern white pine (343000 g m^{-3}). The roots were weighed before being reburied and a total weight was obtained, which is referred to as the actual root mass. The average root density was estimated from the values obtained by Lu et al. (2006), Wahlgren et al. (1968) and Woodcock and Shier (2003).

Root volume was estimated from 3-D radar volumes using isometric surfaces calculated using the marching cubes algorithm (Goodman and Klein, 2012). The algorithm locates the surface within a cube, created from eight pixels. A polygon is created that represents the surface that intersects the cube and a value of one is assigned to the cubes vertex if the data value at that point is greater or equal to the value of the surface that is being generated (Lorensen and Cline, 1987). A value of zero is given to vertices that are less than the value being investigated. Linear interpolation is then used to interpolate the surface intersection along the cube's edge and a unit normal is calculated for each triangle vertex (Lorensen and Cline, 1987). This approach is used widely in medical imaging, for example in computed tomography (CT scan). In tomography a tomogram is generated from an x-ray being sent and received at an array of angles around the object creating a two-dimensional slice from the 3-D object. However, the application in this experiment uses echograms, which images the amplitude of the reflected energy from the top and bottom of the root due to the set-up of the survey. The top and bottom of the root are represented by the magnitude of the diffraction amplitude.

GPR-SLICE creates a volume of the Hilbert transform envelope, which is used as a proxy for root diameter. The isometric surfaces displayed are surfaces of the same amplitude in the 3-D volume, which we related to the mass of roots within the plot area (Goodman and Klein, 2012). The 2 × 3 m plot was processed with 5, 10 and 25 cm line spacing. These data sets were then processed in the same manner as the larger plots with equal line intervals. All depth slices created were done using inverse distance. A volume threshold was determined for each data set from the isometric surface. This is the amplitude threshold of the total amplitude range that is representative of root mass. For instance, a threshold of 85 % would mean that 85 % of the maximum amplitude and greater is root biomass. The threshold defines the bounds of the amplitude.

3.3 Results

3.3.1 Root Detection and Soil Moisture in Trench Plot

A depth slice of 46 cm is shown in Figure 3.2 since this depth showed the greatest detail of the buried roots. High amplitude areas, denoted in black, are representative of the location of roots. Figure 3.2a, with 5 cm interval spacing, was able to detect the roots that were placed close together, with the exception of the roots that were 4 cm and 5 cm

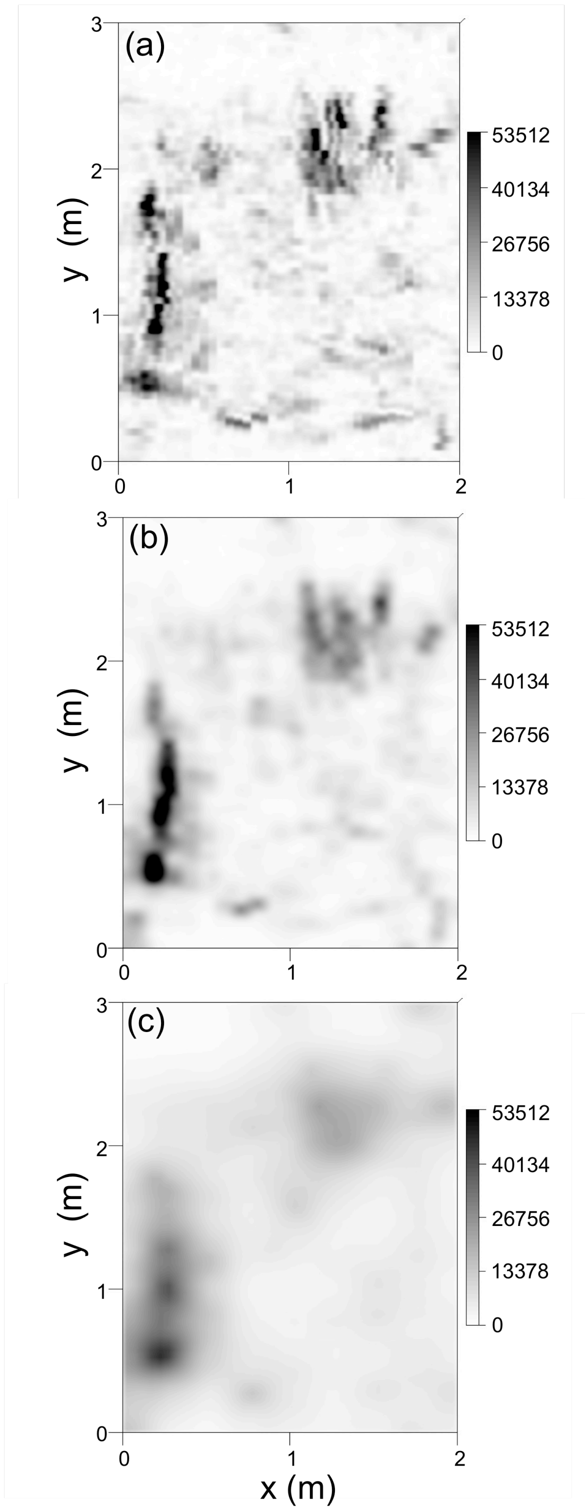

Figure 3.2: Depth slices (46 cm) for 2 x 3 m calibration pit showing effect of varied line spacing. A. 5 cm line spacing. B. 10 cm line spacing. C. 25 cm line spacing.

apart. The smallest diameter root detected was 1.4 cm. Increasing the sampling interval to 10 cm (Figure 3.2b), clumped the five roots that were placed close together. However, roots greater than 1.4 cm were still detected. An increase in the sampling line spacing interval once more to 25 cm (Figure 3.2c), led to a significant decrease in root detection. Only the largest root was detected. The cluster of roots, in the top right corner of the pit, was identified but could not be distinguished from one another.

The images presented in Figure 3.3 show the effect of soil moisture on radargrams. Since the pit was dug and refilled, the boundary conditions were heavily visible in the post-rainfall (wet) radargrams compared to the pre-rainfall (dry) radargrams. Figure 3.3a shows a raw radargram where the direct air and ground waves are apparent near the top of the profile. Background removal eliminates these horizontal bands as shown in Figure 3.3b. The wet radargrams show faint diffractions that are representative of the roots buried at around 40 cm, while the pre-rainfall radargrams show more distinct diffraction hyperbolas. This is due to the larger permittivity contrast between the roots and soil matrix in the dry condition. Bandpass filtering, shown in Figure 3.3c, did not have an effect on either scenario since such a high frequency was used. Stolt migration however was found to be very useful in decomposing the hyperbolas into a more discrete shape that allowed for the identification of roots. It is clear in Figure 3.3d that the wet radargrams were unable to detect the majority of the roots that were buried. Hilbert transform, displayed in Figure 3.3e, provided similar results further distinguishing the roots from the background soil as discrete dark objects. The boundary effects also become evident, located on the far right of the radargram.

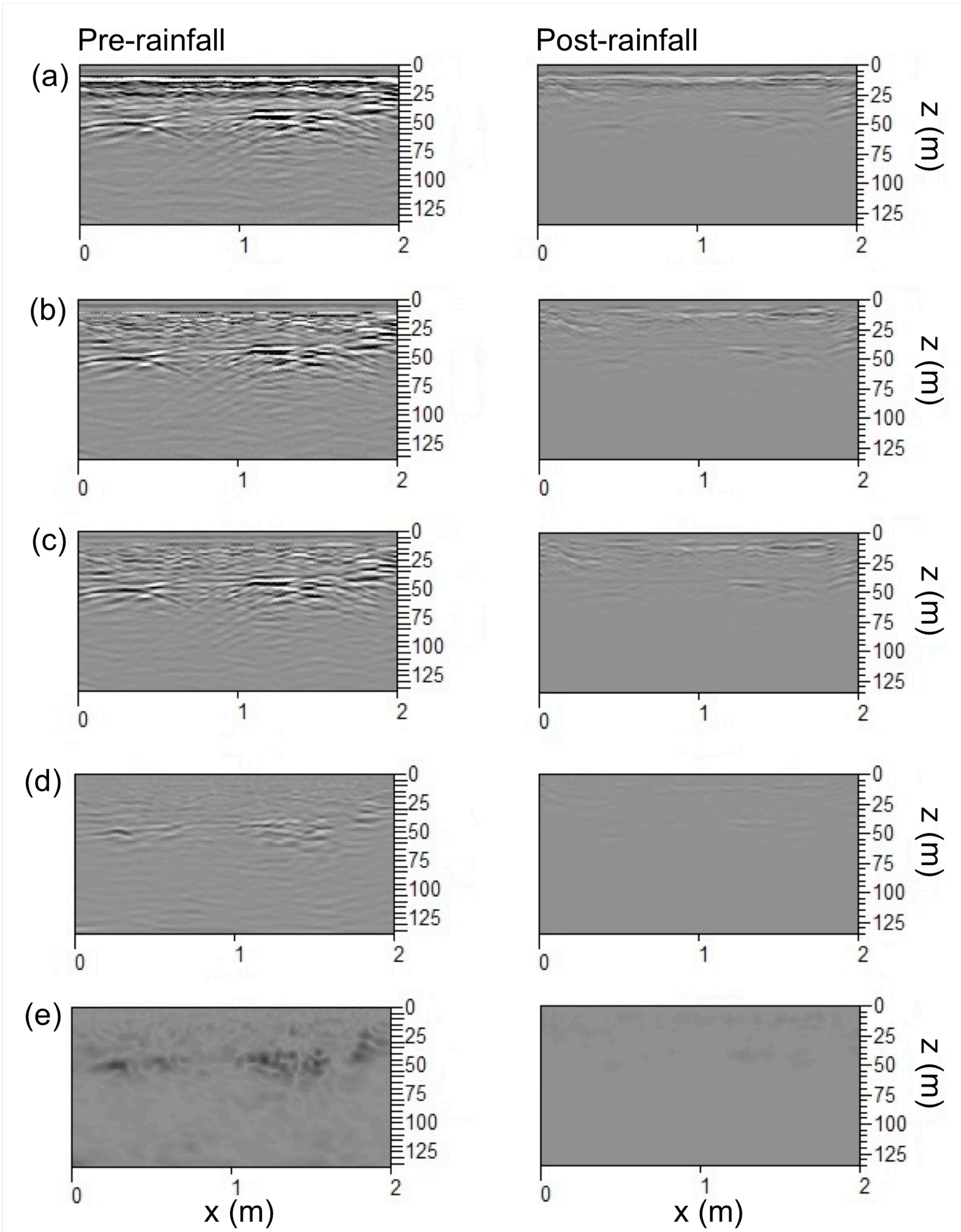

Figure 3.3: Radargrams for 2 x 3 m calibration pit (Line 43) comparing pre-rainfall and post-rainfall conditions. A. Raw 1 GHz radargram. B. Background removal. C. Bandpass filter (761-2605 MHz). D. Stolt migration. E. Hilbert transform.

Using the 2 × 3 m plot with the 5 cm interval spacing, depth slices were created for pre- and post-rainfall surveys. A depth slice of 41 cm was chosen to best represent the difference between the pre- and post-rainfall surveys, provided in Figure 3.4, since the roots were buried around 40 cm. This image further highlights the effects of soil moisture. The post-rainfall depth slice showed boundary effects along the edge of the pit, especially on the far right. The clump of roots as well as the largest root was detected while the remaining roots were not. The minimum root detected was 1.9 cm in diameter. The boundary effects arise due to the difference in compaction of the pit and surrounding area.

3.3.2 Calibration of Root Biomass

Isometric volumes represent the location of root mass in the survey area. Isometric volumes were generated for each sample interval scenario with their volume being equal to 0.02 m^3. The isometric volume of the 2 × 3 m plot with 5 cm line spacing can be seen in Figure 3.5. The 1 GHz antenna allowed for wave penetration up to a depth of 1.5 m, but a depth of 0.78 m was used because no roots were detected beyond this depth. The 5 cm and 10 cm volumes gave a similar result, with the 5 cm volume having a higher resolution. The higher resolution allowed for the differentiation of the clumped roots and created more continuous root structures. Boundary effects were visible horizontally at the top of the pit in both sampling interval volumes. Volume thresholds were found for each sampling interval volume, which was then applied to the 20 × 20 m and 5 × 5 m plots where the corresponding interval was used. The isometric threshold volumes are given in Table 3.1.

Table 3.1: Biomass values estimated from GPR volumes and allometric equation for calibration pit and reference plots.

Plot	5 x 5 m	20 x 20 m	2 x 3 m
Area (m^2)	25	400	6
Isosurface threshold (%)	75	61.9	85
Isosurface volume (m^3)	0.129	2.108	0.020
GPR total root mass (kg)	44.2	723	6.86
GPR total root mass per unit area (kg m^{-2})	1.77	1.81	1.14
GPR total biomass estimate (kgC)	22.6	369	3.50
GPR total biomass estimate per unit area (kgC m^{-2})	0.904	0.922	0.583
Allometric total biomass estimate (kgC)	12.3	2170	3.64*
Allometric total biomass estimate per unit area (kgC m^{-2})	0.492	5.42	0.607

*biomass value calculated prior to reburying

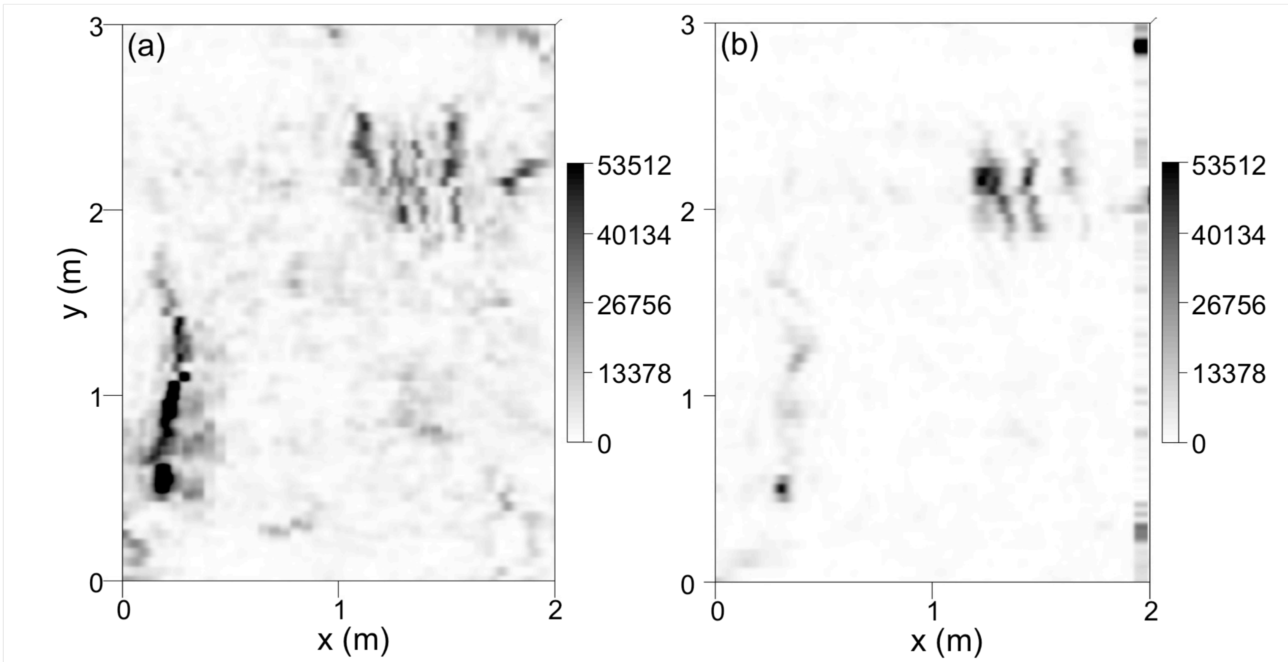

Figure 3.4: Depth slices (41 cm) for calibration pit. A. Pre-rainfall. B. Post-rainfall.

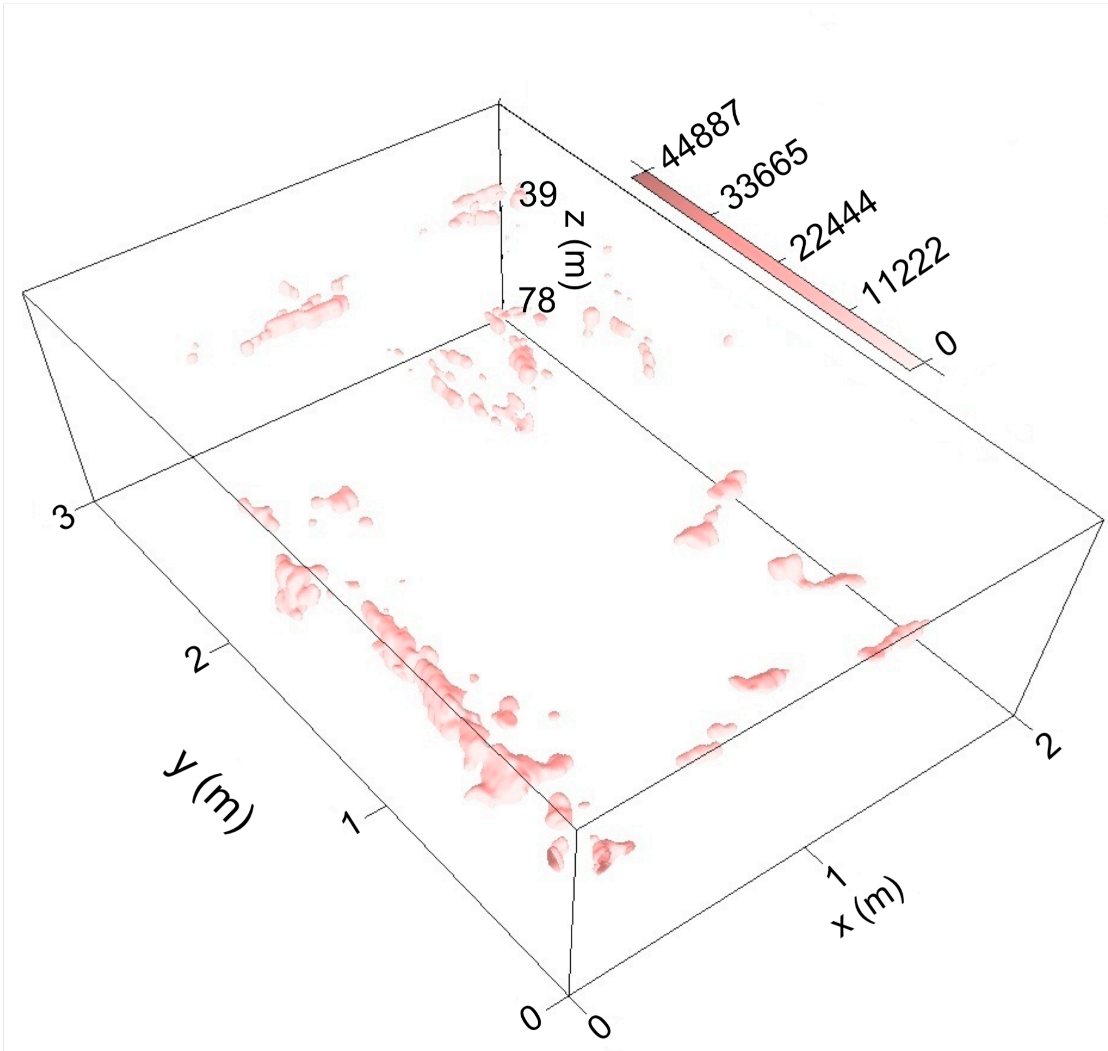

Figure 3.5: Isometric volume of Hilbert-transformed radar amplitudes (0-78 cm) with 5 cm line spacing for calibration pit.

An overlay of the Hilbert transform amplitude surface at 0.45 m on the geo-referenced photograph of the layout of roots is shown in Figure 3.6. Using Figure 3.6, a weak positive relationship between the log of the amplitude diffraction and root diameter was discovered, resulting in an R^2 value of 0.37 shown in Figure 3.7a. Ignoring roots smaller than 4 cm resulted in a slightly weaker relationship ($R^2 = 0.20$) compared to ignoring roots greater than 4 cm ($R^2 = 0.29$) as shown in Figure 3.7c and Figure 3.7b respectively. The relationship was found to be significant ($p < 0.05$), shown by p values calculated from the line of linear fit. However the modified hoerl curve, which is part of the family of power curves, resulted in the best fit for the data as it generally provided the lowest Corrected Akaike's Information Criterion (AICC) value. Therefore the R^2 value obtained from the modified hoerl curve was used to express the relationship between the two variables. Figure 3.8 tests the relationship between picking individual first arrival hyperbolas from the raw log transformed amplitudes and root diameter. An even weaker relationship is found ($R^2 = 0.26$ in Figure 3.8a) while still remaining significant ($p < 0.05$). The same can be said for roots less than 4 cm and greater than 4 cm, which were graphed separately, with an R^2 of 0.26 and 0.28 respectively (Figure 3.8b and Figure 3.8c). The R^2 value corresponding to the line of best fit with the lowest AICC value was used to best represent the data. There was still a significant ($p < 0.05$) relationship when root diameter was less than 4 cm, however the relationship was insignificant when root diameter was greater than 4 cm.

The depth slices created from the 5 × 5 m survey data show roots detected in black and provide their trends (Figure 3.9). The highest root mass was around 34 cm, with the

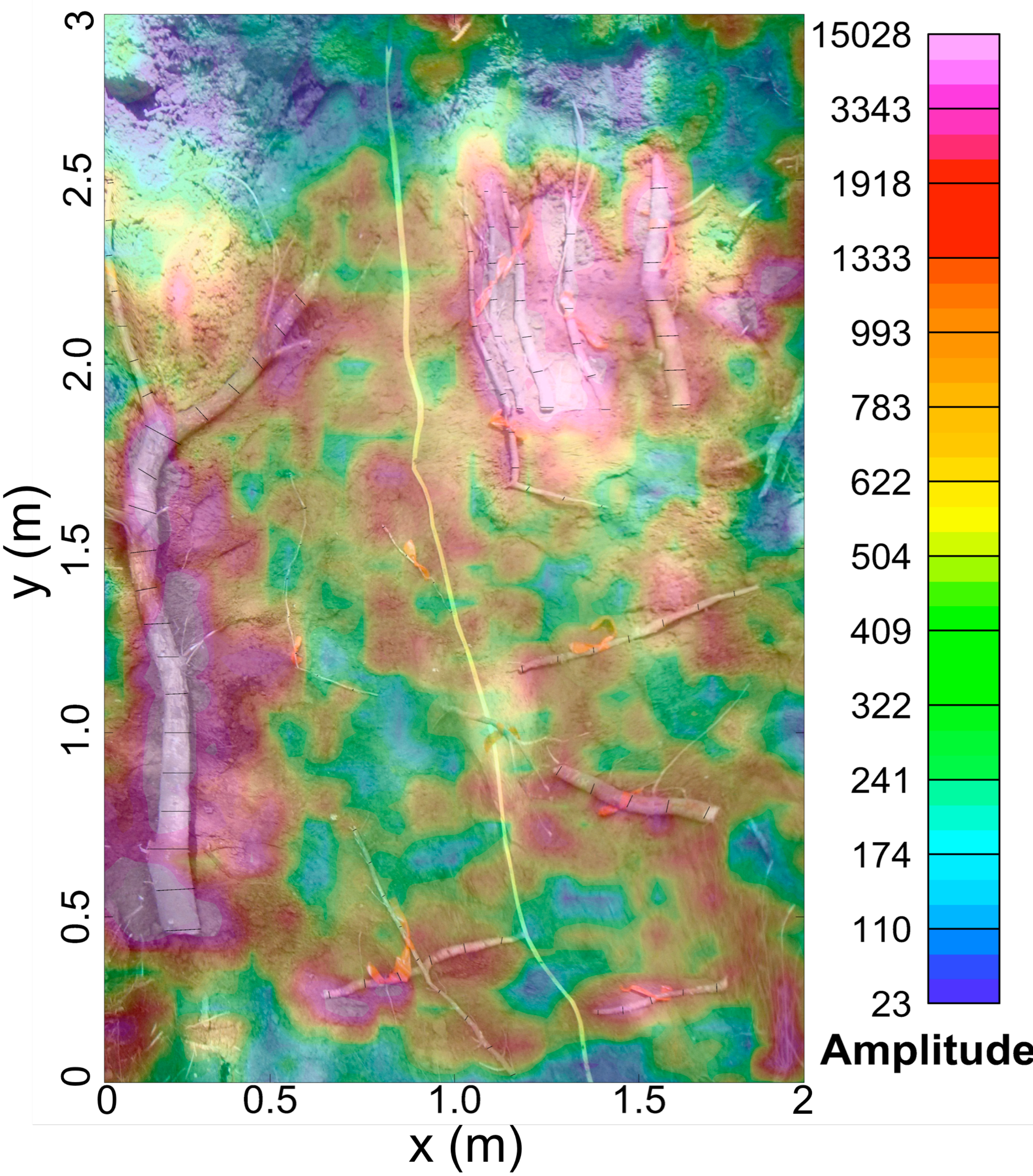

Figure 3.6: GPR depth slice (45 cm) overlaid on geo-referenced photograph of 2 x 3 m calibration plot for comparison of root network with radar amplitudes, with points taken every 10 cm along the length of each root.

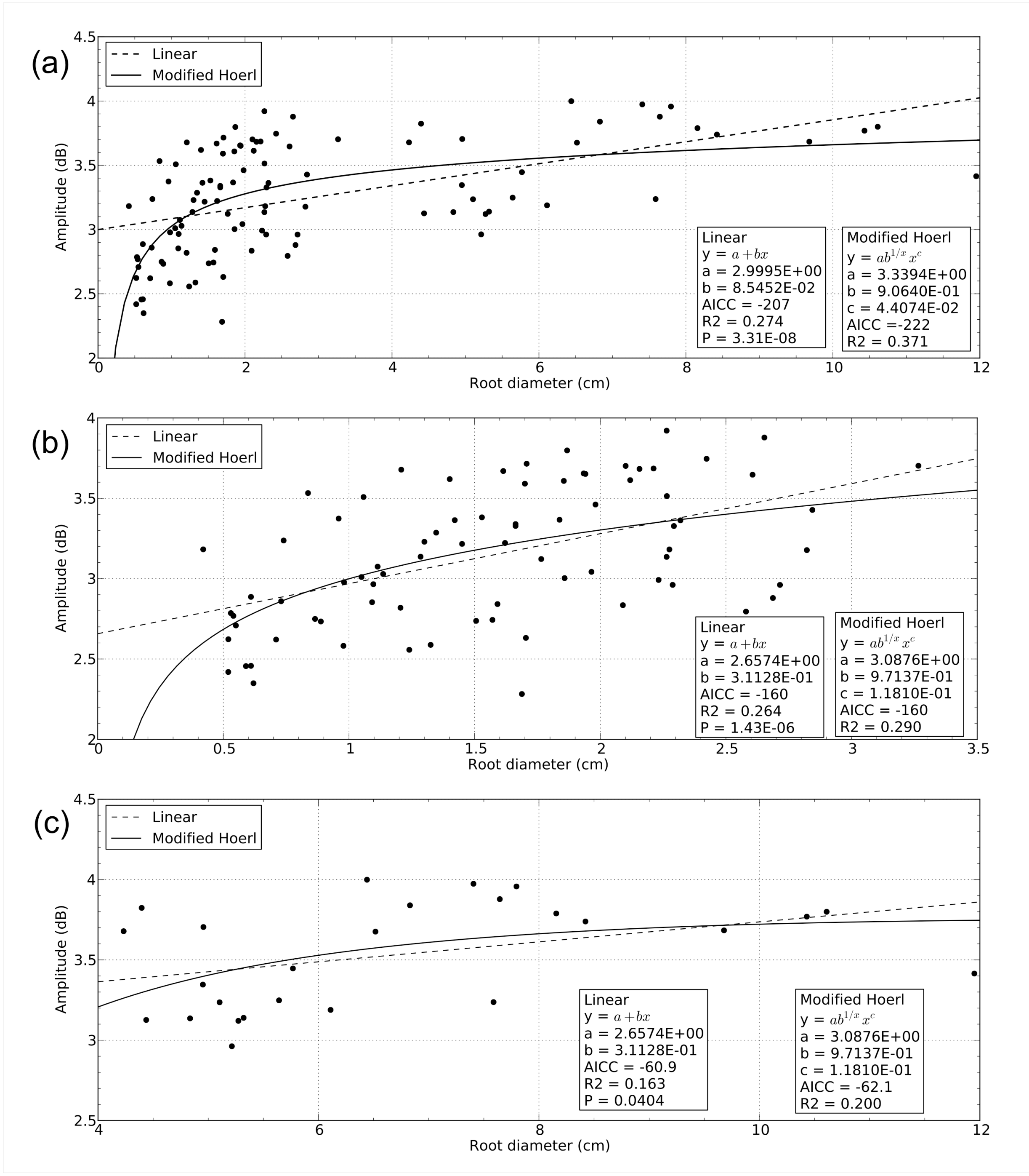

Figure 3.7: A cross-plot of the log of the root diffraction amplitudes from Hilbert transformed data versus root diameter for the calibration pit obtained from the amplitude slice at 45 cm depth overlaid on the geo-referenced photo. A. Entire data set with a linear and power fitted curve. B. Data set where roots less than 4 cm are graphed with linear and power fitted curve. C. Data set where roots greater than 4 cm are graphed with linear and power fitted curve.

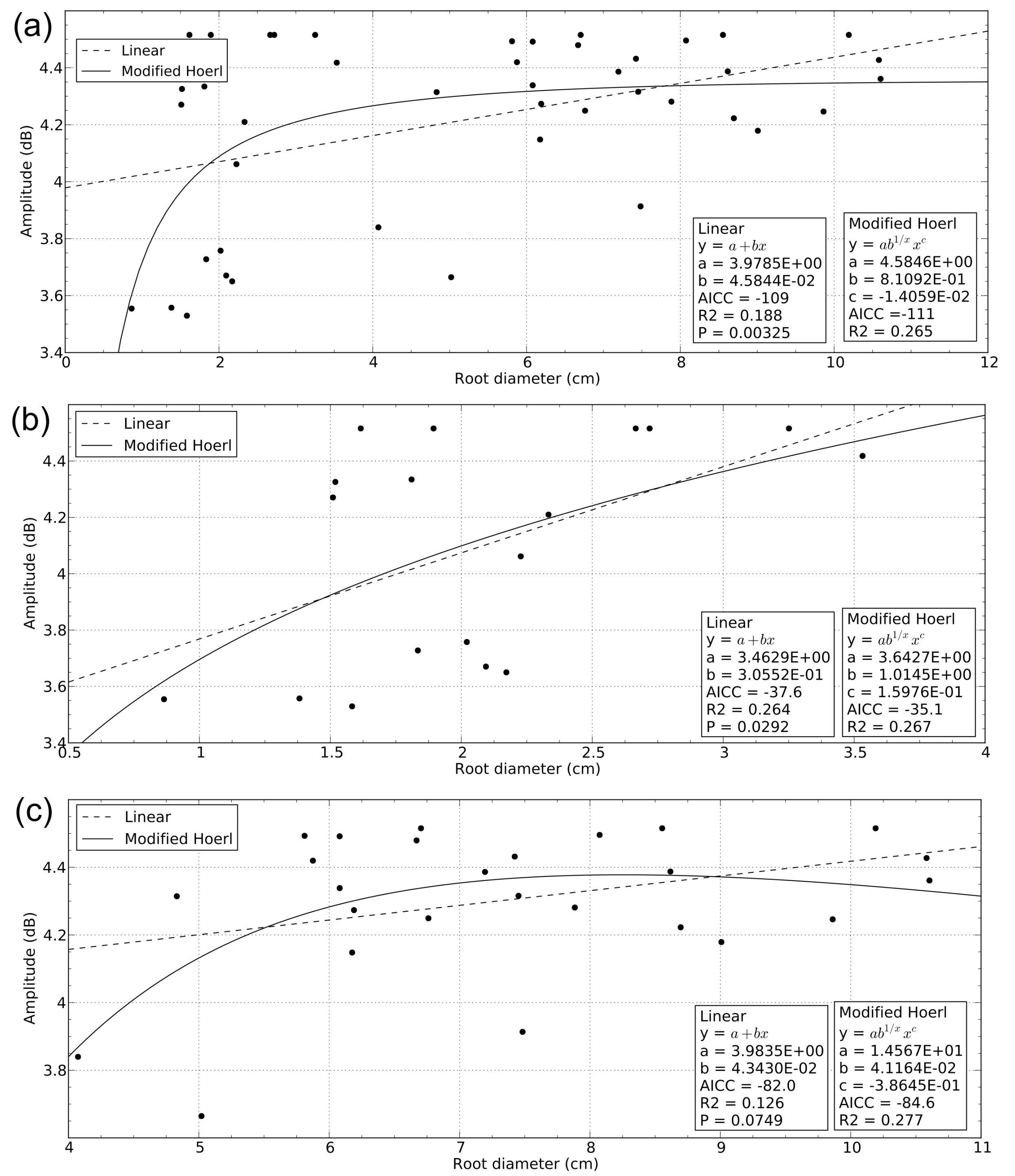

Figure 3.8: A cross-plot of the raw log transformed amplitude values picked from individual hyperbolas versus root diameter. A. Entire data set with a linear and power fitted curve. B. Roots less than 4 cm are graphed with linear and power fitted curve. C. Roots greater than 4 cm are graphed with linear and power fitted curve.

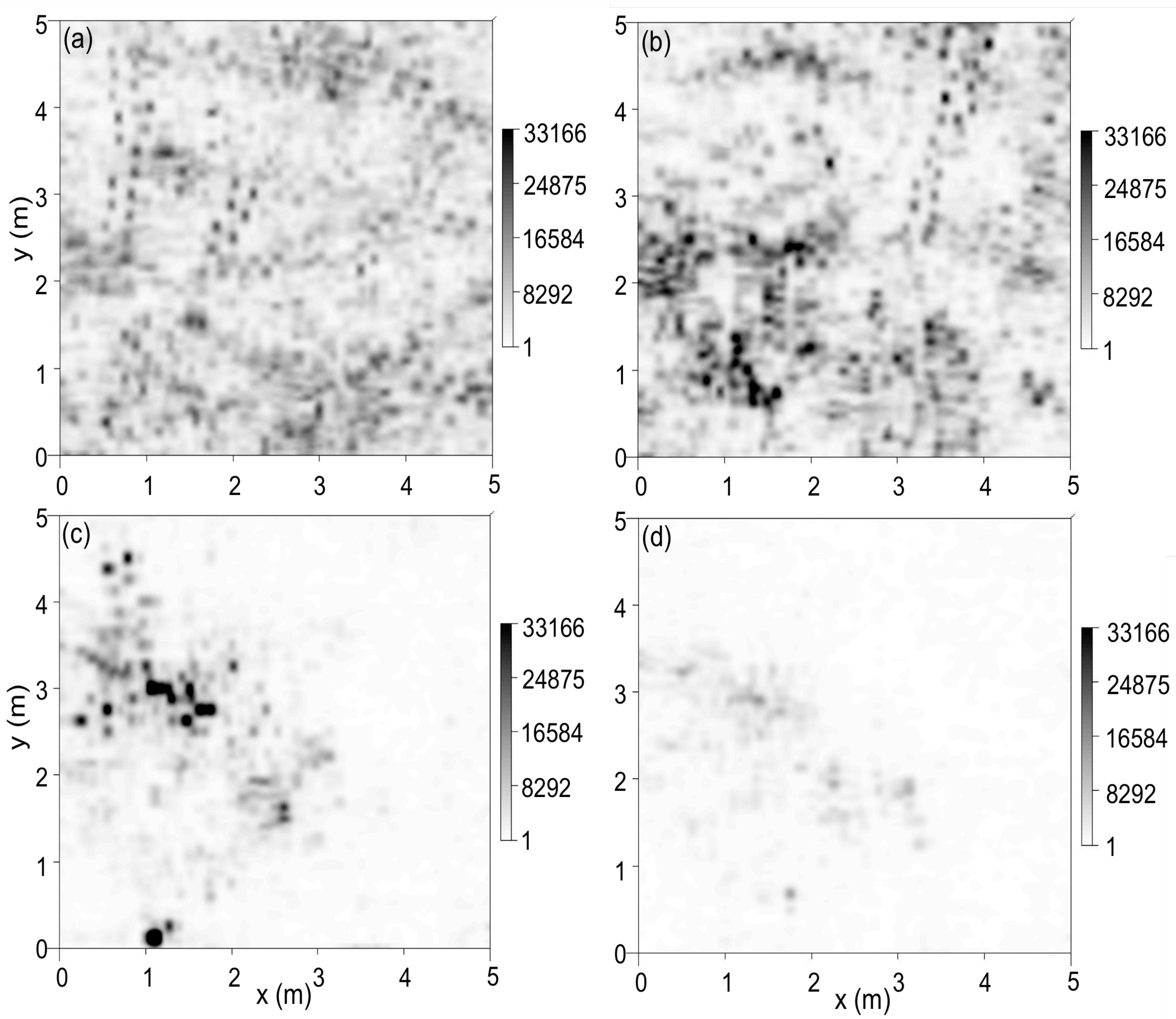

Figure 3.9: Selected depth slices for 5 x 5 m reference plot A. 22 cm. B. 34 cm. C. 66 cm. D. 80 cm.

root mass decreasing away from this depth. The high amplitude areas, represented in black, signify roots. Root mass was low in this area. The same can be said for the 20 × 20 m survey results shown in Figure 3.10, with the majority of the roots located around 34 cm. Root structure was less continuous than the 5 × 5 m inset since the sampling interval was doubled.

Isometric volumes were created for the 20 × 20 m area and 5 × 5 m subset using the threshold volumes generated from the calibration pit. The isometric volumes of the 5 × 5 m and 20 × 20 m plots are shown in Figure 3.11. The majority of the roots are located around 0 to 30 cm, which agrees with Peichl et al. (2010b) who state that the root zone at TPFS is the upper 30 cm. Total biomass values from allometric calculations, and GPR surveys are given in Table 3.1 for each plot. The 5 × 5 m plot had a root volume of 0.129 m^3 and the 20 × 20 m plot had a root volume of 2.11 m^3. The GPR root biomass estimate within the 20 × 20 m plot are a magnitude less than the allometric root biomass estimates whereas in the 5 × 5 m subset the GPR biomass estimate is about double that of the allometric estimate. On average the amount of carbon per area estimated from GPR is 0.913 kgC m^{-2}, where as the allometric total biomass per unit area was estimated to be 2.956 kgC m^{-2}. The allometric method obtained an estimate for biomass per area within the 20 x 20 m reference plot that was 11 times larger than in the 5 x 5 m inset, while a small change was seen in the GPR estimate. A map was created of the 20 x 20 m plot outlining the position of the trees along with their respective DBH (cm) and biomass (kgC) value (Figure 3.12).

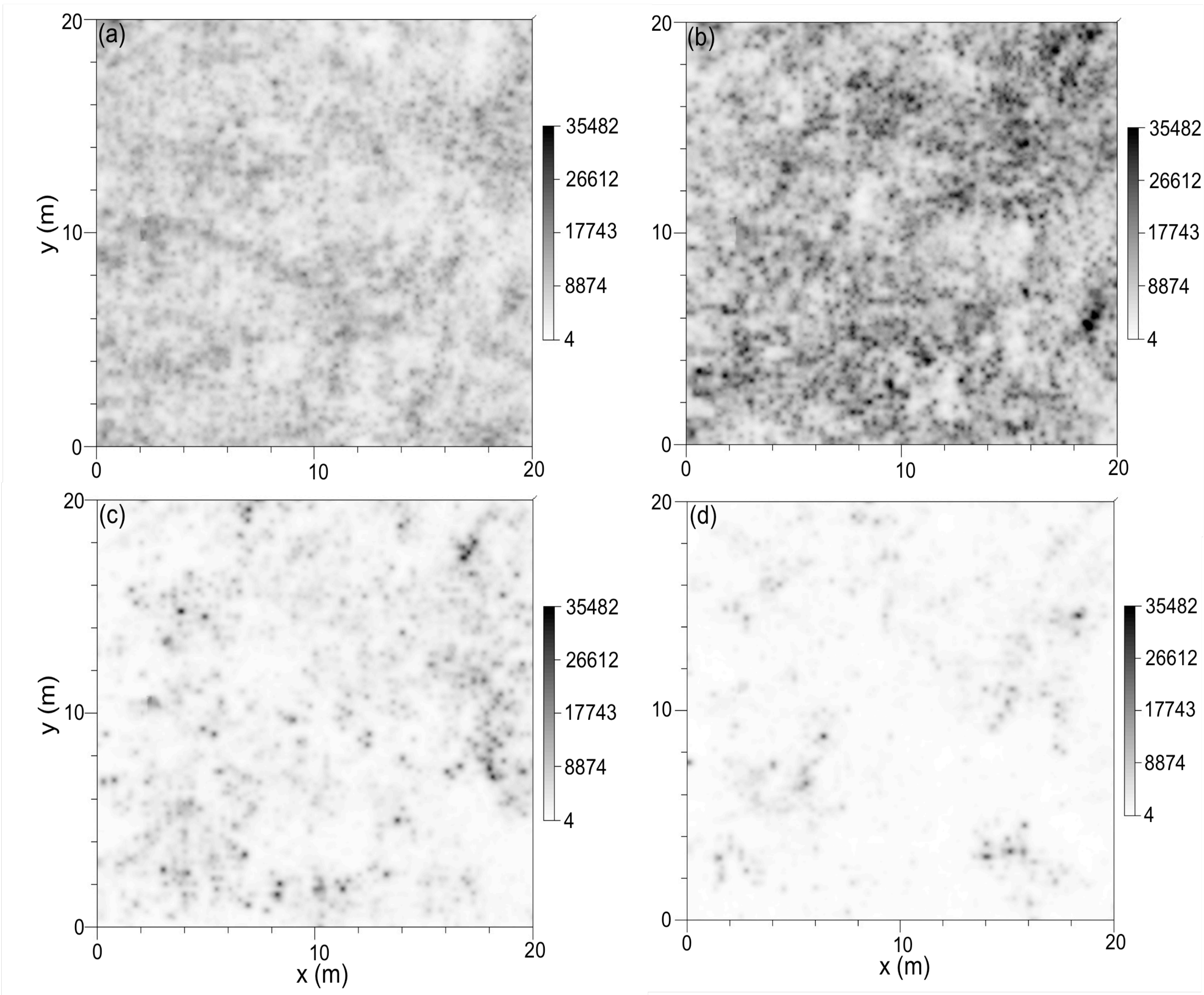

Figure 3.10: Selected depth slices for 20 x 20 m reference plot A. 22 cm. B. 34 cm. C. 57 cm. D. 81 cm.

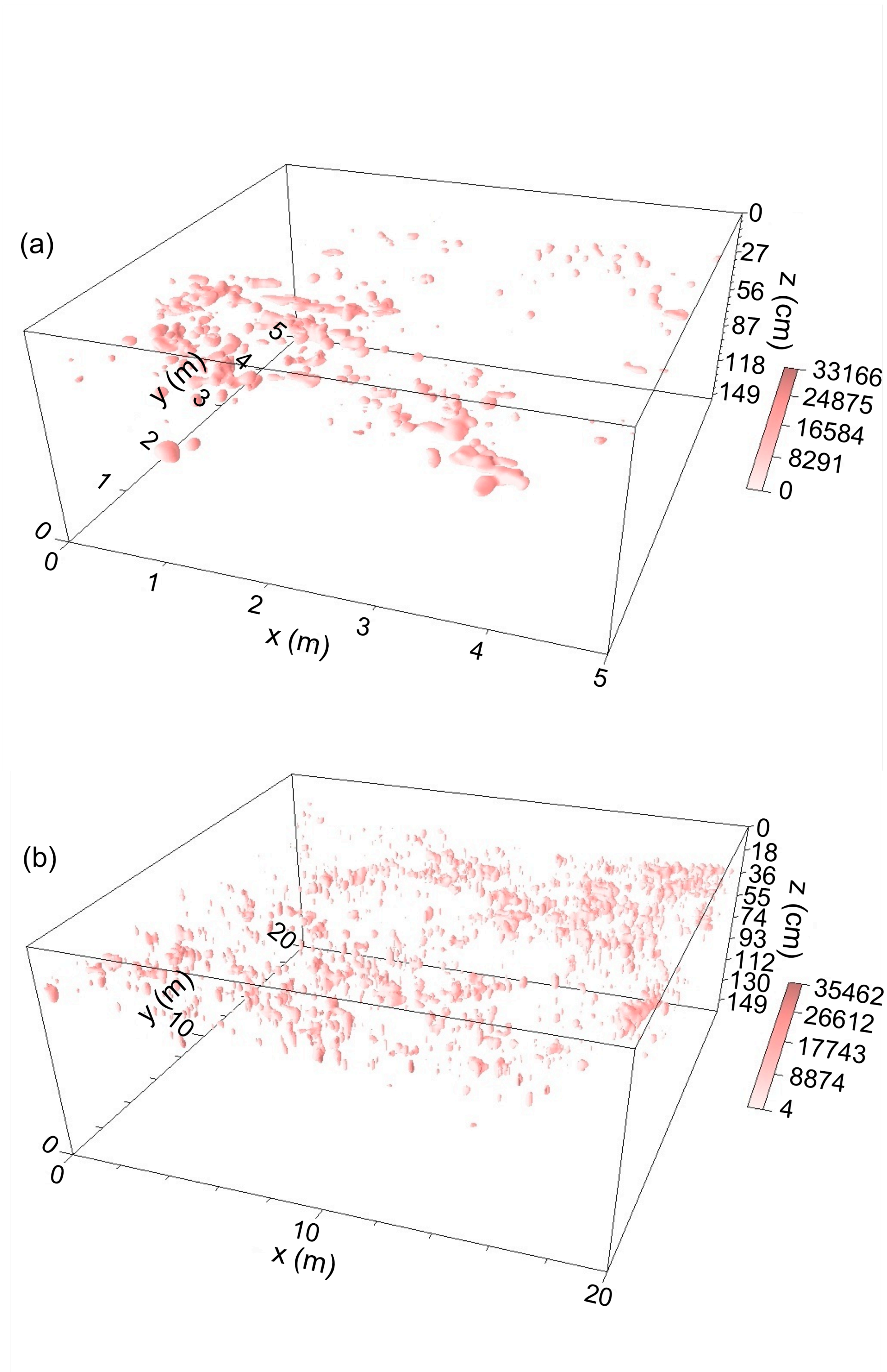

Figure 3.11: Isometric volumes for reference plots. A. 5 x 5 m plot (0.129 m^3). B. 20 x 20 m plot (2.108 m^3).

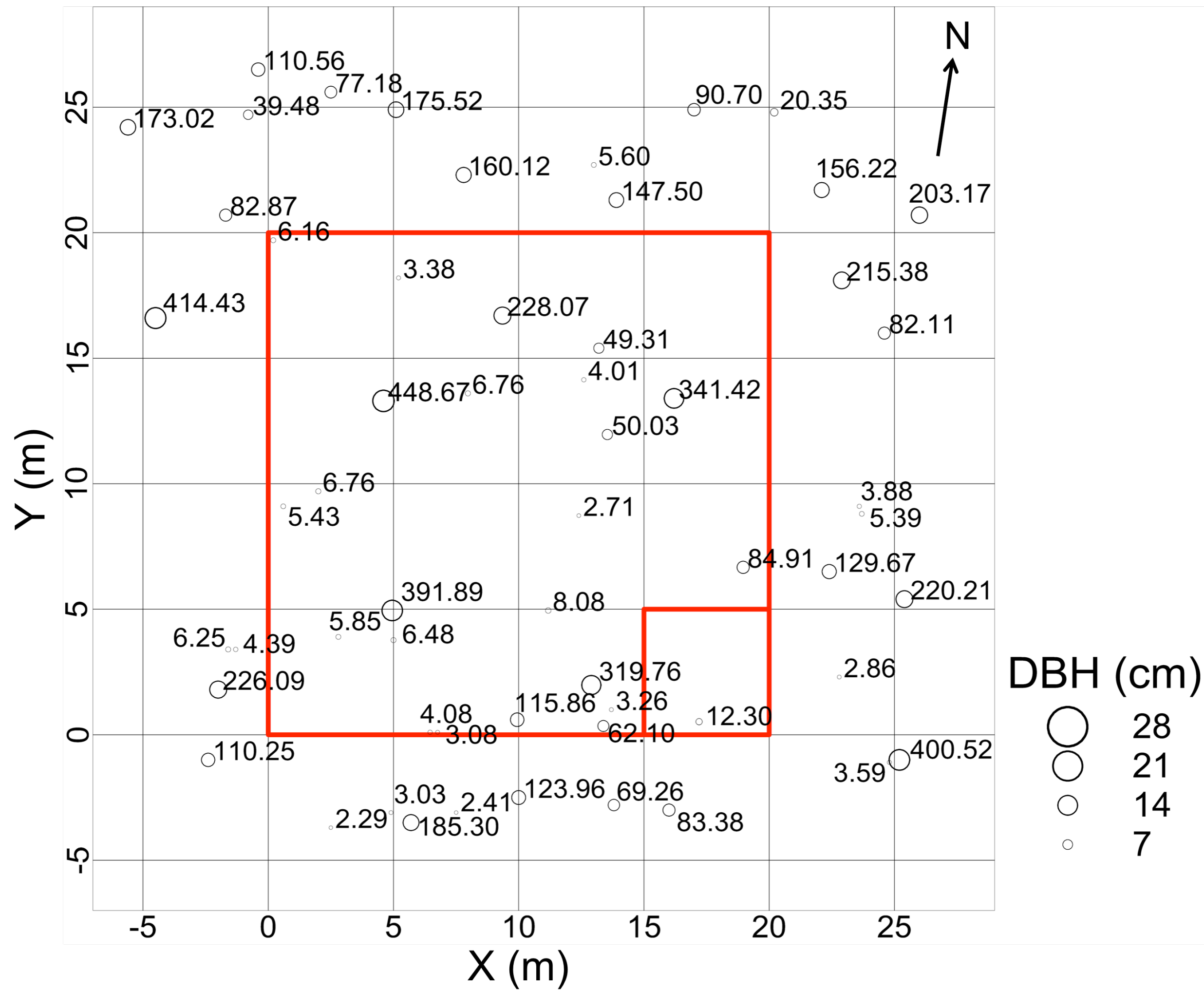

Figure 3.12: Map of Turkey Point reference area (400 m^2) showing location of trees (open circles) with their associated root biomass (kgC) estimated using allometric equation (Peichl and Arain, 2007). Tree diameter at breast height (DBH) indicated by circle diameter.

3.4 Discussion

3.4.1 Root Structure

The radargram profiles obtained by GPR allowed for the production of images of the spatial distribution of roots through interpolation for various scenarios, including pre- and post-rainfall and varied sampling line spacing. Our results rely on the assumption that the density of coarse roots does not change. XiHong et al. (2010) confirms this assumption stating that the density of roots greater than 0.5 cm is relatively uniform. Soil and root moisture play an important role in the detection of roots, particular in sandy soil, which has low water holding capacity. Our study results indicate that a 5% change in soil moisture (0.06 m^3 m^{-3} vs 0.11 m^3 m^{-3}), as observed at our site before and after a rain event, had a significant effect on the outcome of the GPR radargrams. Dannoura et al. (2008) found similar results where the roots were not detected when the soil moisture was higher than that of the root water content. Dead roots would not be detected since they have very low moisture content if not fully dry (Hirano et al., 2009; Dannoura et al., 2008). This limitation may create problems for temporal root biomass studies since soil moisture in winter and spring is much higher. However surveys could be completed on a yearly basis. This could provide incite into the change in root biomass per year resulting in yearly root growth.

Previous studies in literature describe that fine roots (< 2 mm) and small (2-5 mm) roots cannot be detected by GPR but coarse roots (>5 mm) can be detected (Butnor et al., 2001; Hirano et al., 2009; Stover et al., 2007). Hirano et al. (2009) were able to detect roots greater than 1.9 cm with a 900 MHz antenna in dry sand. Roots as small as 0.5 cm can be detected with a 1500 MHz antenna, but only to a depth of 50 cm (Butnor et al., 2001). In our study, the minimum diameter root detected with a 1 GHz antenna was 1.4 cm. Peichl et al. (2010a) found that fine root production contributes about 15 % of net primary productivity (NPP) at TPFS, compared to 10 % contribution from coarse roots. Therefore a higher frequency antenna of 1.5 GHz or even 2 GHz should be used in future work at TPFS to detect smaller diameter roots, leading to the detection of fine roots. We found that in an area with a root zone larger than 50 cm, the 1 GHz antenna would be best as it gives the best compromise between depth and resolution. Taproots also cannot be detected by GPR since they are vertically oriented and are not perpendicular to the GPR survey (Butnor et al., 2001; Zenone et al., 2008). This was shown in the 2 × 3 m calibration pit where the vertical roots remained undetected. Taproots could be detected using borehole GPR or electrical resistivity tomography.

The comparison of the interval spacing in the 2 × 3 m calibration pit (Figure 3.2) highlighted the importance of sampling line spacing. For any size survey area, the line spacing should be no more than 10 cm, with smaller spacing increasing the resolution of the survey. Together antenna frequency and line spacing govern resolution.

The 3-D aspect of our work is unique in estimating the root biomass and has not been done previously in literature. Our 3-D images (Figures 3.5 and 3.11) of root structure over an entire plot clearly show the issue of resolving root mass over depth and how continuity of root structure relates to line spacing. Figure 3.5 also displays the problem with using Hilbert transform as a proxy for root mass. Several cycles are generated from a root due to echoes from the root. This results in the root diameter detected from GPR to be greater than the actual root diameter. This is seen to occur most often in the largest diameter root. The addition of deconvolution to the processing flow could begin to eliminate this problem. Capability to determine the spatial distribution of roots in an area can be very helpful for not only belowground carbon estimates but for various studies and applications. For instance, the spatial distribution of roots can help plan the placement of soil CO_2 flux chambers. This would ensure that the chambers were not placed over an extensive network of roots if they are expected to measure heterotrophic respiration. However it would not be possible to detect roots of <1.4 cm diameter. In addition, accurate estimates of belowground biomass may help to improve the uncertainty in ecosystem models used in climate models. Hruska et al. (1999) were able to produce ground plan and side views of Oak tree root systems in a 6 × 6 m area at 25 cm interval spacing. Planar images of oak tree roots were created by Nadezhdina and Cermak (2003) as well through the interpolation of GPR profiles using image analysis. Zenone et al. (2008) introduced 3-D mapping from the correlation of laser point scan data and GPR profiles. 3-D mapping can be accomplished with the use of GPR-SLICE and small interval spacing of 5 cm.

3.4.2 Root Biomass Estimation

Our results provide a different approach to calculate root biomass. We have used root volume to obtain a quantitative estimate of root biomass. Previous studies have used root density, root diameter, and relationships between actual root biomass and GPR profiles to estimate root biomass (Barton and Montagu, 2004; Butnor et al., 2001, 2003;

XiHong et al., 2010). We found a significant relationship between root diameter and amplitude, although correlation was low. The cluster of roots in Figure 3.6 gives a high amplitude area for small diameter roots since they were placed close together. This could create error and outliers in the data. Roots that are 6 cm and greater appear to peak out at a maximum amplitude (Figures 3.7 and 3.8). Total reflection could be occurring from the largest root, as this is where the maximum amplitude and root diameter is found. In other words, all of the energy is being reflected back from the large root. Amplitudes obtained from the Hilbert transform slice provide a better correlation than raw amplitudes. This could be due to noise or the interference of other buried roots as well as any stratigraphy still present in raw data from changes in soil properties. Butnor et al. (2001) discovered similar results to our Figure 3.6 for a loblolly pine root at 20 cm (R^2=0.30), but they manually chose the apex of the antenna from raw data that correlated with the roots, whereas we used the Hilbert amplitude time slices created. One root was also buried in their pit; therefore there was no interference from other objects such as other roots. They discovered a high correlation (R^2=0.66) for loblolly pine roots at 15 cm. The difference in correlation could be due to the depth and orientation of the roots, the environment (in particular the soil properties), and/or tree species studied. There is however a general trend where high amplitude areas represent roots within the low amplitude soil background. Similar to our work, radar amplitude geometry and magnitude are used from the GPR profiles. Our study relates wave amplitude to the presence of root mass, compared to other studies that relate amplitude to root diameter (e.g. Butnor et al., 2001).

XiHong et al. (2010) also use root bulk volume however they calculate bulk volume based on root diameter derived from the time difference.

Our results indicate that GPR underestimates root biomass compared to the allometric method. This could be due to the large sampling interval. The large sampling interval created discontinuous root structures, which creates a loss of root mass. To confirm which method is best, excavation or air spading of the pit should be used to directly compare results; however this is time consuming and invasive. In our study, the 5 × 5 m inset only had one large tree within it. This may have caused the underestimation of root biomass by the allometric equation since small trees are disregarded, making the GPR estimate more accurate. This can also explain the large difference between total biomass per unit area (kgC m^{-2}) estimated by the allometric equation within both plots. There is also error associated with the allometric equation, including the small sample number and range in DBH, along with the error in annual DBH increment estimates (Peichl et al., 2010a). Peichl and Arain (2007) found a standard error (SE) of 0.354 and a standard error of estimate (SEE) of 0.08 for the allometric biomass equation used in our study. In addition, over the lifespan of a forest stand the allocation of biomass and carbon storage in tree carbon pools changes (Satoo and Madgwick, 1982; Peichl and Arain 2006). The allometric biomass equation used was derived in 2006, therefore this does not take into account any change in growth or carbon allocation over time. Comparing the estimates relative to sample interval shows that smaller interval sampling results in a better estimate of biomass, as the GPR estimate was closer in value to the allometric estimate with a 12.5 cm interval. Our study confirms that grid line spacing must be small (less than 5 cm preferably) for roots to be continuously detected across the two-dimensional profiles (Butnor et al., 2005). Together a high frequency antenna, such as 1 GHz providing a resolution of 2.5 cm, with small line spacing would create a detailed 3-D image resulting in a more accurate biomass estimate.

More detailed 3-D imaging could be completed with tomography surveys of roots using boreholes. Several boreholes could be positioned within a given area and measurements could be taken at various depths within the borehole itself. This would provide a 3-D image of root distribution and structure from direct detection of roots. Root diameter would be better determined since the roots would be imaged from several directions and angles. Multi-channel seismic reflection surveys would also provide a similar result with the root structure being better interpreted from the seismic waves being received from an array of directions from several positions. Other geophysical techniques could be used alongside GPR to obtain a larger database on the root structure, such as the geophysical techniques already stated in our paper and multi-frequency GPR.

A similar study should be conducted with smaller survey intervals for more detail within the large plot, and roots placed at various depths within the calibration pit. Noise was present in the calibration pit created from boundary effects, change in soil density, and the reburying of rocks, roots, organic matter etc., while filling the pit. This noise could be eliminated by the creation of a large pit with the survey completed in the middle, excavation after the survey is finished, allowing the pit to equilibrate to its surrounding for several weeks, and/or filtering the soil. Excavation after the GPR survey is complete could provide the error of the root volume in a large in-situ plot estimated by GPR survey data. Further comparison with the biomass estimates from allometric and GPR methods could then be done. Excavation could be done by air or water spading to limit damage done to the root zone. In areas with slightly undulating forest floors an accelerometer and/or laser scanning could be used to detect changes in topography. To remove the interference of the litter with the GPR unit, air launch GPR could be used.

As noted previously, 3-D images of root structure and distribution can be used in various fields, including the placement of soil CO_2 flux chambers and improving global climate model estimates. They could also be used in urban areas to determine root location and discover the roots of a tree that could be interfering with buried infrastructure. CRB estimates using GPR adds to the research performed to allocate carbon stock due to its importance with the increasing awareness of carbon mitigation. Although fine roots cannot be detected, they are typically ignored in methods such as excavation and therefore allometry due to the difficulty in gathering accurate estimates. The aspect of obtaining CRB and structure from root volume generated from 3-D GPR images is new to the field and should be built upon with further research. This new aspect begins to improve upon the allometric equation that has been used extensively in past research. GPR is a non-destructive technique that can be repeated over time for biomass estimates to be obtained from year to year.

3.5 Conclusions

Our study results show that:

(1) GPR can be used to create 3-D images that provide root distribution, size, and volume of coarse roots, where root volume can be related to larger (25 m^2 and 400 m^2 area) plot sizes for biomass estimation.

(2) Large line spacing will lower resolution leading to the underestimation of root mass and root biomass; therefore a line spacing of at most 10 cm should be used.

(3) High soil moisture decreases the detection of coarse roots.

(4) GPR biomass estimates underestimate biomass compared to that of the allometric equation due to the lack of continuity of root structure however ignoring small trees (< 9 cm) creates error within the allometric equation in small plot sizes.

(5) We also found that GPR has the capability to identify roots that are 10 cm apart and greater before the roots appear to be one large root, with the optimum line spacing.

3.6 Acknowledgements

This study was funded by the Natural Sciences and Engineering Research Council (NSREC) Discovery and Strategic grants. The Ontario Ministry of Environment (MOE) also provided funds. Support from the Canadian Foundation of Innovation (CFI), the Ontario Innovation Trust (OIT) and the Ontario Ministry of Natural Resources (OMNR) is also acknowledged. We thank Emily Nicholas, Suo Huang, Bin Chen, Robin Thorne and Steve Williams (OMNR) for their help.

CHAPTER 4: CONCLUSION AND FUTURE RESEARCH

Our study introduces the use of an accelerometer mounted on a high frequency (1 GHz) GPR unit to account for antenna tilt and the generation of 3-D images. The 3-D images display root structure, distribution and overall root location. We have also created a standard field procedure when using GPR for root detection and introduced volume as a parameter to relate total belowground biomass to geophysical parameters.

Micro-topographic effects brought about by the small size of the high frequency GPR unit create antenna tilt. Accounting for antenna tilt provides more accurate and precise images of root location and structure, as vector data enhances (15.5 % amplitude increase) and localizes the high amplitude signal. An accelerometer is also beneficial in forest environments where canopy cover would interfere with GPS signals. Radial surveys were found to be advantageous for root detection since the antenna runs perpendicular to the root structure, providing clear hyperbolas, indicating root location. Radial surveys at a line spacing of 10 cm provide better continuity of root structure than the typical rectilinear survey grid. In addition, we found that high soil moisture decreases the detection of roots and a line spacing of more than 10 cm (≤ 5 cm is optimal for 3-D images) results in discontinuous root structures. The lack of continuity leads to an underestimate of the root biomass (369 kgC) from GPR data when compared to the allometric equation (2170 kgC). With smaller line spacing (12.5 cm), the coarse root biomass estimated by GPR and allometry are more comparable, 22.6 kgC compared to 12.3 kgC respectively. However the allometric equation is subject to error, as it does not take into account small trees (DBH < 9 cm). The smallest root detected by GPR was 1.4

cm, which is considered a coarse root (> 5 mm). Therefore the standard field procedure for coarse root detection in a sandy environment with a high frequency antenna would require: low soil moisture, line spacing of a maximum of 10 cm, and an accelerometer (along with GPS for topography correction if canopy cover is minimal) to account for antenna tilt. With this field procedure, GPR has the potential to provide 3-D images of root distribution, size, and volume of coarse roots, leading to the estimation of coarse root biomass. However, under non-ideal conditions, allometry and excavation should be used. Before geophysical methods can be used extensively for estimating belowground biomass, further research should be completed to test its accuracy and precision in various field conditions with a variety of species. Until this occurs, allometry and GPR should be used alongside one another.

Additional research needs to be conducted in situ for root detection and belowground biomass estimates using GPR. More research should also be performed that integrates root biomass and soil water content estimation before GPR can be used temporally or in more topographically diverse sites (Butnor et al., 2003). Further investigation into the application of other geophysical methods, such as borehole radar, time domain reflectometry and multi-frequency GPR, for root detection should be completed. This would introduce tomography imaging of root structure. An assemblage of geophysical methods and GPR frequencies used simultaneously could lead to the detection of roots and estimation of belowground biomass with the requirement of little to no destructive techniques. Expanding on the work done in our study, smaller line spacing should be used for the 20 x 20 m and 5 x 5 m plots. Roots should also be placed at various depths in the calibration pit to determine if the relationship between amplitude and root diameter changes with depth. Furthermore, a mound should be created with known locations of buried metal objects where the effects of micro-topography and topography will be explored on antenna tilt using GPS and an accelerometer mounted on a GPR unit. Improvements could be made to the antenna tilt algorithm as well as corrections to the time stamps of the GPS and accelerometer data.

CHAPTER 5: REFERENCES

Amato, Mariana., Basso, Bruno., Celano, Giuseppe., Bitella, Giovanni., Morelli, Gianfranco., and Rossi, Roberta. (2008) In situ detection of tree root distribution and biomass by multi-electrode resistivity imaging. Tree Physiology., 28, 1441-1448

Arain, M.A. and Restrepo-Coupe, N. (2005) Net ecosystem production in a temperate pine plantation in southeastern Canada. Agricultural and Forest Meteorology., 128, 223-241.

Arora, K.Vivek., and Montenegro, Alvaro. (2011) Small temperature benefits provided by realistic afforestation methods. Nature Geoscience., 4, 514-518

Barton, Craig., and Montagu, Kelvin. (2004) Detection of tree roots and determination of root diameters by ground penetrating radar under optimal conditions., Tree Physiology., 24, 1323-1331

Benson, Alvin K. (1995) Applications of ground penetrating radar in assessing some geological hazards: examples of groundwater contamination, faults, cavities. Journal of Applied Geophysics., 33, 177-193

Beres, Milan., and Haeni, F.P. (1991) Application of Ground-Penetrating-Radar Methods in Hydrogeologic Studies. Groundwater., 29, 375-386

Bolte, A., Rahmann, T., Kuhr, M., Pogoda, P., Murach, D., and Gadow, K. (2004) Relationships between tree dimension and coarse root biomass in mixed stands of European beech (*fagus sylvatica L.*) and Norway spruce (Picea abies [L.] Karst.). Plant and Soil., 264, 1-11

Butnor, J.R., Doolittle, J.A., Hognsen, K.H., Samuelson, T., Stokes, T., and Kess, L. (2003) Utility of Ground-Penetrating Radar as a Root Biomass Survey Tool in Forest Systems. Soil Science Society of America., 67, 1607-1615

Butnor, J.R., Doolittle, J.A., Kress, L., Cohen, S. and Johnsen, K.H. (2001) Use of ground penetrating radar to study tree roots in the southeastern United States. Tree Physiology., 21, 1269-1278

Butnor, John., Roth, Brian., and Johnsen, Kurt. (2005) Feasibility of using ground-penetrating radar to quantify root mass in Florida's intensively managed pine plantations. Forest Biology Research Cooperative Report Number 38. Gainsville, Florida, USA.

Cairns, Michael., Brown, Sandra., Helmer, Eileen., and Baumgardner, Greg. (1997) Root biomass allocation in the world's upland forests. Oecologia., 111, 1-11

Cermak, Jan., Hruska, Jiri., Martinkova, Milena., and Prax, Alois. (2000) Urban tree root systems and their survival near houses analyzed using ground penetrating radar and sap flow techniques. Plant and Soil., 219, 103-116

Chen, J.M., Govind, A., Sonnentag, O., Zhang, Y., Barr, A., and Amiro, B. (2006) Leaf area index measurements at Fluxnet-Canada forest sites. Agricultural and Forest Meteorology., 140, 257-268.

Conyers, Lawrence B., and Leckebusch, Juerg. (2010) Geophysical Archaeology Research Agendas for the Future: Some Ground-penetrating Radar Examples. Archaeological Prospection., 17, 117-123

Dannoura, Masako., Hirano, Yasuhiro., Igarashi, Tetsuro., Ishii, Masahiro., Aono, Kenji., Yamase, Keitaro., and Kanazawa, Yoishi. (2008) Detection of *Cryptomeria japonica* roots with ground penetrating radar. Plant Biosystems., 142, 375-380

Dixon, R.K., Brown, S., Houghton, R.A., Solomon, A.M., Trexler, M.C., and Wisniewski, J. (1994) Carbon Pools and Flux of Global Forest Ecosystem. Science., 263, 185-191

Doolittle, James., and John, Butnor. (2009) Soils, Peatlands, and Biomonitoring. In Jol. Harry (Eds.), Ground Penetrating Radar Theory and Applications (pp. 179-202). Slovenia: Elsevier.

Fisher, C. Steven., Stewart, R. Robert., and Jol, M. Harry. (1992) Processing ground penetrating radar (GPR) data. CREWES Research Report., 4, 1-22

Gaul, Dirk., Hertel, Dietrich., Borken, Werner., Matzner, Egbert., and Leuschner, Christoph. (2008) Effects of experimental drought on fine root system of mature Norway spruce. Forest Ecology and Management., 256, 1152-1159

Goodale, Christine., Apps, Michael., Birdsey, Richard., Field, Christopher., Heath, Linda., Houghton, Richard., Jenkins, Jennifer., Kohlmaier, Gundolf., Kurz, Werner., Liu, Shirong., Nabuurs, Gert-Jan., Nilsson, Sten., and Shvidenko, Anatoly. (2002) Forest carbon sinks in the northern hemisphere. Ecological Applications., 12, 891-899

Goodman, Dean., and Klein, Justin. GPR-Slice v7 User's Manual. United States: Geophysical Archaeometry Laboratory Inc., 2012.

Goodman, Dean., Nishimura, Yasushi., Hongo, Hiromichi., and Higashi, Noriaki. (2006a) Correcting for Topography and the Tilt of Ground-penetrating Radar Antennae. Archaeological Propsection., 13, 159-163

Goodman, Dean., Nishimura, Yasushi., Hongo, Hiromichi., and Higashi, Noriaki. (2006b) Imaging of the Saitobaru Burial Mount #111: Correcting for topography and the tilt of the GPR antenna. Journal of Archaeological Prospection Society of Japan., 8, 3-8

Goodman, Dean., Schneider, Kent., Piro, Salvatore., Nishimura, Yasushi., and Pantel, Agamemnon G. Remote Sensing in Archaeology: Ground Penetrating Radar Advances in Subsurface Imaging for Archaeology. New York, USA: Springer Science and Business Media LLC, 2007

Grasmueck, Mark. (1996) 3-D ground-penetrating radar applied to fracture imaging in gneiss. Geophysics., 61, 1050-1064

Heeraman, D. A., Hopmans, J. W., and Clausnitzer, V. (1997) Three dimensional imaging of plant roots in situ with X-ray Computed Tomography. Plant and Soil., 189, 167-179

Hirano, Yasuhiro., Dannoura, Masako., Aono, Kenji., Igarashi,Tetsurou., Ishii, Masahiro., Yamase, Keitarou., Makita, Naoki., and Kanasawa, Yoichi. (2009) Limiting Factors in the detection of tree roots using ground penetrating radar. Plant Soil., 319, 15-24

Hruska, Jiri., Cermak, Jan., and Sustek, Svatopluk. (1999) Mapping tree root systems with ground-penetrating radar. Tree Physiology., 19, 125-130

Huisman, J.A., Sperl, C., Buoten, W., and Verstraten. J.M. (2001) Soil water content measurements at different scales: accuracy of time domain reflectometry and ground-penetrating radar. Journal of Hydrology., 245, 48-58

IPCC, 2007. Working Group I: The scientific Basis. (http://www.ipcc.ch/ipccreports/tar/wg1/ 505.htm, Sept. 20th 2010)

Lassoie, J.P. and T.M. Hinckley. 1991. Techniques and approaches in forest tree ecophysiology. CRC Press, Boston, 208-221

Leucci, Giovanni. (2010) The use of three geophysical methods for 3D images of total rot volume of soil in urban environments. Exploration Geophysics., 41, 268-278

Lorensen, William E., and Cline, Harvey E. (1987) Marching Cubes: A high resolution 3D surface construction algorithm. Computer Graphics., 21 N.4, 163-169

Lu, Pengxin., and Sinclair, Robert. W. (2006) Survival, growth and wood specific gravity of interspecific hybrids of Pinus strobus and P. wallichiana grown in Ontario. Forest Ecology and Management., 234, 97-106

Nadezhdina, Nadezhda., and Cermak, Jan. (2003) Instrumental methods for studies of structure and function of root systems of large trees. Journal of Experimental Botany., 54, 1511-1521

Neal, Adrain. (2004) Ground-penetrating radar and its use in sedimentology: principles, problems and progress. Earth Science Reviews., 66, 261–330

OceanServer Technology Inc. OceanServer Compass Manual Revision 4. United States: OceanServer Technology Inc., 2010

Ouimet, Rock., Camire, Claude., Brazeau, Marcel., and Moore, Jean-David. (2008) Estimation of coarse root biomass and nutrient content for sugar maple, jack pine, and black spruce using stem diameter at breast height. Can. J. Res., 38, 92-100

Peichl, Matthias., and Arain, M. Altaf. (2006) Above- and belowground ecosystem biomass and carbon pools in an age-sequence of temperate pine plantation forests. Agriculture and Forest Meteorology., 140, 51-63

Peichl, Matthias and Arain, M. Altaf. (2007) Allometry and partitioning of above- and belowground tree biomass in an age-sequence of white pine forests. Forest Ecology and Management., 253, 68-80

Peichl, Matthias., Brodeur, Jason, Khomik, Myroslava., and Arain, M.Altaf., (2010a) Biometric and eddy-covariance based estimates of carbon fluxes in an age sequence of temperate pine forests. Agriculture and Forest Meteorology., 150, 952-965

Peichl, Matthias., Arain, M.Altaf., and Brodeur, Jason. (2010b) Age effects on carbon fluxes in temperate pine forests. Agriculture and Forest Meteorology., 150, 1090-1101

Peichl, M., Arain, M.A., Ullah, S., Moore, T.R., (2009) Carbon dioxide, methane, and nitrous oxide exchanges in an age-sequence of temperate pine forests. Global Change Biology., 16, 2198-2212

Pesant, E.W. and Acton, C.J., (1984) The soils of the Regional Municipality of Haldimand-Norfolk. Vol. 1 & 2, Report 57, Land Resource Research Institute.

Prokhorenko, Vitalii., Ivashchuk, Volodymyr., Korsun, Sergiy., Musiyachenko, Sergiy., and Borodavka, Vladyslav. Topographic Correction of GPR Profile Based on Odometer and Inclinometer Data. 14th International Conference on Ground Penetrating Radar, June 4-8, 2012, Shanghai, China

OceanServer Technology Inc. OceanServer Compass Manual Revision 4. United States: OceanServer Technology Inc., 2010

Reynolds, John. An Introduction to Applied and Environmental Geophysics. England: John Wiley and Sons Ltd, 1997. Print.

Rossi, R., Amato, M., Bitella, G., Bochicchio, R., Ferreira Gomes, J. J., Lovelli, S., Martorella, E., and Favale, P. (2010) Electrical resistivity tomography as a non-destructive method for mapping root biomass in an orchard. Eurpean Journal for Soil Science., doi: 10.1111/j.1365-2389.2010.01329.x

Satriani, A., Loperte, A., Proto, M., and Bavusi, M. (2010) Building damage caused by tree roots: Laboratory experiments of GPR and ERT surveys. Advances in Geosciences., 24, 133-137

Sensors and Software Inc., Practical Processing of GPR data. 1999. http://www.ees.nmt.edu/outside/Geop/Classes/Geop446/Docs/GPR_data_process.pdf

Stokes, Alexia., Fourcaud, Thierry., Hruska, Jiri., Cermak, Jan., Nadyezdhina, Nadezhda., Nadyezhdin., and Praus, Ludek. (2002) An evauluation of different methods to investigate root system architecture of urban trees *in situ*: I. Ground-penetrating radar. Journal of Arboriculture., 28(1), 2-10

Stover, Daniel. B., Day, Frank. P., Butnor, John. R. and Drake. Bert. G. (2007) Effect of elevated CO2 on coarse-root biomass in Florida scrub detected by ground-penetrating radar. Ecology., 88, 1328-1334

Vadeboncoeur, Matthew., Hamburg, Steven., and Yanai Ruth. (2007) Validation and refinement of allometric equations for roots of northern hardwoods. Can. J. For. Res., 37, 1777-1783

Vincke, Caroline., and Thiry, Yves. (2008) Water table is a relevant source for water uptake by a Scots pine (Pinus sylvestris L.) stand: Evidences from continuous evapotranspiration and water table monitoring. Agriculture and Forest Meteorology., 148, 1419-1432

Wahlgren, H.E., Baker, G., Maeglin, R.R., Hart, A.C., (1968) Survey of specific gravity of eight Maine conifers. USDA For. Serv. Res. Pap., 95, 11

Wielopolski, Lucian., Hendrey, George., Daniels, Jeff., and McGuigan, Michael. (2002) Imaging tree root systems in situ. International conference on ground penetrating radar N^{o}9. 4758, 58-62

Woodcock, D.W., and Shier, A.D. (2003) Does Canopy Position Affect Wood Specific Gravity in Temperate Forest Trees. Annals of Botany., 91, 529-537

XiHong, Cui., Chen, Jin., JinSong, Shen., Cao, Kin., Chen, XueHong., and Zhu, XiaoLin. (2010) Modeling tree root diameter and biomass by ground penetrating radar. Sci China Earth Sci., doi: 10.1007/s11430-010-4103-z

Yokota, Yuya., Matsumoto, Masayoshi., Gaber, Ahmed., Grasmueck, Mark., and Sato, Motoyuki. 2011 Estimation of biomass of tree roots by GPR with high accuracy positioning system. Geoscience and Remote Sensing Symposium, Vancouver, BC, July 2011

Zenone, Terrenzio., Morelli, Gianfranco., Teobaldelli, Maurizio., Fischanger, Federico., Matteucco, Marco., Sordini, Matteo., Armani, Alessio., Ferre, Chiara., Chiti, Tommasco., and Seufert, Guenther. (2008) Preliminary use of ground-penetrating radar and electrical resistivity tomography to study tree roots in pine forests and poplar populations. Functional Plant Biology., 35, 1047-1058